

A Dissertation

entitled

Analysis of Deactivation Mechanism on a Multi-Component Sulfur-Tolerant

Steam Reforming Catalyst

by

Satish L. Lakhapatri

Submitted to the Graduate Faculty as partial fulfillment of the requirements for the

Doctor of Philosophy Degree in Engineering

Dr. Martin A. Abraham, Advisor

Dr. Glenn Lipscomb, Committee Member

Dr. Maria Coleman, Committee Member

Dr. Sasidhar Varanasi, Committee Member

Dr. Pannee Burckel, Committee Member

Dr. Patricia Komuniecki, Dean
College of Graduate Studies

The University of Toledo

August 2010

Report Documentation Page

Form Approved
OMB No. 0704-0188

Public reporting burden for the collection of information is estimated to average 1 hour per response, including the time for reviewing instructions, searching existing data sources, gathering and maintaining the data needed, and completing and reviewing the collection of information. Send comments regarding this burden estimate or any other aspect of this collection of information, including suggestions for reducing this burden, to Washington Headquarters Services, Directorate for Information Operations and Reports, 1215 Jefferson Davis Highway, Suite 1204, Arlington VA 22202-4302. Respondents should be aware that notwithstanding any other provision of law, no person shall be subject to a penalty for failing to comply with a collection of information if it does not display a currently valid OMB control number.

1. REPORT DATE

AUG 2010

2. REPORT TYPE

3. DATES COVERED

00-00-2010 to 00-00-2010

4. TITLE AND SUBTITLE

Analysis of Deactivation Mechanism on a Multi-Component Sulfur-Tolerant Steam Reforming Catalyst

5a. CONTRACT NUMBER

5b. GRANT NUMBER

5c. PROGRAM ELEMENT NUMBER

6. AUTHOR(S)

5d. PROJECT NUMBER

5e. TASK NUMBER

5f. WORK UNIT NUMBER

7. PERFORMING ORGANIZATION NAME(S) AND ADDRESS(ES)

University of Toledo, 2801 Bancroft, Toledo, OH, 43606-3390

8. PERFORMING ORGANIZATION REPORT NUMBER

9. SPONSORING/MONITORING AGENCY NAME(S) AND ADDRESS(ES)

10. SPONSOR/MONITOR'S ACRONYM(S)

11. SPONSOR/MONITOR'S REPORT NUMBER(S)

12. DISTRIBUTION/AVAILABILITY STATEMENT

Approved for public release; distribution unlimited

13. SUPPLEMENTARY NOTES

14. ABSTRACT

Conventional fuels exist in limited reserves and have adverse environmental impacts. Researchers are striving hard to either introduce alternative sources to replace conventional fuels or use the existing sources efficiently. Towards attaining sustainable development, it is considered an obligation to use the existing energy reserves efficiently with reduced environmental issues. Fuel cells are energy conversion devices which convert chemical energy into electricity. They are promising in that they do not cause pollution at source and can operate at relatively high energy efficiencies. The only by-product coming out of a fuel cell is water. Use of the fuel cell in transportation sector has been an area of active research. While car manufacturers are rigorously looking at challenges in replacing internal combustion engine with fuel cell stack, it has attracted also attracted a great deal of attention from heavy duty trucks. Trucks generally idle about 20-40% of the time the engine is running, depending on season and operation. During idling of trucks, the internal combustion engine is known to operate at much lower efficiencies, typically less than 5%. It is here where fuel cells can be used effectively as auxiliary power units (APUs). While the efficiency in a typical internal combustion engine of a truck rarely exceeds 20%, a fuel cell normally operates at around 40% to 60%. The maximum theoretical efficiency of a hydrogen fuel cell is around 83% and the higher efficiencies can be attributed to the fact that they do not operate on a themal cycle unlike internal combustion engines. Hydrogen used to run a fuel cell can be produced from transportation fuels. Given the advantages such as their availability, relatively low cost, and existing infrastructure for delivery and transportation, they are likely to play a major role in hydrogen production in the near future. Hydrogen production via transportation fuels such as diesel, gasoline and jet fuel is hindered by catalyst deactivation during its production via reforming. Deactivation of reforming catalyst used for hydrogen production from diesel or jet fuel creates a significant barrier to commercialization of fuel cell technologies. In order to design better catalysts, it is vital to understand the mechanisms of catalyst deactivation and then use the understanding for better catalyst development. In an attempt to address the fundamental problem of catalyst deactivation, two catalyst systems, NM4 and 3J1, were extensively studied for deactivation. NM4 is a binary catalyst consisting of Ni and Rh while 3J1 consists of Ni, Pd and Rh. In the first part of the study, deactivation on NM4 was studied using n-hexadecane doped with thiophene as the surrogate fuel for diesel. 3J1 was the focus of study in the second part where a mixture of hydrocarbons (

15. SUBJECT TERMS

16. SECURITY CLASSIFICATION OF:			17. LIMITATION OF ABSTRACT	18. NUMBER OF PAGES	19a. NAME OF RESPONSIBLE PERSON
a. REPORT	b. ABSTRACT	c. THIS PAGE			
unclassified	unclassified	unclassified	Same as Report (SAR)	211	

An Abstract of
Analysis of Deactivation Mechanism on a Multi-Component Sulfur-Tolerant Steam
Reforming Catalyst

by

Satish L. Lakhapatri

Submitted to the Graduate Faculty in partial fulfillment of the requirements for the
Degree of Doctor of Philosophy in Engineering

The University of Toledo

August 2010

Conventional fuels exist in limited reserves and have adverse environmental impacts. Researchers are striving hard to either introduce alternative sources to replace conventional fuels or use the existing sources efficiently. Towards attaining sustainable development, it is considered an obligation to use the existing energy reserves efficiently with reduced environmental issues. Fuel cells are energy conversion devices which convert chemical energy into electricity. They are promising in that they do not cause pollution at source and can operate at relatively high energy efficiencies. The only by-product coming out of a fuel cell is water. Use of the fuel cell in transportation sector has been an area of active research. While car manufacturers are rigorously looking at challenges in replacing internal combustion engine with fuel cell stack, it has attracted

also attracted a great deal of attention from heavy duty trucks. Trucks generally idle about 20-40% of the time the engine is running, depending on season and operation. During idling of trucks, the internal combustion engine is known to operate at much lower efficiencies, typically less than 5%. It is here where fuel cells can be used effectively as auxiliary power units (APUs). While the efficiency in a typical internal combustion engine of a truck rarely exceeds 20%, a fuel cell normally operates at around 40% to 60%. The maximum theoretical efficiency of a hydrogen fuel cell is around 83% and the higher efficiencies can be attributed to the fact that they do not operate on a thermal cycle unlike internal combustion engines. Hydrogen used to run a fuel cell can be produced from transportation fuels. Given the advantages such as their availability, relatively low cost, and existing infrastructure for delivery and transportation, they are likely to play a major role in hydrogen production in the near future. Hydrogen production via transportation fuels such as diesel, gasoline and jet fuel is hindered by catalyst deactivation during its production via reforming. Deactivation of reforming catalyst used for hydrogen production from diesel or jet fuel creates a significant barrier to commercialization of fuel cell technologies. In order to design better catalysts, it is vital to understand the mechanisms of catalyst deactivation and then use the understanding for better catalyst development.

In an attempt to address the fundamental problem of catalyst deactivation, two catalyst systems, NM4 and 3J1, were extensively studied for deactivation. NM4 is a binary catalyst consisting of Ni and Rh while 3J1 consists of Ni, Pd and Rh. In the first part of the study, deactivation on NM4 was studied using n-hexadecane doped with thiophene as the surrogate fuel for diesel. 3J1 was the focus of study in the second part where a

mixture of hydrocarbons (n-hexadecane, toluene, tetralin and 1-methylnaphthalene) was used to represent jet fuel. The tests were also performed on real jet fuel (Jet A) obtained from the NASA Glenn Research Center. The basic difference between these fuels is the high content of aromatics and naphthenes in case of jet fuel in addition to high organic sulfur. The studies were aimed at understanding the effect of this difference on deactivation characteristics. Analysis of fresh catalysts showed the presence of two groups of particles, primarily distinguished by their size and composition; particles in the range of few nanometers to 6 nm were predominantly made of rhodium while nickel was generally seen as large crystallites. Palladium was seen in close proximity to nickel and generally present as large crystallites. Steam reforming caused sintering of crystallites containing nickel while no identifiable growth in rhodium crystallites was observed. The steam reforming activity was measured in terms of H₂ yields. The catalysts showed superior activity and stability during steam reforming of paraffins represented by n-hexadecane. In the presence of naphthenic species such as 1-methylnaphthalene, the catalysts deactivated rapidly leading to quick drops in hydrogen yields. The catalysts were stable in the absence of sulfur but deactivated over a period of 10 h when sulfur was present at high loading. Stability and activity were higher with higher amounts of rhodium content when nickel was kept constant. Palladium was seen to cause excessive cracking and thereby leading to significant deactivation.

Sulfur compounds were converted to primarily hydrogen sulfide via hydrodesulfurization. It was found when complete conversion of sulfur compounds to hydrogen sulfide was observed, the catalyst lost only a small portion of its activity. Only when thiophene started to exit unconverted, the catalyst started to deactivate steadily. In

addition, presence of sulfur led to significantly increased amounts of cracking products which indicated that sulfur deactivated primarily active sites responsible for steam reforming. STEM-EDS of used catalysts revealed preferential adsorption of sulfur on the surface of nickel crystallites; EDS and XRD analysis showed no bulk sulfide formation. No detectable sulfur was seen on rhodium crystallites. Excessive carbon deposition was observed during steam reforming of sulfur-containing fuel. Graphitic carbon was present at all stages of catalyst life irrespective of the catalyst composition and it was significantly higher for sulfur-containing fuels. Blocking of reactant species on the surface of the catalyst due to the formation of aromatic/polymeric carbon on the support was also seen, although higher rhodium content inhibited this phenomenon.

**Dedicated to my parents, Shashikala & Limbadri and my brothers, Sachin &
Santosh**

Acknowledgment

First and foremost I offer my sincerest gratitude to my supervisor, Dr. Martin Abraham, who has supported me throughout my thesis with his patience and knowledge whilst allowing me the room to work in my own way. I am not sure many graduate students are given the opportunity to develop their own individuality and self-sufficiency by being allowed to work with such independence. I attribute the level of my PhD degree to his encouragement and effort and without him this thesis, too, would not have been completed or written. Working on this project was an excellent opportunity and I would like to thank Dr. Abraham for the same. It has been a great learning experience and I am certain it is something that will shape my future.

I would like to thank Dr. Arunan Nadarajah for offering me with the opportunity of pursuing my graduate studies at the Chemical and Environmental Engineering Department of The University of Toledo. My sincere thanks to Dr. Glenn Lipscomb for his constant support throughout my doctoral studies, especially after Dr. Abraham left the University. I would also like to express my sincere gratitude to Catacel, our industrial partner, for their support throughout my research. I would like to acknowledge Wright Fuel Cell group and US Army for the funding throughout my research.

I would like to also express my thanks to my other dissertation committee members, Dr. Sasidhar Varanasi, Dr. Maria Coleman and Dr. Pannee Burckel for their constructive

comments during my proposal and final defense.

I am heartily thankful to Dr. Kai Sun, University of Michigan Electron Microbeam Analysis Laboratory) whose supervision and support on advanced catalyst characterization techniques from the preliminary to the concluding level enabled me to direct my research.

This work would not have been possible without the support and encouragement of my colleagues and labmates Sandeep Goud and Atish Kataria under whose supervision I began working toward my thesis. I would like to thank my other labmates Sadashiv, Pradeep, Preshit, Ayyappan and Amanda for generously sharing their knowledge about various concepts and also time to help me setting up my reactions. No words can describe the support rendered by a special friend Rohini, whose constant moral support helped me immensely during the last two years of my doctoral work. I am grateful to my roommates Vaibhav, Rangarajan and Desikan for their continued moral support. A special thanks also to Kamal, Santhosh, Alope, Rahul, Abbas, Devdutt, Rachit and Amey. It would be unfair not to mention these guys who have made my stay at UT a memorable one.

Finally, I would like to acknowledge the most important people of my life, my parents and my two brothers. I am forever indebted to my family for their understanding, endless patience and encouragement when it was most required. Dedicating my work to them is just a small token of appreciation.

Table of Contents

Abstract.....	iii
Acknowledgment.....	viii
Table of Contents	x
List of Figures.....	xv
List of Tables	xxv
1. Introduction.....	1
1.1. Types of Fuel Cells.....	3
1.1.1. Alkaline Fuel Cells (AFC).....	4
1.1.2. Proton Exchange Membrane Fuel Cells (PEMFC).....	5
1.1.3. Direct Methanol Fuel Cells (DMFC).....	6
1.1.4. Phosphoric Acid Fuel Cell (PAFC)	6
1.1.5. Molten Carbonate Fuel Cell (MCFC).....	7
1.1.6. Solid oxide Fuel Cell (SOFC).....	7
1.2. Fuel Options	8
1.2.1. Hydrogen.....	8
1.2.2. Natural gas	9
1.2.3. Methanol	9
1.2.4. Biomass.....	10
1.2.5. Logistic fuels.....	10

1.3. Fuel Processing – Stationary or On-board	11
1.3.1. Reforming in a stationary plant.....	11
1.3.2. Reforming on-board.....	12
1.3.3. General Fuel Processing Scheme for a Fuel Cell.....	13
1.4. Desulfurization technologies	13
1.4.1. Conventional HDS technologies.....	15
1.4.2. ‘Non-HDS’ based desulfurization technologies	16
1.5. Fuel Processing Technologies.....	17
1.5.1. Steam Reforming (SR).....	18
1.5.2. Partial Oxidation (POX)	19
1.5.3. Auto thermal reforming (ATR).....	19
1.6. Motivation and Objective.....	20
2. Experimental and Analytical	26
2.1. Experimental Set-up for Steam Reforming.....	26
2.1.1. Summary of experimental and analytical section	26
2.1.2. Details of experimental and analytical section	27
2.2. Catalyst preparation.....	35
2.2.1. NM4	36
2.2.2. 3J1	37
2.3. Catalyst loading.....	39
2.4. Catalyst testing.....	40
2.4.1. Definition of hydrogen yield.....	41

2.5. Catalyst characterization	42
2.5.1. Pulse Chemisorption	42
2.5.2. Temperature Programmed Reduction (TPR)	43
2.5.3. Temperature Program Oxidation (TPO)	44
2.5.4. Temperature Program Ammonia Desorption (TPAD)	44
2.5.5. BET surface area	45
2.5.6. X-ray Diffraction (XRD)	45
2.5.7. Transmission Electron Microscopy (TEM)	46
2.5.8. X-ray Photoelectron Spectroscopy	47
2.5.9. Scanning Electron Microscopy (SEM)	47
3. Literature Review	49
3.1. Operating parameters	49
3.1.1. Temperature	49
3.1.2. Steam-to-carbon ratio (S/C)	52
3.2. Steam reforming of Methane	52
3.2.1. Thermodynamics	53
3.2.2. Kinetics	54
3.2.3. Catalysts	55
3.3. Steam reforming of higher hydrocarbons	56
3.3.1. Thermodynamics	56
3.3.2. Kinetics	57
3.3.3. Catalysts	59

3.4. Catalyst Deactivation.....	62
3.4.1. Carbon deposition.....	62
3.4.2. Sulfur Poisoning.....	67
3.4.3. Metal particle sintering.....	69
3.4.4. Catalyst deactivation in higher hydrocarbons / transportation fuels.....	71
4. Analysis of deactivation mechanism on NM4 catalyst.....	74
4.1. Introduction.....	74
4.2. Steam reforming of n-hexadecane.....	76
4.2.1. Activity and deactivation.....	76
4.2.2. Extent of cracking.....	83
4.2.3. Hydrogen sulfide in the product stream.....	85
4.3. Characterization of fresh catalysts.....	86
4.3.1. Phase structure and Ni crystallite size.....	87
4.3.2. Microscopic structure and composition.....	89
4.4. Characterization of used catalysts.....	91
4.4.1. Phase structure and Ni crystallite size.....	92
4.4.2. Sulfur adsorption studies.....	95
4.4.3. Carbon deposition studies.....	99
5. Analysis of deactivation mechanism on 3J1.....	108
5.1. Introduction.....	108
5.2. Selection of process parameters to study deactivation.....	110
5.3. Hydrogen yield.....	110

5.4. Steam reforming of Simulated fuel and Jet A	111
5.4.1. Activity and deactivation	112
5.4.2. Extent of cracking	120
5.4.3. Hydrogen sulfide in the product stream.....	121
5.4.4. Long time study on 3J1	122
5.5. Characterization of fresh catalysts.....	124
5.5.1. Phase structure using XRD, TPR and XPS.....	125
5.5.2. Microscopic structure and composition using STEM-EDS.....	132
5.6. Characterization of used catalysts.....	141
5.6.1. Phase structure and crystallite growth using XRD, XPS and TPR.....	141
5.6.2. Sulfur adsorption studies.....	151
5.6.3. Carbon deposition studies	159
6. Summary of results and proposed mechanism of deactivation	166
7. Conclusions.....	174
References.....	176

List of Figures

Figure 1-1. Generalized flow diagram for a fuel processor-fuel cell system.....	13
Figure 2-1. Schematic of the experimental set-up used for steam reforming.....	27
Figure 2-2. Stacked coil arrangement for feed vaporization.....	29
Figure 2-3. Reactor assembly	30
Figure 2-4. Condenser section	32
Figure 2-5. Automatic gas injection and separation using two 6-way valves	34
Figure 3-1. A CHEMCAD simulation of steam reforming of n-hexadecane at S/C 3	50
Figure 3-2. A CHEMCAD simulation on steam reforming of n-hexadecane showing the change in the hydrogen yield, n-hexadecane conversion and CO ₂ selectivity with temperature	51
Figure 4-1. Gas chromatograph of diesel performed on Hewlett Packard 6890/5973 GC/MS	75
Figure 4-2. Relative H ₂ yields of catalyst NM4 during steam reforming of sulfur- free and sulfur-laden n-hexadecane at 800°C, S/C 3 and 1 atm	77

Figure 4-3. Relative H ₂ yields of catalyst Ni/a during steam reforming of sulfur-free and sulfur-laden n-hexadecane at 800°C, S/C 3 and 1 atm	78
Figure 4-4. Relative H ₂ yields of catalyst Rh/a during steam reforming of sulfur-free and sulfur-laden n-hexadecane at 800°C, S/C 3 and 1 atm	78
Figure 4-5. Relative H ₂ yields of catalyst (2.5RhNi)/a during steam reforming of sulfur-free and sulfur-laden n-hexadecane at 800°C, S/C 3 and 1 atm	79
Figure 4-6. Initial activity in terms of hydrogen yield evaluated by straight line fitting of reaction data for different catalyst formulations during steam reforming of sulfur-free and sulfur-laden n-hexadecane at 800°C, S/C 3 and 1 atm	80
Figure 4-7. Deactivation rate in terms of hydrogen yield per hour evaluated by straight line fitting of reaction data for different catalyst formulations during steam reforming of sulfur-free and sulfur-laden n-hexadecane at 800°C, S/C 3 and 1 atm	81
Figure 4-8. Dry product gas composition over 10 h during steam reforming of sulfur-free and sulfur-laden n-hexadecane at 800°C, S/C 3 and 1 atm	82
Figure 4-9. H ₂ /CO, H ₂ /CO ₂ and CO ₂ /CO in the dry product gas over 10 h during steam reforming of sulfur-free and sulfur-laden n-hexadecane at 800°C, S/C 3 and 1 atm	83

Figure 4-10. Extent of cracking in the dry product gas over 10 h during steam reforming of sulfur-free and sulfur-laden n-hexadecane at 800°C, S/C 3 and 1 atm	84
Figure 4-11. Total % sulfur out over 10 h during steam reforming of sulfur-free and sulfur-laden n-hexadecane at 800°C, S/C 3 and 1 atm	86
Figure 4-12. XRD profiles of fresh catalysts calcined in air at 800°C and reduced in 5% H_2/N_2 at 800°C	89
Figure 4-13. TPR profiles of fresh catalysts calcined in air at 800°C.....	89
Figure 4-14. EDS analysis of fresh NM4, calcined in air at 800°C and reduced in 5% H_2/N_2 at 800°C. (a) STEM image, (b) Magnification of box in image a, and (c) EDS signature of particles A and B, as seen in b	91
Figure 4-15. XRD patterns of used catalysts, after steam reforming of sulfur-laden n-hexadecane at 800°C, S/C 3 and 1 atm	93
Figure 4-16. XRD patterns of used catalysts, after steam reforming of sulfur-free n-hexadecane at 800°C, S/C 3 and 1 atm	93
Figure 4-17. XRD patterns of used catalyst NM4 at different TOS, after steam reforming of sulfur-laden n-hexadecane at 800°C, S/C 3 and 1 atm.....	94
Figure 4-18. HRTEM images of used catalysts, after steam reforming of sulfur-free and sulfur-laden n-hexadecane at 800°C, S/C 3 and 1 atm	95

Figure 4-19. EDS analysis of used NM4 after steam reforming of sulfur-laden n-hexadecane at 800°C, 1 atm, S/C=3 and 1000 ppm sulfur (a) STEM image, and (b) EDS signature at positions 1, 2 and 3	97
Figure 4-20. Elemental mapping analysis of used NM4 after steam reforming of sulfur-laden n-hexadecane at 800°C, 1 atm, S/C=3 and 1000 ppm sulfur (a) STEM image, (b) nickel mapping, and (c) sulfur mapping.....	98
Figure 4-21. Elemental mapping analysis of used (2.5RhNi)/a after steam reforming of sulfur-laden n-hexadecane at 800°C, 1 atm, S/C=3 and 1000 ppm sulfur (a) STEM image, (b) nickel mapping, and (c) sulfur mapping.....	99
Figure 4-22. TPO of used catalyst NM4 after steam reforming of sulfur-free and sulfur-laden n-hexadecane at 800°C, S/C 3 and 1 atm	100
Figure 4-23. Carbon deposition on the catalyst (based on integration of TPO, as described in text) and C ₂ + in dry exit gas during steam reforming n-hexadecane at 800°C, 1 atm, S/C=3.	101
Figure 4-24. Carbon mapping of used catalysts, after steam reforming of sulfur-laden n-hexadecane at 800°C, 1 atm, S/C=3 and 1000 ppm sulfur (a) STEM image and (b) carbon mapping of NM4, and (c) STEM image and (d) carbon mapping of (2.5RhNi)/a.	103

Figure 4-25. C 1s XPS of used catalysts, after steam reforming of n-hexadecane at 800°C, 1 atm and S/C=3 (a) sulfur-free and sulfur laden runs, and (b) sulfur-laden run on NM4 taken as a function of time on stream.....	105
Figure 4-26. STEM image of used NM4 catalyst showing presence of carbon whiskers after steam reforming of sulfur-laden n-hexadecane at 800°C, 1 atm and S/C=3	107
Figure 5-1. Gas chromatograph of kerosene performed on Hewlett Packard 6890/5973 GC/M.....	110
Figure 5-2. Relative H ₂ yields of catalyst Ni/b during steam reforming of Simulated fuel No sulfur and Jet fuel 1000 ppm sulfur at 800°C, S/C3 and 1 atm	113
Figure 5-3. Relative H ₂ yields of catalyst Pd/b during steam reforming of Simulated fuel No sulfur and Jet fuel 1000 ppm sulfur at 800°C, S/C3 and 1 atm	113
Figure 5-4. Relative H ₂ yields of catalyst Rh/b during steam reforming of Simulated fuel No sulfur and Jet fuel 1000 ppm sulfur at 800°C, S/C3 and 1 atm	114
Figure 5-5. Relative H ₂ yields of catalyst Ni-Pd/b during steam reforming of Simulated fuel No sulfur and Jet fuel 1000 ppm sulfur at 800°C, S/C3 and 1 atm	114

Figure 5-6. Relative H ₂ yields of catalyst Ni-Rh/b during steam reforming of Simulated fuel No sulfur and Jet fuel 1000 ppm sulfur at 800°C, S/C3 and 1 atm	115
Figure 5-7. Relative H ₂ yields of catalyst (PdRh)/b during steam reforming of Simulated fuel No sulfur and Jet fuel 1000 ppm sulfur at 800°C, S/C3 and 1 atm	115
Figure 5-8. Relative H ₂ yields of catalyst 3J1 during steam reforming of SF No S and JF 1000 ppm S at 800°C and 1 atm.	116
Figure 5-9. Initial activity in terms of hydrogen yield evaluated by straight line fitting of reaction data for different catalyst formulations during steam reforming of Simulated fuel No sulfur and Jet fuel 1000 ppm sulfur at 800°C, S/C3 and 1 atm	117
Figure 5-10. Deactivation rate in terms of hydrogen yield per hour evaluated by straight line fitting of reaction data of different catalyst formulations during steam reforming of Simulated fuel No sulfur and Jet fuel 1000 ppm sulfur at 800°C, S/C3 and 1 atm	118
Figure 5-11. Dry product gas composition over 10 h during steam reforming of Simulated fuel No sulfur and Jet fuel 1000 ppm sulfur at 800°C, S/C3 and 1 atm	119

Figure 5-12. H ₂ /CO, H ₂ /CO ₂ and CO ₂ /CO in the dry product gas over 10 h during steam reforming of Simulated fuel No sulfur and Jet fuel 1000 ppm sulfur at 800°C, S/C3 and 1 atm	119
Figure 5-13. Extent of cracking in the dry product gas over 10 h during steam reforming of Simulated fuel No sulfur at 800°C, S/C3 and 1 atm	120
Figure 5-14. Extent of cracking in the dry product gas over 10 h during steam reforming of Jet fuel 1000 ppm sulfur at 800°C, S/C3 and 1 atm.....	121
Figure 5-15. Total % sulfur out over 10 h during steam reforming of Jet fuel 1000 ppm sulfur at 800°C, S/C3 and 1 atm.....	122
Figure 5-16. Hydrogen and sulfur yield over 10 h during steam reforming of Jet fuel 1000 ppm sulfur at 800°C, S/C3 and 1 atm.....	123
Figure 5-17. Evolution of H ₂ S and thiophene peak with time on stream during steam reforming of Jet fuel on Ni/b and 3J1 at 1000 ppm sulfur, 800°C, S/C3 and 1 atm	124
Figure 5-18. XRD profiles of fresh reduced catalysts	125
Figure 5-19. TPR profiles of fresh calcined catalysts.....	127
Figure 5-20. Al 2p XPS profiles of fresh calcined catalysts.....	128
Figure 5-21. Al 2p XPS profiles of fresh reduced catalysts	129
Figure 5-22. Ni 2p XPS profiles of fresh calcined catalysts.....	130

Figure 5-23. Ni 2p XPS profiles of fresh reduced catalysts	130
Figure 5-24. Rh 3d XPS profiles of fresh calcined catalysts	131
Figure 5-25. Rh 3d XPS profiles of fresh reduced catalysts.....	132
Figure 5-26. EDS analysis of fresh reduced 3J1 catalyst (a) STEM image and (b and c) EDS of particles shown in (a).....	134
Figure 5-27. EDS analysis of small particles in fresh reduced 3J1 (a) STEM image and (b and c) EDS of particles shown in (a).....	136
Figure 5-28. EDS analysis of small particles in fresh reduced Ni-Rh/b (a) STEM image and (b and c) EDS of particles shown in (a).....	138
Figure 5-29. EDS analysis of big particles in fresh reduced (PdRh)/b (a) STEM image and (b and c) EDS of particles shown in (a).....	140
Figure 5-30. XRD profiles of (a) fresh catalysts and (b) used catalysts after steam reforming of Jet fuel 1000 ppm sulfur at 800°C, S/C=3 and 1 atm.....	143
Figure 5-31. TPR profiles of (a) fresh catalysts and (b) used catalysts catalysts after steam reforming of Jet fuel 1000 ppm sulfur at 800°C, S/C=3 and 1 atm	144
Figure 5-32. Ni 2p XPS of (a) fresh catalysts and (b) used catalysts after steam reforming of Jet fuel 1000 ppm sulfur at 800°C, S/C=3 and 1 atm.....	147

Figure 5-33. Ni 2p XPS of used catalyst 3J1 at different times on stream, catalysts after steam reforming of Jet fuel 1000 ppm sulfur at 800°C, S/C=3 and 1 atm	148
Figure 5-34. EDS analysis of small particles in used 3J1 catalysts after steam reforming of Jet fuel 1000 ppm sulfur at 800°C, S/C=3 and 1 atm.....	150
Figure 5-35. STEM images of used (a) 3J1 and (b) Ni-Rh/b catalysts steam reforming of Jet fuel 1000 ppm sulfur at 800°C, S/C=3 and 1 atm.....	151
Figure 5-36. EDS analysis of small particles in used Ni-Rh/b catalysts after steam reforming of Jet fuel 1000 ppm sulfur at 800°C, S/C=3 and 1 atm.....	153
Figure 5-37. EDS analysis of large particles in used Ni-Rh/b catalysts after steam reforming of Jet fuel 1000 ppm sulfur at 800°C, S/C=3 and 1 atm.....	155
Figure 5-38. EDS analysis of large particles in used 3J1 catalysts after steam reforming of Jet fuel 1000 ppm sulfur at 800°C, S/C=3 and 1 atm.....	157
Figure 5-39. EDS analysis of large particles in used 3J1 catalysts after steam reforming of Jet fuel 1000 ppm sulfur at 800°C, S/C=3 and 1 atm.....	159
Figure 5-40. TPO of used catalysts catalysts after steam reforming of Jet fuel 1000 ppm sulfur at 800°C, S/C=3 and 1 atm.....	160
Figure 5-41. EDS analysis of Ni/Pd particle in used 3J1 catalysts after steam reforming of Jet fuel 1000 ppm sulfur at 800°C, S/C=3 and 1 atm.....	161

Figure 5-42. TPO of used 3J1 at different times on stream after steam reforming of Jet fuel 1000 ppm sulfur at 800°C, S/C=3 and 1 atm.....	162
Figure 5-43. C 1s XPS of used catalysts after steam reforming of Jet fuel 1000 ppm sulfur at 800°C, S/C=3 and 1 atm.....	164
Figure 5-44. C 1s XPS of used 3J1 at different times on stream catalysts steam reforming of Jet fuel 1000 ppm sulfur at 800°C, S/C=3 and 1 atm.....	165
Figure 6-1. Proposed deactivation mechanism on a noble metal promoted nickel based sulfur-tolerant steam reforming catalyst	173

List of Tables

Table 2-1. Composition of catalysts synthesized for part I – NM4	37
Table 2-2. Composition of catalysts synthesized for part II – 3J1	38
Table 5-1. Nickel crystallite sizes estimated by Scherrer equation	126
Table 5-2. EDS peak position assignments.....	132

Chapter 1

Introduction

In an age of ever increasing prices of conventional fuels, uncertainty of fossil fuel supplies and concern over the rising carbon dioxide levels in the atmosphere, the role of fuel cell as clean and efficient energy conversion device is being studied vigorously. As we move towards a sustainable future, it is also important to use the existing energy resources efficiently.

The scientific community is striving to introduce alternative energy sources with minimal environmental issues. In the last decade, there has been significant attention to the application of fuel cells for mobile and stationary settings. After the discovery of a fuel cell principle by Sir William Grove in 1839, it took almost 80 years to develop a practical fuel cell. The fuel cell running on hydrogen has been identified as an attractive long term option for both trucks and passenger cars because it is efficient, quiet, clean and long-lasting. While it can be used as an auxiliary power unit in trucks, it is envisioned to be used as a replacement of internal combustion engine in case of passenger cars. The concept can reduce emission of pollutants in tank-to-wheel path besides utilizing the fuel efficiently.

Fuel cells are clean energy conversion devices that use a fuel and an oxidant to generate electricity. In general, all the fuel cells operate without combusting fuel and with few moving parts. It is for this reason that they became attractive from both energy and environmental standpoints. Based on reports from US Department of Energy, fuel cells have emerged over the last decade as one of the most promising new technologies for meeting the US energy needs for power generation and transportation well into the 21st century.^{1,2,3} The desirable characteristics of a fuel cell include: (1) high overall efficiency; (2) low pollution; (3) silent operation; (4) effective reduction of greenhouse gas formation at the source and (5) process simplicity for conversion of chemical energy to electrical energy.⁴ A fuel cell can be two to three times more efficient than an internal combustion (IC) engine in converting fuel to electricity.⁵ While an IC engine operates at less than 20% efficiency, the efficiency of a fuel cell based propulsion system can be much higher. This is partly because it is not limited by any thermodynamic cycle unlike internal combustion engine. The challenges facing the use of hydrogen in passenger cars include its storage, transport and distribution. The well-to-wheel efficiency for fuel cell vehicle, because of all these challenges generally drops down to 30%. Use of fuel cell as auxiliary power unit in heavy duty trucks is very promising from economics point of view. When idling, an internal combustion engine operates at very low efficiency, typically less than 5%. Use of fuel cell APUs could be a promising in that it can reduce fuel consumption and cause less pollution. It is estimated that approximately 700 million gallons of diesel can be saved annually through the use of fuel cell APUs in the trucking industry, resulting in a reduction of 8.9 million metric tons of CO₂ per year.

1.1. Types of Fuel Cells

Fuel cells generate electricity from a simple electrochemical reaction in which oxygen and hydrogen combine to form water.

The most important features in a fuel cell are:

- Electrolyte which usually defines of the type of the fuel cell
- Fuel, the most common being hydrogen
- The anode catalyst, which breaks down the fuel into electrons and ions. The anode catalyst is usually made up of noble metals, like platinum.
- The cathode catalyst, which turns the ions into water. The cathode catalyst is often made up of nickel.

There are several different types of fuel cell but they are all based around a central design which consists of two electrodes, a negative anode and a positive cathode. These are separated by a solid or liquid electrolyte that carries electrically charged particles between the two electrodes. A catalyst, such as platinum, is often used to speed up the reactions at the electrodes. At the anode a catalyst oxidizes the fuel, usually hydrogen, turning the fuel into a positively charged ion and a negatively charged electron. The electrolyte is a substance specifically designed so ions can pass through it, but the electrons cannot. The freed electrons travel through an external circuit creating current. The ions travel through the electrolyte to the cathode. Once reaching the cathode, the ions are reunited with the electrons and the two react with a third chemical, usually oxygen, to

create water. This process occurs in all fuel cells except for molten carbonate fuel cells. The molten carbonate cell transfers the carbonate ions formed by the reaction of oxygen and carbon monoxide in the presence of electrons from the cathode side to the anode side to react with hydrogen and form water and two electrons for current.

Fuel cells are usually classified based on the type of electrolyte employed. However, Direct Methanol Fuel Cell (DMFC) is an exception to this classification (in which methanol is the fuel, directly oxidized in the fuel cell without undergoing reforming). They are also classified based on the operating temperatures, thus there are low temperature and high temperature fuel cells. Alkaline Fuel Cell (AFC), Proton Exchange Membrane Fuel Cell (PEMFC), DMFC and Phosphoric Acid Fuel Cell (PAFC) are low temperature fuel cells while Molten Carbonate Fuel Cell (MCFC) and Solid Oxide Fuel Cell (SOFC) are high temperature fuel cells. The high temperature fuel cells operate between 500 °C-1000 °C depending on their detailed configuration. The low temperature fuel cells operate below 200 °C.

1.1.1. Alkaline Fuel Cells (AFC)

AFCs use an aqueous solution of KOH retained in a porous stabilized matrix. KOH concentration can be varied depending upon the operating temperatures in the range 50-225°C. They also use a variety of non-precious metal catalysts which makes them relatively cheaper. AFCs are known to offer very high chemical reaction rate in addition to giving very high electrical efficiencies, high power densities and high currents.⁶ One of the limitations is the poisoning of AFCs with small quantities of carbon dioxide. Carbon dioxide reacts with the electrolyte and severely degrades the performance of the

fuel cell. They are therefore used in controlled aerospace and underwater applications. Because of their fast-starting nature and early development, these fuel cells have been used by NASA to produce power and drinking water for astronauts since the 1960s.

1.1.2. Proton Exchange Membrane Fuel Cells (PEMFC)

Proton exchange membrane fuel cells are said to be the best type of fuel cells to replace the internal combustion engine, both as use in an auxiliary power unit and for propulsion. PEMFCs use a solid polymer membrane as an electrolyte. Platinum is employed as the catalyst on the electrode. Hydrogen fuel is supplied as hydrogen gas or is reformed from methanol, ethanol, natural gas or liquefied petroleum gas and then fed into the fuel cell. They usually operate at low temperatures (60-100°C), primarily due to the restrictions on the temperature of the membranes. A major breakthrough in the use of PEMFCs came with the discovery of Nafion membranes (DuPont). These membranes were more stable than the earlier polystyrene sulfonate membranes. In 1987, Ballard started using Dow membrane and achieved four times increase in current densities at the same voltage with Nafion membranes. **Error! Bookmark not defined.** Moreover, recent investigations have led to the development of high temperature membranes (stable up to 200°C) but not yet commercialized. Among all the fuel cell types, PEMFCs have the highest power generating capacity per unit volume or weight of the fuel cell. **Error! Bookmark not defined.** Moreover, the low operating temperature allows for rapid start-up and shut down. These advantages make PEMFCs preferred for use in automotive applications. Quick-starting PEMFCs can also provide back-up power to telecommunications and other sites requiring uninterrupted power supplies.

There are, however, many challenges which make them economically challenging. Platinum catalysts are expensive and also subject to CO poisoning which is why catalyst improvements, non-precious metal catalysts and other alternatives are under investigation.

1.1.3. Direct Methanol Fuel Cells (DMFC)

The main advantage of DMFCs lies around the fact that it uses unreformed methanol rather than pure hydrogen as the fuel. This eliminates one of the important and costly steps of fuel processing for hydrogen production. They operate at about the same temperatures as PEMFCs (50-120°C). Efficiencies are around 40%. These fuel cells are rightly targeted at small mobile power applications such as laptops and cell phones, using replaceable methanol cartridges at power ranges of 1-50 W. Many of the major electronics companies are demonstrating miniature DMFCs powering their equipment and smaller fuel cell companies are partnering with military and communications contractors.

1.1.4. Phosphoric Acid Fuel Cell (PAFC)

PAFCs were the first commercial fuel cells. These fuel cells use phosphoric acid at concentration up to 100% as the electrolyte medium. PACFs suffer from poor start-up problems, primarily due to the fact that electrolyte solidifies at a temperature of 40°C, making them inappropriate for continuous operation. Moreover, because of lower power density, large and heavy units are used; making PAFC's suitable only for stationary applications. Since the ionic conductivity in phosphoric acid is low at low temperatures, these fuel cells are generally operated at slightly high temperatures (150-220°C). This

also makes them more tolerant to impurities in the fuel. Simple construction, low electrolyte volatility and long-term stability are additional advantages. The power range of existing PAFCs is 25-250 kW. However, if several units are linked, PAFCs can achieve a combined power output greater than 1 MW.

1.1.5. Molten Carbonate Fuel Cell (MCFC)

MCFCs are the high temperature fuel cells operating at around 600-750°C and use a molten alkali carbonate mixture for an electrolyte. They typically range between 75-250 kW, but when using combined units, have been used for as much as 5 MW. They have been operated on a variety of fuels including hydrogen, carbon monoxide, natural gas, propane, landfill gas, marine diesel, and simulated coal gasification products.

The challenges to both SOFC (described below) and MCFC development include slow start up, strong thermal shielding requirements, and difficulty in developing durable materials for the high temperature operating environment. Research is being done on reduction of size and cost, as well as possible integration with gas turbines to increase performance.

1.1.6. Solid oxide Fuel Cell (SOFC)

SOFCs are one of the high temperature fuel cells, with operating temperatures around 700-1000°C. The electrolyte used is dense yttria (Y_2O_3)-stabilized zirconia (ZrO_2), which is an excellent conductor of negatively charged oxygen (oxide) ions at high temperatures. The anode of SOFC is generally a porous nickel–zirconia ($Ni-ZrO_2$) or cobalt–zirconia ($Co-ZrO_2$) cermet, while the cathode is magnesium (Mg)-doped lanthanum manganate or

strontium (Sr)-doped lanthanum manganate LaMnO_3 .⁷ Due to operation at high temperature, low cost non-precious metals can replace precious metals. Waste heat is used for internal steam reforming of hydrocarbon fuels. One of the main advantages of SOFCs is that it is tolerant to CO poisoning. These fuel cells are known to produce a power output of 2-100 kW and can attain 220 kW-300 kW when used in a SOFC/gas turbine hybrid system. SOFCs are well-suited for medium-to-large scale, on-site power generation and are also being used recently for telecommunications back up and as auxiliary power units (APUs) for military vehicle on-board equipment. Bloom Energy Server, manufactured by Bloom Energy, is a reliable and affordable SOFC based distributed power generator and offers high fuel flexibility.

1.2. Fuel Options

While polymer electrolyte membrane fuel cell is widely accepted as the fuel cell of choice for automotive applications, much less can be said of the source of hydrogen to be used. Although hydrogen is the best fuel for a fuel cell, other fuels such as natural gas and methanol can be used without processing them for hydrogen or syngas. This is the reason why numerous research groups in the world are actively involved in fuel processing for synthesis gas and hydrogen for fuel cells. Brown, in his study, compared seven fuels for their utility as hydrogen sources for fuel cells in automotive applications.⁸ The paper also discusses various processes to convert these fuels into hydrogen.

1.2.1. Hydrogen

Keeping other things same, a fuel cell is most efficient using hydrogen as the fuel. Moreover, it eliminates a bulky on-board reformer which may be necessary to generate

hydrogen from on-board fuel. Momirlan and Veziroglu in a paper discussing the transition from the present fossil fuel era to hydrogen economy, present an indicative graph showing 200 EJ hydrogen production in 2030 (about 23% of total primary energy) and 750 EJ in 2050 (75% of total energy).⁹ For immediate use, hydrogen can be supplied via steam reforming of natural gas which is technologically matured. Over a medium-to-long timescale, it is conceived to produce hydrogen with emphasis on sustainability, mainly via biomass. However, the storage of hydrogen on board a vehicle creates a serious challenge due to its low density. Some of the storage technologies include using liquid hydrogen, compressed hydrogen, or hydrides. These technologies are not economically viable.

1.2.2. Natural gas

One of the possibilities is to use the natural gas as it is instead of processing it for hydrogen production. In addition, natural gas is particularly suitable for distributed power system due to the existing transportation infrastructure throughout the world. The storage options are similar to those for hydrogen, but not as technically demanding. On-board reforming of natural gas can be used to drive a fuel cell on hydrogen. One of the problems with this system is that an additional gas clean-up system also needs to be installed to remove CO and other impurities (except in case of SOFCs).

1.2.3. Methanol

Third fuel that has been investigated and is known to be a promising choice is methanol. This alcohol offers some major advantages for a mobile application. Its reforming characteristics are favorable as compared to other fuels since it can be reformed at a

much lower temperature.¹⁰ It has a high energy density in range of other transportation fuels while its storage characteristics are similar. It is used as a chemical feedstock in large quantities today, produced mostly from natural gas. When produced from natural gas, its cost is comparable to that of other logistic fuels. However, there are a few serious disadvantages in using methanol, including its toxicity, hygroscopic nature and corrosiveness. Few technological breakthroughs can help to combat these problems.

1.2.4. Biomass

Bio-derived materials, including bio-ethanol, bio-diesel and other high molecular weight bio-based compounds are considered promising raw materials for hydrogen generation. One of the biggest advantages is their carbon cycling neutrality. Generally, hydrogen/syngas is produced via gasification/pyrolysis followed by an additional catalytic reforming unit. However, due to the difficulty in volatilizing these biomass products that have high boiling points, technologies like aqueous phase reforming and supercritical water oxidation are being researched as an alternative to the conventional solid catalyzed gas-phase reforming process.^{11,12} One of the disadvantages in these processes is the formation of methane and other lower alkanes. These lower alkanes can be further reformed to hydrogen but disturbs the economics of the process to a negative side. Efforts are ongoing to study the elementary reactions (C-H and C-C bond cleavage) and achieve higher yields with minimal methane formation.

1.2.5. Logistic fuels

All of the above mentioned fuels (hydrogen, natural gas, methanol and biofuels) suffer from the absence of a dense network of fueling stations. This forms a serious obstacle in

introducing these fuels to drive the fuel cell technology. Therefore, fuels with good network for transportation are becoming potential candidates for use in the fuel cells. Gasoline, diesel and jet fuels have existing infrastructure for manufacture and distribution, for hydrogen production for fuel cell applications either for stationary or mobile devices. **Error! Bookmark not defined.** This may not be sustainable or desirable in the long term, owing to the relatively high carbon content and relatively low hydrogen content of these fuels. It would, however, provide an entry for a hydrogen economy in the short to medium time scale. Moreover, given the advantages inherent in fossil fuels - such as their availability, relatively low cost, and existing infrastructure for delivery and transportation - they are likely to play a major role in hydrogen production in the near future. Generally, hydrogen can be produced from transportation fuels via steam reforming, partial oxidation and auto-thermal reforming. However, one of the major challenges in reforming these fuels is the deactivation of the catalyst used in reforming. Catalyst deactivation is pronounced due the presence of sulfur even in ppm levels. Although desulfurization of these fuels is done to remove sulfur, it is still present in few ppm levels. For example, ultra low sulfur diesel has 15 ppm sulfur.

1.3. Fuel Processing – Stationary or On-board

1.3.1. Reforming in a stationary plant

Steam reforming of natural gas is the method of choice for bulk production as it results in a hydrogen rich gas. Gas clean-up is done by means of pressure swing adsorption (PSA) which produces hydrogen with a purity of 99.99%. The CO content of the hydrogen is in the range 10 ppm and thus poses no serious threat to the new breed of fuel cells.

However, the biggest disadvantage to reforming in a large plant is the transportation and storage of hydrogen, for which there is no adequate infrastructure at present. Research activities in the field of hydrogen storage include metal hydrides, carbon nanotubes and metal organic frameworks.

1.3.2. Reforming on-board

To overcome the problem of infrastructure for the storage of hydrogen on the vehicle, it is conceived to produce hydrogen through on-board reforming. One of the critical issues on board a vehicle is the removal of CO. Apart from CO poisoning, another important disadvantage of an on-board reformer is the start-up time. In a conventional fuel processing system for hydrogen production for PEMFCs, the fuel stream is first pre-heated or evaporated to a certain temperature, then mixed with water, followed by conversion to hydrogen-rich reformat at temperatures ranging from 400–850°C (depending on the type of fuel). Subsequent to fuel conversion to hydrogen-rich reformat, gas clean-up is done via water gas shift and preferential oxidation. In a combined reformer–fuel cell system, the off-gas from the anode of the PEMFC can be combusted to preheat the reactant or provide heat for reactions together with the heat recovered from other parts of the system. Simultaneously, water condensed from both the anode and the cathode sides of the PEMFCs can be recycled as a feed to the whole system. In practice, a variety of configurations can be adopted with different integration schemes, each having different degrees of efficiency and compactness. It can be understood that the main limitation comes from integrating a reformer into the existing vehicle model. Lindermeir *et al* presents a possible on-board diesel fuel processing configuration for SOFC-APU for passenger cars and trucks.¹³

1.3.3. General Fuel Processing Scheme for a Fuel Cell

The schematic diagram of a generalized conventional reforming process is shown in Fig. 1.¹⁴ Qi *et al* presents the key technological progress made over the last two decades in the integrated fuel processor designs.

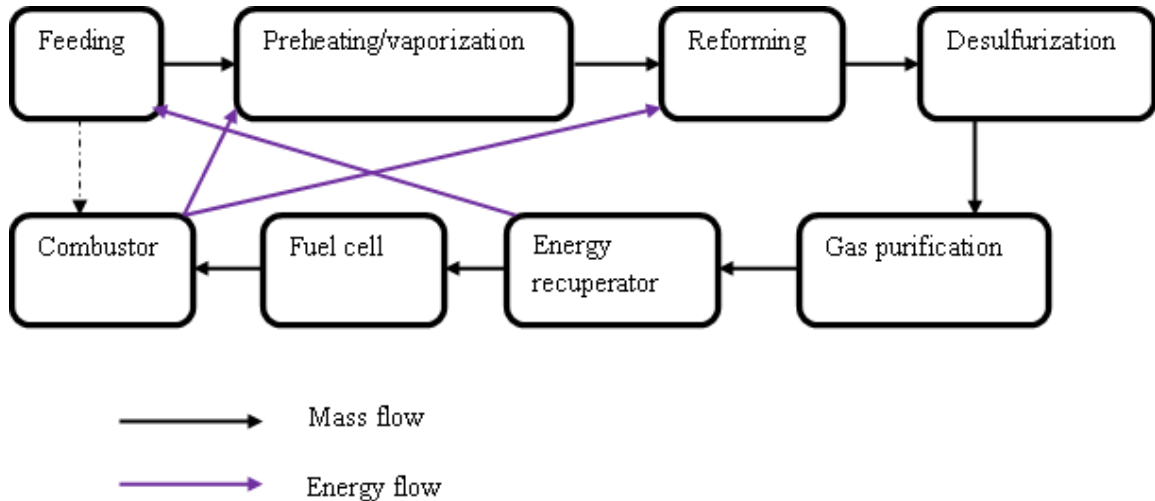


Figure 1-1. Generalized flow diagram for a fuel processor-fuel cell system

Moreover, it should be noted that the fuel processing system could be a stand-alone system. CO clean up unit is not necessary for high-temperature fuel cells (SOFCs) as they are fairly resistant to small amounts of CO. In some cases, hydrogen purification system may remove CO thereby eliminating the need for separate CO clean up system. Desulfurization may be carried out either downstream or upstream of reforming step. A cracking/pre-reforming unit may be included prior to the main reforming unit to avoid catalyst deactivation due to carbon deposition on the catalyst.

1.4. Desulfurization technologies

Fuel cells are known to get poisoned by small amounts (ppm level) of sulfur compounds. It is therefore necessary to look at the desulfurization technologies and their relevance to the fuel cell industry.

Most of the desulfurization technologies deal with gasoline, diesel and non-transportation fuels as they constitute around 70-75% of the refinery units. New sulfur limits of 10-15 ppm sulfur are already in practice in European and USA markets. In fact, zero-emission and, as a consequence, zero levels of sulfur are anticipated worldwide in the coming 5–10 years.

The desulfurization processes can be divided into three groups depending on whether the sulfur compounds are separated from refinery stream without decomposition, or decompose on separation. Conventional desulfurization is achieved via hydrodesulfurization (HDS) which includes adding hydrogen to remove sulfur. All the desulfurization processes can be broadly classified into two groups, ‘HDS based’ and ‘non-HDS based’. In HDS based processes, hydrogen is used to decompose organosulfur compounds and eliminate sulfur from refinery streams while non-HDS based processes do not require hydrogen. Babich and Moulijn have reviewed the applicability and perspectives of various desulfurization technologies taking into account the requirements of the produced fuels.¹⁵

1.4.1. Conventional HDS technologies

1.4.1.1. Catalysis based HDS technologies

Catalytic HDS involves reacting crude oil/refinery stream with hydrogen at high temperature to yield hydrogen sulfide and hydrocarbon. Generally, CoMo/Al₂O₃ and NiMo/Al₂O₃ catalysts are used for conventional HDS.¹⁶ The performance of a catalyst depends of a number of factors, some of which are catalyst active species concentration, support properties, synthesis route, the reaction conditions (sulfiding protocol, temperature, partial pressure of hydrogen and hydrogen sulfide), nature and concentration of the sulfur compounds present in the feed stream, and reactor configuration. Generally, conventional HDS of thiophenic compounds proceeds via two reaction pathways. Via the first pathway the sulfur atom is directly removed from the molecule (hydrogenolysis pathway). In the second pathway the aromatic ring is hydrogenated and sulfur is subsequently removed (hydrogenation pathway). Both pathways occur in parallel employing different active sites of the catalyst surface.

1.4.1.2. Advanced HDS

Advanced HDS is required when deep desulfurization is desired. Deep desulfurization of refinery streams becomes possible when the severity of the HDS process conditions is increased. Unfortunately, more severe conditions may also result in undesired side reactions. Instead of applying more severe conditions, HDS catalysts with improved activity and selectivity are being developed. One of the approaches is to employ advanced reactor designs and new types of catalysts and catalyst support. The best results

are usually achieved by a combination of the latter two approaches, namely, using an appropriate catalyst with improved activity in a reactor of advanced design.¹⁵

In 1998, Akzo Nobel introduced highly active CoMo and NiMo catalysts referred to as STARS (Super Type II Active Reaction Sites).^{17,18} These catalysts were shown to result in streams with less than 5 ppm of sulfur and significantly reduce polyaromatic content. Another Akzo Nobel catalyst preparation technology has been claimed to result in extremely active hydrotreating catalysts (NEBULA).¹⁹ In these catalysts, the active phase and the carrier are different in nature from conventional HDS catalysts while they are active even in the sulfided form.

1.4.2. 'Non-HDS' based desulfurization technologies

Technologies that do not use hydrogen for catalytic decomposition of organosulfur compounds are designated as non-HDS based desulfurization technologies.

1.4.2.1. Shifting the boiling point by alkylation

This is based on the fact that shifting the boiling temperature of organosulfur compounds, they can be removed easily from light fractions via distillation.

1.4.2.2. Desulfurization via extraction

Some organosulfur compounds are more soluble than most hydrocarbons in an appropriate solvent. The sulfur compounds are transferred from the refinery stream into the solvent due to their higher solubility in the solvent. The organosulfur compounds are separated by distillation and the solvent is recycled.

1.4.2.3. Selective oxidative desulfurization

Generally, desulfurization by selective oxidation consists of two main steps: oxidation of sulfur compounds and subsequent purification.²⁰

1.4.2.4. Desulfurization by adsorption on a solid sorbent

The ability of a solid sorbent to selectively adsorb organosulfur compounds from refinery streams is used to desulfurize refinery streams. This can be further divided into 'adsorptive desulfurization' and 'reactive adsorption desulfurization' based on the type of interaction between the organosulfur compound and the adsorbent.¹⁵

1.4.2.5. Desulfurization by membrane pervaporation

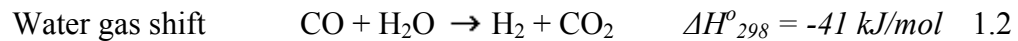
Patented and commercialized by Grace, these membranes use a pervaporation technology to cost effectively meet the new, tougher worldwide specifications for petrochemicals desulfurization.

1.5. Fuel Processing Technologies

One possible method to produce hydrogen for use in an automotive fuel cell is to convert a liquid fuel to hydrogen through thermochemical methods achieved onboard the vehicle. Some of the important technologies include steam reforming, partial oxidation and autothermal reforming. Steam reforming has the advantage of high hydrogen concentration in the effluent. Nickel based catalysts supported on alumina are widely used in steam reforming of natural gas.

1.5.1. Steam Reforming (SR)

On large scale level, hydrogen is generally produced via catalytic steam reforming of natural gas. This reaction is operated at temperatures above 800°C at around 20 atm to optimize the economics. The steam reforming of methane can be represented as:

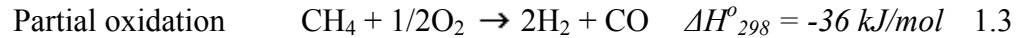


The reforming reaction is endothermic and external heat is required to drive the reaction forward. The effluent coming out of the reformer consists of hydrogen, carbon monoxide, carbon dioxide and water. This effluent is sent to the water gas shift (WGS) reactors to convert CO to CO₂. Since WGS is equilibrium controlled, it is generally done in two steps, high temperature shift and low temperature shift. CO levels can be reduced below 1%. Further purification of hydrogen is typically done using pressure swing adsorption (PSA).

Of the presently available commercial technologies to produce hydrogen, steam reforming remains one of the most economical alternatives because of the relatively high yield and concentration of hydrogen in the effluent gas.²² It has been proposed that proper heat integration makes this process more suitable for small scale reformer and fuel cells. Although steam reforming is an attractive technology for hydrogen production, catalyst deactivation due to coke formation and sulfur poisoning during reforming of logistic fuel remain the main challenges.^{23,24}

1.5.2. Partial Oxidation (POX)

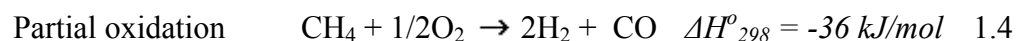
In partial oxidation, the fuel is converted to hydrogen and carbon monoxide through selective oxidation in stoichiometrically oxygen deficient environment. Partial oxidation of methane can be represented as:



The reaction is fairly exothermic in nature and hence has the advantage that heat integration allows heat recovery from the system. One of the disadvantages is relatively low hydrogen yields and low concentration of hydrogen in the effluent gas as compared to steam reforming. Hydrogen is further diluted due to the presence of high concentration of nitrogen present in air used for oxidation. CO can be cleaned up using WGS reactors which also serves to increase the hydrogen concentration in the effluent. Since steam is not used as a reactant, lot of coke is formed during the reforming of higher hydrocarbons leading to deactivation of the catalyst. Oxygen is derived from air, hence the reactor size must be large making them unsuitable for compact design. One of the ways to reduce the reactor size is to use pure oxygen in place of air, although it works against the economics of the plant.

1.5.3. Auto thermal reforming (ATR)

The auto-thermal reforming process combines the advantages of steam reforming and partial oxidation in a single process. In this process the hydrocarbon feed is reacted with a proper mixture of steam and air. ATR of methane can be represented as:





Since the heat required for the steam reforming reaction is derived via the partial oxidation reaction, no external addition of heat is required and the process is thermally neutral if operated at appropriate conditions. Since heat integration is not required in this process, ATR reactors can be made compact and suitable for small scale applications. The amount of hydrogen obtained through this process is lower than that obtained via steam reforming but this process has a higher overall efficiency than a POX system. The main challenge with this system is to obtain the proper mixture of fuel, water, and air.

1.6. Motivation and Objective

A large proportion of trucks spend considerable amount of time idling. When idling, engines operate at low levels of efficiencies, experience high wear conditions, and emit high levels of NO_x, particulate matter, and carbon oxides. The US Department of Energy estimates that annually \$ 1 billion worth of diesel is consumed during idling with additional \$ 1 billion spent on increased engine maintenance costs. The desire to increase fuel economy and decrease greenhouse gas emissions has led researchers to look for alternatives. One of the options being suggested is a hybrid system consisting of a conventional internal combustion engine (ICE) for propulsion and a fuel cell powered auxiliary power unit (APU). This could potentially reduce greenhouse gas emissions and also provide increased fuel efficiencies.

PEMFC and SOFC are the most suitable fuel cells for integration with transportation applications. PEMFC operates at a relatively low temperature of about 100-120°C and thus requires very little time to start up, while on the other hand, SOFC operates at a

much higher temperature of about 800-1000°C, requiring significant time to warm up. The main disadvantage of PEMFC is that it is intolerant to CO and requires secondary reactors for CO clean-up. In the case of SOFC, CO acts as fuel and is converted to CO₂ providing additional energy. Due to the high operating temperature of SOFC, water produced during the process is available as high temperature steam to be used in the reformer for hydrogen production. Thus, using a SOFC will not require additional components such as CO oxidation unit, steam generation unit, and as a result will reduce the system requirements from the reformer, making it a favored option for generation of electricity on-board a vehicle.

General approaches to convert fuel to hydrogen and carbon oxides are steam reforming (SR), partial oxidation (POX) and autothermal reforming (ATR). ATR has many disadvantages in case of liquid hydrocarbons; most notably the formation of hot spots and thermal cracking of the reactants. The yields of hydrogen in POX are relatively low and because it is highly exothermic, it generates hot spots. Steam reforming yields high hydrogen concentration in the effluent. It was therefore intended to use steam reforming as the process to convert fuel into hydrogen and carbon oxides.

Conventional nickel based catalysts are neither adequately active nor very stable for steam reforming if used for high molecular weight fuels including logistic fuels. Presence of high molecular weight components along with sulfur leads to severe coking of the catalyst. Due to high average molecular weight, these hydrocarbons need to be reformed at high temperatures. The high temperature associated with reforming to produce hydrogen also favors the formation of coke. It is well established that heavy hydrocarbons undergo steam assisted cracking before being reformed on the catalyst

surface. Cracked products consist of olefins apart from several other lower hydrocarbons. Olefins and aromatics are known to have high coking ability. Apart from hydrocarbons, it is well known that sulfur forms strong bond with metals and thereby inhibit reforming to a large extent. The regeneration of sulfur poisoned catalyst is particularly very difficult.

There is extensive literature on understanding deactivation due to coking in case of methane steam reforming but there is not enough effort in case of heavier fuel reforming. Simultaneous deactivation due to both coking and sulfur further complicates the problem. Although there is ample work accomplished in developing improved catalysts to process logistic fuels, there have been no systematic studies that look at catalyst development from the deactivation point of view. Semi-empirical and random experiments have resulted in sufficiently stable and active catalysts but their further improvement certainly requires in-depth understanding of deactivation phenomenon. A systematic study of deactivation due to coking and sulfur will certainly lead us to resolve issues involved in designing better catalysts. It is therefore undertaken to study deactivation due to sulfur and coking systematically in case of logistic fuels.

With the discussion above, we know that two of the primary hurdles in developing a better catalyst for logistic fuels are the presence of high molecular weight hydrocarbons and also its high sulfur content. To study sulfur poisoning and carbon formation is not only important from mechanistic understanding point of view, but also in developing a stable and active catalyst.

A stable and active catalyst was previously developed in our laboratory for steam reforming of diesel. It was basically a bimetallic catalyst (NM4) and consisted of 10%Ni

promoted by 0.5%Rh supported on γ -alumina. The catalyst was prepared by wet-impregnation with co-impregnation of both active metals. Catalyst preparation method is detailed in the experimental section of this thesis. More details can be found in Goud's work.²⁵

N-hexadecane was used as the surrogate to represent aliphatic hydrocarbon part of diesel while thiophene was used to mimic sulfur present. Aromatic compounds present in the logistics fuel were represented by toluene while 1-methylnaphthalene was used to mimic naphthenes.

The first part was concentrated on studying deactivation on the catalyst NM4 in steam reforming of diesel represented by n-hexadecane and thiophene. NM4 was a bimetallic catalyst consisting of 0.5%Rh and 10%Ni supported on γ -alumina. Understanding deactivation in a catalyst containing two active metals was difficult. For this reason, two monometallic catalysts, one containing 2.5%Rh and other 10%Ni, were prepared separately to understand the performance of NM4. The percentage of rhodium in the monometallic catalyst was higher than that present in the bimetallic catalyst. This was done as 0.5%Rh was too low for analysis in various analytical techniques. There was also a bimetallic catalyst containing 2.5%Rh and 10%Ni supported on γ -alumina, which was prepared with a similar intention. Steam reforming reactions were run at 800°C at 1 atm pressure at a steam to carbon (S/C) ratio of 3. Reactions were run for 10 hr time on stream on each of the catalysts while NM4 catalyst was run for different time on stream ranging from 15 min to 10 hr. Post reaction catalysts were then analyzed using different analytical techniques to study deactivation. Techniques used included temperature programmed oxidation, reduction and desorption (TPO, TPR and TPD), X-ray

photoelectron spectroscopy (XPS), scanning electron microscopy (SEM), high resolution transmission electron spectroscopy (HRTEM), scanning tunneling electron microscopy (STEM), electron energy loss spectroscopy (EELS) and energy dispersive spectroscopy (EDS).

In the second part of the study, an improved multi-component catalyst 3J1 was studied for deactivation. It contained 10%Ni, 1.55%Pd and 1%Rh supported on γ -alumina. The catalyst was prepared by a modified method of metal impregnation. For details, refer to the work of Kataria.²⁶ For comparison purposes, steam reforming reactions were run at 800°C at 1 atm pressure at a steam to carbon (S/C) ratio of 3. Reactions were run for different times on stream ranging from 1 h to 45 h while only catalysts recovered after 10 h were extensively characterized for understanding deactivation. Post reaction catalysts were analyzed using different analytical techniques mentioned above.

The following section outlines the objectives set to understand the deactivation mechanism during steam reforming of sulfur-containing liquid fuels on multi-component sulfur-tolerant catalysts:

1. Determine catalyst activity in terms of hydrogen yield and deactivation during steam reforming of sulfur-containing liquid fuels (diesel surrogate and jet fuel) on NM4 and 3J1 series catalysts, both in the absence and presence of sulfur. Also, correlate sulfur yield with deactivation over time.
2. Characterize fresh catalysts to understand its microscopic structure and composition, primarily using XRD, XPS, STEM and temperature programmed oxidation and reduction studies.

3. Characterize used catalysts NM4 and 3J1 to understand deactivation mechanism due to sulfur poisoning and carbon deposition during steam reforming of sulfur-containing liquid fuels.
4. Propose a universal deactivation mechanism on a multi-component sulfur-tolerant steam reforming catalyst.

The aim of this study was to understand the mechanisms of deactivation on a multi-component sulfur-tolerant reforming catalyst. The name ‘sulfur-tolerant’ catalysts refers to a catalyst synthesized previously in our laboratory and has shown to be promising towards reforming sulfur-containing liquid fuels. However, the catalyst deactivates at longer time on stream. Although this was not the scope of the present study to design a better catalyst, the knowledge of deactivation mechanisms can help immensely in designing a better catalyst for heavy fuel reforming applications.

Chapter 2

Experimental and Analytical

2.1. Experimental Set-up for Steam Reforming

2.1.1. Summary of experimental and analytical section

A schematic of the experimental set-up used to conduct steam reforming of the fuel is shown in figure 2.1. The reactor tubing was made of quartz to minimize coke formation. Experiments confirmed that coking on the inner walls of the quartz tube was negligible.²⁷ Quartz wool was used to support the catalyst on either side. The temperature of the preheater and the reactor were maintained using single-zone tube furnaces controlled by temperature controllers. A K-type thermocouple was placed at the center of the catalyst bed to record and control its temperature. The line carrying the effluent stream was insulated to avoid condensation. The products from the reactor were sent to a glass condenser to separate condensable components such as water and other organic species formed or unconverted. The gaseous products were then withdrawn by an online gas chromatograph equipped with a pulsed discharge ionization detector (PDID) and a flame photometric detector (FPD). A known volumetric flow of argon was also simultaneously fed into the reactor using a mass flow controller to enable quantitative analysis of the

reaction products. Molar fractions of H_2 , Ar, CO, CO_2 , CH_4 and other light hydrocarbons were obtained using PDID while FPD was used to obtain composition of sulfur products.

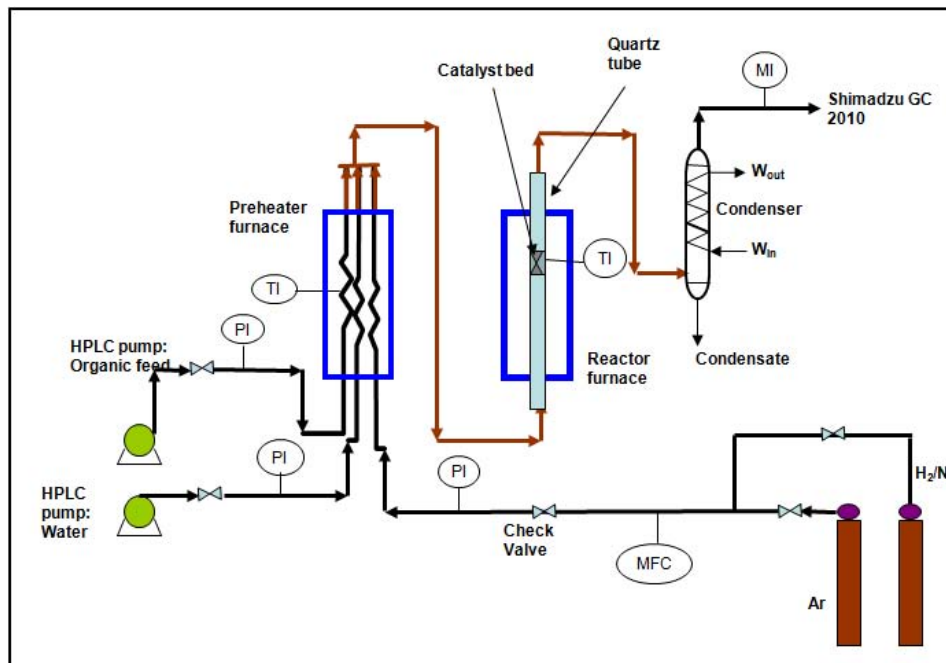


Figure 2-1. Schematic of the experimental set-up used for steam reforming

2.1.2. Details of experimental and analytical section

2.1.2.1. Feeding system

The liquid feeds were pumped using two HPLC pumps (Series II Isocratic HPLC Digital, Lab Alliance) while the flow of the gases was controlled using mass flow controllers (MC-500SCCM-D, Alicat Scientific). The HPLC pump for organic feed (diesel, jet fuel and hydrocarbon mixture) had a flow rate range of 0-10 ml/min with 0.01 ml/min increments and the pump for water had a 0-40 ml/min range with 0.1 ml/min increments. The outlets of these pumps was connected to microbore tubing in order to create a sufficient pressure drop so that these pumps would inject a set amount of liquid flow. The

flow of the inert gas (Ar, Airgas) and reduction gas (5% H_2/N_2 , Airgas) was controlled using mass flow controllers via a PID control configuration. The parameters required for PID configuration were automatically adjusted by the controller. The inert gas served both as the internal standard for the gas chromatograph and as a carrier gas through the reactor system. The fuel, water and inert lines separately entered the evaporator section through 0.32 cm stainless steel tubes (SS-T2-S-028-20, Swagelok), each fitted with non-return valves (SS-2C-1/3, Swagelok) to avoid any back flow due to pressure build up in the system. Pressure gauges (PGI-40M-PG100-LANX, Swagelok) were installed on each line to monitor the pressure. The inert gas feed line had a filter (SS-2F-05, Swagelok) installed between the gas cylinder and the mass flow controller.

2.1.2.2. Feed vaporizer

Feed vaporization was accomplished using a single zone tubular furnace (Hoskins Mfg.), mounted vertically. The furnace had an internal bore diameter of 1 inch. Its rating was 110 V, 5 A. Temperature of the preheater furnace was controlled using a temperature controller (CNI1622-C24, Omega Engineering) with solid state relay (SSRDIN660DC25, Omega Engineering) and a K type thermocouple (KQSS-116G-12, Omega Engineering). The temperature controller for furnace was auto-tuned for reaction conditions before being put to actual use for reactions. Auto-tuning helped prevent temperature fluctuations, thereby assisting in repeatability of the data. Vaporization unit also consisted of three separate feed lines, for the flow of fuel, water and inert gas (or reduction gas) which are drawn from their respective pumps and mass flow controller. The feed lines were approximately 50 cm long and coiled separately to make a 10 cm long coiled section. This was done so that the liquid feeds remained in the preheater

furnace long enough for complete vaporization. Sufficient length was left on both sides of the tube for fitting arrangements. Figure 2.2 shows the stacked coil arrangement.



Figure 2-2. Stacked coil arrangement for feed vaporization

The aim of the vaporizing section was to completely vaporize all the liquid feeds without causing excessive cracking, as it may lead to clogging in the lines. The temperature of the furnace was maintained at 550°C, since greater temperatures resulted in excessive cracking of the hydrocarbon.²⁸ The vaporized feeds were then mixed together using a cross connection. The mixed feed then passed through the Swagelok SS tube heated with heating tapes. The heated feed at 550°C then entered at the bottom of the reactor.

2.1.2.3.Reactor

The reactor section is shown in figure 2.3. It consisted of a high temperature tubular reactor inside a furnace and a temperature controller to control the temperature of the

catalyst bed. The reactor consisted of quartz tubing (20x25 Fused Quartz tubing, Technical Glass Products), 50 cm in length with ID 2.5 cm and thickness 0.25 cm. The two ends of the reactor were fitted using 2.54 cm Swagelok fittings and graphite ferrules (14361, Grace Davison). The thermocouple was inserted into the catalyst bed through the top fitting using 0.32 cm bored-through fitting. The bored-through fitting allows for the insertion of the thermocouple, which otherwise is not possible through a normal fitting. The furnace used in the reactor set-up was a single zone split furnace (Series 3210, Applied Test Systems). The effluent coming from the top of the reactor was passed to the condenser section using a ¼ in OD SS316 line (SS-T4-S-035-20, Swagelok). The line carrying the effluent was heated using a heating tape (EW-36115-12, Cole-Parmer) to avoid any condensation before the glass condenser.

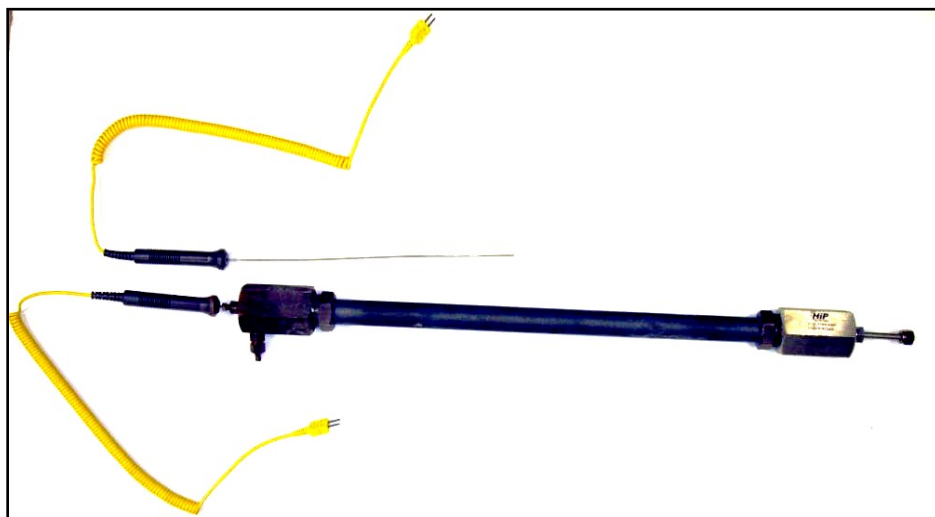


Figure 2-3. Reactor assembly

2.1.2.4. Condenser

The condenser was made of glass and was used to condense the liquid products and the unreacted water and organic fuel. The glass condenser had a shell and tube design for the effective cooling of the condensables. The condenser was operated with circulating cooling water using a peristaltic pump (Masterflex, Cole Parmer). Ice was added to the cooling water at regular intervals to maintain the temperature of the circulating water at around 10-15°C. The condenser, shown in Figure 2.4, was built in-house with the help of a glass blower. The liquid products were condensed in the conical separating flask, attached to the condenser at the bottom. The non-condensable gases were separated and passed over a cold trap (Z225789, Sigma Aldrich). Cold trap was used to remove any uncondensed liquid and thereby prevent them from going to the analytical system. The cold trap was maintained at -20°C using a mixture of dry ice and isopropyl alcohol.



Figure 2-4. Condenser section

2.1.2.5.Process Automation via LabVIEW

The main purpose of using LabVIEW (LabVIEW ver. 8.1, National Instruments) was reproducibility of reaction data. All the mass flow controllers and HPLC pumps were operated using the LabVIEW interface via RS232 serial cable connecting the device with the computer. A general reaction protocol was developed and was used for all the reactions. The software was programmed to control the flows to the system, so that irregularities arising out of manual operation could be avoided.

2.1.2.6.Analytical section

The main unit in the analytical system consisted of a gas chromatograph (GC-2010, Shimadzu). The dry effluent gas exiting the condenser units was sent to the GC. The

effluent gases coming out the reactor were mainly H₂, Ar, CO, CH₄, CO₂, C₂H₂, C₂H₄, C₂H₆ and trace amounts of C₃H₈, C₄H₁₀ and H₂S. In order to analyze all the gases, two suitable columns were used to separate the gases in the GC as shown in figure 2.5. The Shincarbon micro-packed column (ShinCarbon ST 100, Restek) was used to separate the gases (other than H₂S), and the pulsed discharge ionization detector was used to detect the gases. The second column (SPB-1, Restek) was used to separate sulfur compounds which were eventually sent to flame photometric detector for sulfur compounds analysis.

The GC was operated in the temperature programmed mode to separate gases in about 20.7 min. The oven temperature was maintained at 45°C for the first 5.2 min and then ramped to 280°C at 25°C/min and held at 280°C for 5.9 min. This gave a total run time of 20.7 min. In between the runs, the GC took about 8-9 min. to cool down while the equilibration time of 0.2 min was kept to initialize the next sample injection. So, each GC sample took about 30 min for analysis. This GC was used inline and operated in automatic acquisition mode. Helium was used as a carrier gas. Hydrogen and air were used to ignite the flame of the FPD detector. While hydrogen was supplied directly from the UHP H₂ cylinder (Airgas), zero air was obtained from zero air generator.

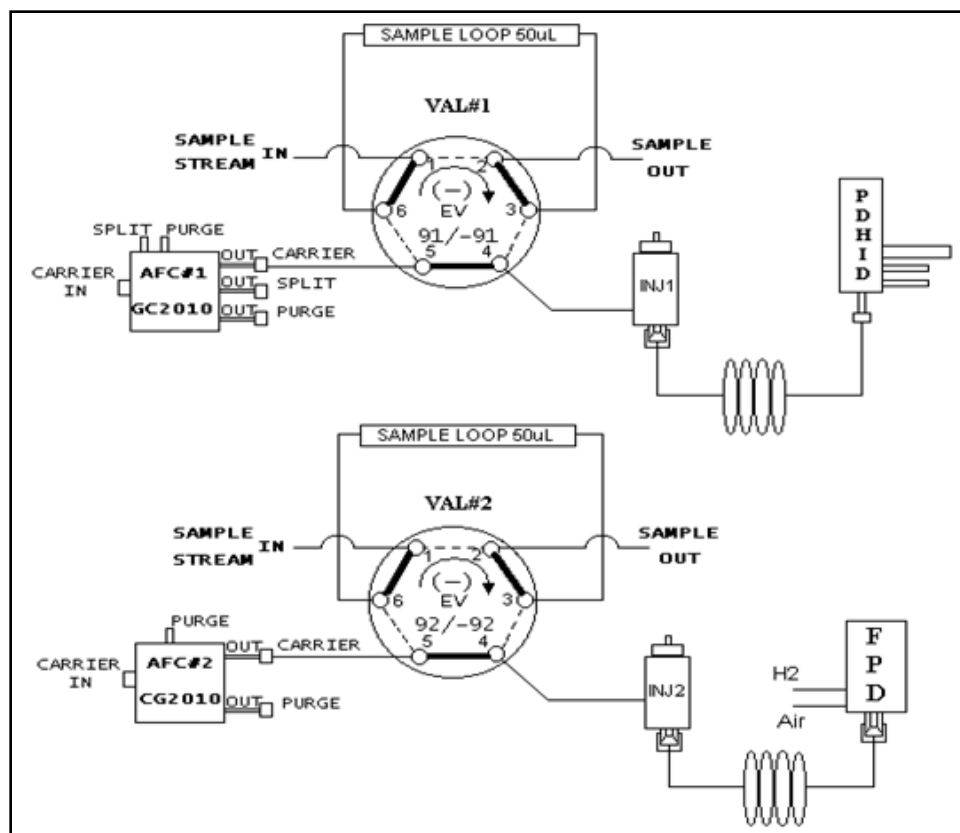


Figure 2-5. Automatic gas injection and separation using two 6-way valves

Gas samples were automatically injected simultaneously into both sampling lines of the GC using an auto-sampler system as shown in figure 2.5. A six-port valve was used to sample 50 µl of gas. When loading the sample loop, ports 1 and 6 as well as ports 2 and 3 are connected to flow the effluent gas through the loop. At the time of injection, the valve position switches to connect 5 and 6 as well as 3 and 4 to allow the flow of carrier gas through the sample loop driving the gas sample in the injector section. In order to avoid condensation of moisture, the sampling system is covered with a heated and insulated box to maintain a temperature of 120°C.

GC calibration was crucial to obtain reliable product gas concentration data. At least 4-5 concentration points were used for calibration of each of the gases. Gas mixtures with desired gas compositions were prepared in a lecture bottle in the laboratory using pure gases. A vacuum pump was used to empty the lecture bottle of any residual gas, following which its weight was recorded. The bottle was then filled with the pure gases and their weight was recorded. Using the weight difference, the amount of gas added in each step was calculated to identify the gas composition in the lecture bottle. This calibration gas was then introduced into the GC sample loops using a mass flow controller to ensure that the sample loops were loaded with gases at atmospheric pressure. Thus, by knowing the volume of sample loops and using the ideal gas equation, the number of moles of each gas injected into the GC was calculated. The area under the peaks for each gas was correlated with the moles of each gas injected. Moles of gas were used as the calibration basis to eliminate any error due to pressure fluctuations in the line carrying the gases to the GC. The percentage error was below 2%.

2.2. Catalyst preparation

Studies were focused on two catalysts, namely NM4 and 3J1. NM4 is a binary catalyst containing base metal Ni and a small amount of noble metal Rh. 3J1 is a ternary catalyst containing Ni, Rh and Pd. Both the catalysts were prepared via wet impregnation using a commercially available stabilized alumina support (MI386, Grace Davison). Details on the composition and preparation technique for catalysts are given below:

2.2.1. NM4

First part of the thesis was concentrated on understanding the deactivation mechanisms during steam reforming of model diesel compound on a previously developed catalyst NM4. Compositionally, it contains 10% by weight Ni and 0.5% by weight Rh supported on stabilized alumina. Stabilizers present in the commercial alumina which includes mainly lanthanum are not accounted for in compositions. Metal precursors used to prepare NM4 were nickel nitrate (10816, Alfa Aesar) and rhodium acetylacetonate (10561, Alfa Aesar) while the solvent used is tetrahydrofuran (THF) (44608, Alfa Aesar). The catalyst was prepared in batches of 10 g. In the first step, both the metal precursors were added into the solvent contained in a round bottom flask and stirred until they were completely dissolved. The amounts of salts were calculated to make the required metal concentration in the final catalyst. To this solution, 9.0 g of previously dried alumina support was added. The round bottom flask was then attached to the rotary evaporator and it was then rotated slowly at a speed of about 45 rpm for 18 hours, to ensure uniform contact between the metal and the support. This was a very crucial step and is assumed to result in proper metal binding with the support and a dispersion of each individual metal on the support. The solvent was then removed at a rate of 50 ml/min by applying vacuum and maintaining the round bottom flask temperature close to 30°C. When using THF as the solvent, the water bath temperature was increased to 50°C after removing the vacuum to ensure complete removal of THF. The obtained powder was then dried in an oven for 2 hours at 120°C to remove all the remaining moisture and solvent and then calcined at 800°C.

A set of catalysts were synthesized in order to study the effect of individual metals. The catalysts were prepared using similar single step impregnation technique. Two monometallic catalysts, one containing 10%Ni and the other containing 2.5%Rh, were prepared. A bimetallic catalyst containing 2.5%Rh and 10%Ni was also prepared to study the effect of Rh in the bimetallic catalyst. The sole purpose of testing this set of catalysts was to gain information about the deactivation mechanism on NM4 catalyst; it was not our intention in this work to formulate a more active or more stable catalyst.

Table 2-1. Composition of catalysts synthesized for part I – NM4

Catalyst name	Metals loading (%)	Impregnation sequence	Calcination temperature (°C)
Ni/a	Ni(10)	-	800
Rh/a	Rh(2.5)	-	800
(0.5RhNi)/a or NM4	Ni(10), Rh(0.5)	Co-impregnation	800
(2.5RhNi)/a	Ni(10), Rh(2.5)	Co-impregnation	800

Notice that the catalysts were designated by letter ‘a’ at the end of each formulation name. This was done to differentiate between these catalyst formulations from the set of catalysts prepared in the second part of the study. The catalysts in the second part, described below, were prepared by a different method and they are designated by letter ‘b’ at the end of their label.

2.2.2. 3J1

To prepare 3J1, a two step impregnation was used. In the first step, 5 ml of ammonium hydroxide was added to 30 ml of distilled water, contained in a round bottom flask. Then,

nickel nitrate precursor was added to the water, followed by alumina support. This was then mixed in a rotary evaporator for 18 h and the solvent was removed as described in the earlier section. The solvent was evaporated at a rate of 50 ml/min by applying vacuum and maintaining the round bottom flask temperature close to 60°C. When using water as the solvent, the water bath temperature was increased to 80°C after removing the vacuum to ensure complete removal of water. The obtained powder was then dried in an oven for 2 hours at 120°C to remove all the remaining moisture and then the powder was calcined at 300°C. This powder was then used for second step impregnation to incorporate Rh and Pd in a single step using THF solvent. In the second step, the calcined nickel catalyst was added into 30 ml of THF solvent in which Rh and Pd precursors were initially added. The mixture was then rotated in the rotavap for 18 h and the solvent was evaporated at 30°C. The powder was dried at 120°C and calcined at 500°C.

Table 2-2. Composition of catalysts synthesized for part II – 3J1

Catalyst name	Metals loading (%)	Impregnation sequence	Calcination temperature (°C)
Ni/b	Ni(10)	-	300
Pd/b	Pd(1.5)	-	500
Rh/b	Rh(1.0)	-	500
Ni-Pd/b	Ni(10), Pd(1.5)	Ni-Pd	300-500
Ni-Rh/b	Ni(10), Rh(1.0)	Ni-Rh	300-500
(RhPd)/b	Rh(1.0), Pd(1.5)	Co-impregnation	300-500
Ni-(RhPd)/b or 3J1	Ni(10), Rh(1.0), Pd(1.5)	Ni-(RhPd)	300-500

Similar to the first part, a series of catalysts were prepared to study the effect of each of the metals. It should be again mentioned that the sole purpose of these set of catalysts was to study deactivation mechanisms and it was not our intention to formulate a more stable or active catalyst. Three monometallic and three bimetallic catalysts in addition to 3J1 were synthesized, details of which are given below in the table.

2.3. Catalyst loading

Catalyst location within the reactor was regarded as one of the most critical steps in obtaining reproducible data, as changes in the placement of the catalyst bed in the tubular reactor led to variations in the catalyst performance. Utmost care was taken in loading the catalyst at the same position along the length of the reactor tube. For the same, the length of the reactor was kept constant and so is the distance of the catalysts bed from one of the ends of the reactor. Generally, the reactor was loaded with 1.0 g of powder catalyst unless otherwise mentioned. The catalyst bed was located at such a height that temperature measurement at the center of the bed was possible.

Care was taken in an attempt to obtain an ideal fixed bed reactor system. The fixed bed configuration required the catalyst bed to be placed on top of a flat surface and also to have a flat top. For this reason, the catalyst bed was placed on top of fine quartz wool. This was necessary as the catalyst powder size was in the range of 40 micron and such a quartz wool support bed would prevent catalyst from falling and moving across the reactor. A 2 inch long roll of dense quartz wool was inserted in the quartz tube from the top, keeping some part of it outside the tube. The quartz wool roll was then slid into the reactor to a specific distance from the top. A measured amount of catalyst was then

poured into the tube from a weighing pan. The tube was then shaken to obtain a flat top of the catalyst bed. After the required catalyst amount was loaded, it was covered by a 2 inch bed of quartz wool. Such an arrangement would avoid the entrainment of powder from the top of the reactor. The remaining vacant portion over the downstream quartz wool was filled up using additional wool. At high gas flowrate and GHSV, there was a tendency of the entire bed to move across the reactor. To avoid such an effect, all the remaining space above the catalyst bed was filled with additional quartz wool. In order to ensure that the tip of the thermocouple was placed at the center of the catalyst bed, the length of the thermocouple tip from the coupling was measured. The quartz tube was placed at a specific distance into the coupling bearing the thermocouple, which provided the distance at which the thermocouple tip would be inside the tube. Taking into account the catalyst bed height, this was the distance to which the upstream quartz wool was slid into the reactor tube.

2.4. Catalyst testing

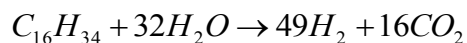
The two sets of catalysts were tested for their activity and reactivity towards steam reforming of fuel. Throughout the study, the reactions were run at 800°C, 1 atm pressure, and a steam to carbon ratio of 3. Catalysts were reduced at 800°C before reaction, as described below. A fixed start-up and shut down procedure was used for reproducibility. This was accomplished using a standard reaction protocol, interfaced with the computer using LabVIEW software.

Catalyst was reduced *in situ* at 800°C in flowing 5% H₂/N₂ at 50 sccm for 2 h. After reduction, the flow of 5% H₂/N₂ was stopped and immediately replaced by Ar at the same

flowrate. After 25 min of inert flow, the rate was reduced to 20 sccm and simultaneously steam was introduced into the system. After 10 minutes, the vaporized fuel mixture, consisting of either pure n-hexadecane or n-hexadecane doped with 1000 ppm thiophene, was introduced into the system. Steam reforming was conducted at 800°C, steam to carbon (S/C) ratio of 3 and atmospheric pressure for 10 h time on stream at 52,000 h⁻¹ gas hourly space velocity. After 10 h time on stream, the reaction was terminated by stopping steam and organic feed while turning off the furnace simultaneously. This was quickly followed by flow of argon to flush the reactor so that the catalyst did not undergo further changes. It should be mentioned that the mass flow controllers and HPLC pumps were controlled via standard reaction protocol developed using LabVIEW software.

2.4.1. Definition of hydrogen yield

Hydrogen yield was used as a quantitative measure of catalyst performance and a means of comparison amongst various catalysts. It was defined as the percentage ratio of the flow rate of hydrogen obtained in the product stream to the flow rate of hydrogen one would expect if all of the fuel were converted to hydrogen and carbon dioxide. In case of hexadecane, complete steam reforming is given by:



Forty nine moles of hydrogen are formed per mole of hexadecane converted when complete conversion to carbon dioxide and hydrogen is achieved. Thus, hydrogen yield for hexadecane steam reforming would be percentage ratio of molar flow rate of hydrogen in the product gas to 49 times the molar flow rate of hexadecane fed in.

$$H_2 yield = \frac{F_{H_2,out}}{49F_{nHex,in}} \times 100 \quad 4.1$$

2.5. Catalyst characterization

Both the fresh and used catalysts were characterized using various techniques, including pulse chemisorption, temperature programmed reduction, temperature programmed oxidation, temperature programmed desorption, scanning electron microscopy (SEM), transmission electron microscopy (TEM), scanning transmission electron microscopy (STEM), energy dispersive spectroscopy (EDS), electron energy loss spectra (EELS), X-ray photoelectron spectroscopy (XPS) and X-ray diffraction (XRD).

2.5.1. Pulse Chemisorption

Dispersion is the fraction of active metal atoms exposed to the surface or is accessible to the reacting species. It is a critical parameter for catalyst since only atoms which are exposed to the surface can take part in the surface catalyzed reactions. Due to high temperatures encountered during different steps (calcination, reduction, reaction), some of the metal may become inaccessible to the reactants due to migration into the support bulk, formation of a new product, sintering, or otherwise. All of these processes lead to a decrease in the metal dispersion values. The change in the dispersion of metals can be measured by pulse chemisorption experiment using CO or H₂ as required. This analytical method provides information about the particle size and dispersion of metal.

Pulse chemisorption experiments were conducted using an automated catalyst characterization instrument (Micromeritics Autochem 2910). A 10% by volume H₂/Ar

mixture was used to carry out the experiment and the amount of H₂ chemisorbed was used to determine the exposed metal atom in the catalyst. Experiments were carried out in a U tube quartz reactor using 0.1 g of catalyst supported on the quartz wool. Sample preparation included heating the catalyst to 120°C with a ramp rate of 10°C/min and holding it at that temperature for 30 min in Ar to remove any absorbed moisture, after which the catalyst was cooled to ambient temperature. Pulses of the 10% H₂/Ar mixture were dosed repeatedly until the catalyst surface was saturated. The total amount of H₂ chemisorbed was measured using a thermal conductivity detector (TCD) and the metal dispersion was calculated.

2.5.2. Temperature Programmed Reduction (TPR)

Temperature programmed reduction is employed mainly to study the reduction behavior of metals present on the support. The data obtained from TPR is useful to estimate reduction temperatures of metals on the support, degree of reduction, metal-support interactions and any important findings regarding interaction of metal with other metals and support. The reduction temperature depends on the degree of interaction between the active species and the support. Stronger interactions lead to higher reduction temperatures. A mixture of 10% H₂-Ar was used for studying TPR. Experiments were carried out using the Micromeritics Autochem 2910. Sample preparation was the same as that used in pulse chemisorption. After sample preparation, the catalyst was heated to 825°C at a rate of 10°C/min in 10% H₂/Ar mixture. The consumption of hydrogen was recorded using TCD.

2.5.3. Temperature Program Oxidation (TPO)

During catalytic hydrocarbon processing, the catalyst deactivates due to coke formation [9, 10, 13, and 14]. Temperature program oxidation (TPO) coupled with a mass spectrometer was used to determine the amount of carbon deposited on the deactivated catalyst. 0.1 g of used catalyst was analyzed in the Micromeritics Autochem 2910 using 3% O₂/He mixture. The sample preparation method was the same as in the chemisorption experiment. The temperature of the sample was increased at a constant rate of 10°C/min in 3% O₂/He mixture. The exhaust from the instrument was coupled with Ametek quadruple mass spectrometer to estimate the amount of CO₂ formed during TPO. The consumption of oxygen was also monitored using TCD, thereby providing qualitative information about the amount of oxidation. In the TPO experiment, the metals present in the catalyst may also oxidize, hence the difference between the amounts of oxygen consumed by fresh catalyst (reduced) and used catalyst was used to find the approximate amount of carbon being burnt.

2.5.4. Temperature Program Ammonia Desorption (TPAD)

Support acidity plays an important role in catalyst deactivation. Studies have revealed that acidity of the support is critical in deactivation via carbon deposition. It is a general practice to conduct ammonia desorption studies to study support acidity. The experiments were carried out using the Micromeritics Autochem 2910. The amount of ammonia absorbed was used to determine the acidity of the catalyst. A mixture of 15% NH₃/He was used to carry out TPD of ammonia. At room temperature, ammonia was allowed to

absorb on the surface until saturation. The temperature of the catalyst bed was slowly increased at 5°C/min and NH₃ desorption was monitored and recorded using TCD.

2.5.5. BET surface area

It is well established that a loss in the catalyst surface area is directly related to the extent of deactivation during any catalytic process [10, 12]. One of the reasons for loss of surface area is sintering of metal and support. While sintering of metal can be easily estimated using chemisorptions, sintering of support is evaluated using Brunauer-Emmett-Teller (BET) surface area. Micromeritics Autochem 2910 was used to determine the BET surface area. The sample preparation method was the same as in the chemisorption experiment. After sample preparation, a mixture of 30% N₂/He was passed over the catalyst. Temperature of quartz reactor was lowered to -178°C using a liquid nitrogen bath during which the nitrogen was allowed to physically absorb on the surface of the catalyst. Consumption of nitrogen was monitored using TCD. After saturation, liquid N₂ bath was removed and the reactor was allowed to come to room temperature. The desorption peak was recorded using TCD. The area under desorption peak of nitrogen gave the amount of nitrogen adsorbed on the catalyst surface. This information was used to find out the BET surface area of the catalyst.

2.5.6. X-ray Diffraction (XRD)

X-ray diffraction is used to decode any phase changes that might have occurred during either pretreatment or reaction. It is also possible to roughly estimate the average crystallite size. XRD experiments were performed on the Philips X'pert Pro instrument

using $\text{CuK}\alpha$ radiation with nickel filter at 40 kV and 45 mA, step size of 0.02° , and scan rate of $5^\circ/\text{min}$. Sufficient amount of catalyst was packed in a Plexiglas holder.

The crystal size of the catalysts was calculated using the Scherrer equation and the XRD spectra. The mean size (D) of the crystallite in the catalyst is determined using the following equation:

$$D = \frac{k\lambda}{B_{1/2} \cos\theta} \quad 2.1$$

k, is the constant ranging between 0.9 to 1

λ , is the wavelength of X-ray, Å

θ , is the angle measured from the diffraction patterns

$B_{1/2}$, is measured from the diffraction pattern figure obtained at the different 2θ angles (degrees), as it can be approximated as width of the line breadth at half the intensity.

In short, a broader peak means that the corresponding crystallite is present as relatively small particles. A sharp peak usually is attributed to crystallites of relatively large size.

2.5.7. Transmission Electron Microscopy (TEM)

The images were taken using a JEOL 2010F field emission gun analytical electron microscope located in the Electron Microbeam Analysis Laboratory (EMAL), University of Michigan, Ann Arbor. This technique coupled with EDS helped identify compositional changes in the catalyst structure. High resolution TEM images were obtained using JEOL 3011 operated at 300 kV. Energy dispersive spectroscopy (EDS), electron energy loss

spectroscopy (EELS) and scanning transmission electron microscopy (STEM) images were obtained using JEOL 2010F operated at 200 kV. EDS was performed with a Horizontal Ultra-thin Window Si-Li X-ray detector and a Gatan Imaging Filter (GIF) was used to get EELS. High angle annular dark field (HAADF) was used to record STEM images. For microscopy, powder sample of the catalyst was dispersed on a 300 mesh Cu grid with a lacey carbon film.

2.5.8. X-ray Photoelectron Spectroscopy

X-ray photoelectron spectroscopy (XPS) was performed using the Kratos Axis Ultra XPS analyzer located in the Electron Microbeam Analysis Laboratory (EMAL), University of Michigan, Ann Arbor. The instrument was operated with mono-aluminum source at 8 mA and 15 kV with 0.5 eV resolution. The vacuum in the analysis chamber was maintained below 10^{-9} torr. A pass energy of 20 eV and a dwell time of 450 ms was applied for individual elemental analysis while survey scan was obtained at a pass energy of 160 eV and a dwell time of 250 ms. The charge neutralizer was turned on to eliminate surface charging for nonconductive samples. The charge shifts in the binding energies were corrected with reference to Al 2p at 74.7 eV.

2.5.9. Scanning Electron Microscopy (SEM)

Images were obtained using Philips XL30 Field Emission Gun (FEG) SEM located in the Electron Microbeam Analysis Laboratory (EMAL), University of Michigan, Ann Arbor. The instrument was generally operated at an accelerating voltage of 15 kV but was varied depending on the charging effects associated with the catalyst samples. The vacuum inside the chamber was maintained below 10^{-6} torr. Similar to TEM, the instrument was

coupled with Energy Dispersive Spectroscopy (EDS) for compositional analysis. EDS was performed with a Horizontal Ultra-thin Window Si-Li X-ray detector using EDAX acquisition software.

Chapter 3

Literature Review

Knowledge of thermodynamics and reaction kinetics is of great help in designing better catalysts. While thermodynamics helps in knowing the theoretical equilibrium limits, kinetics can yield information on reaction pathways and transition states. The following section summarizes some of the literature on thermodynamics and kinetic data for both simple molecules like methane and high molecular weight molecules like those found in transportation fuels.

3.1. Operating parameters

3.1.1. Temperature

Temperature of steam reforming is critical parameter as it can significantly alter the deactivation characteristics of the catalyst. It was the aim of the research was to study deactivation at optimized temperature from process economics point of view. Steam reforming is an endothermic reaction; its hydrogen yield therefore increases with increasing temperature. A CHEMCAD simulation was carried out using a Gibbs reactor to determine equilibrium conversions. Results from the Gibbs reactor simulation are obtained by minimization of global Gibbs free energy. The simulation was carried out for a temperature range of 200-950°C with 25°C step increments. A ChemCAD simulation

of n-hexadecane steam reforming was performed at a S/C of 3 and atmospheric pressure; the equilibrium composition predicted from this simulation is shown in figure 4.2. The mole fractions are estimated on water free basis.

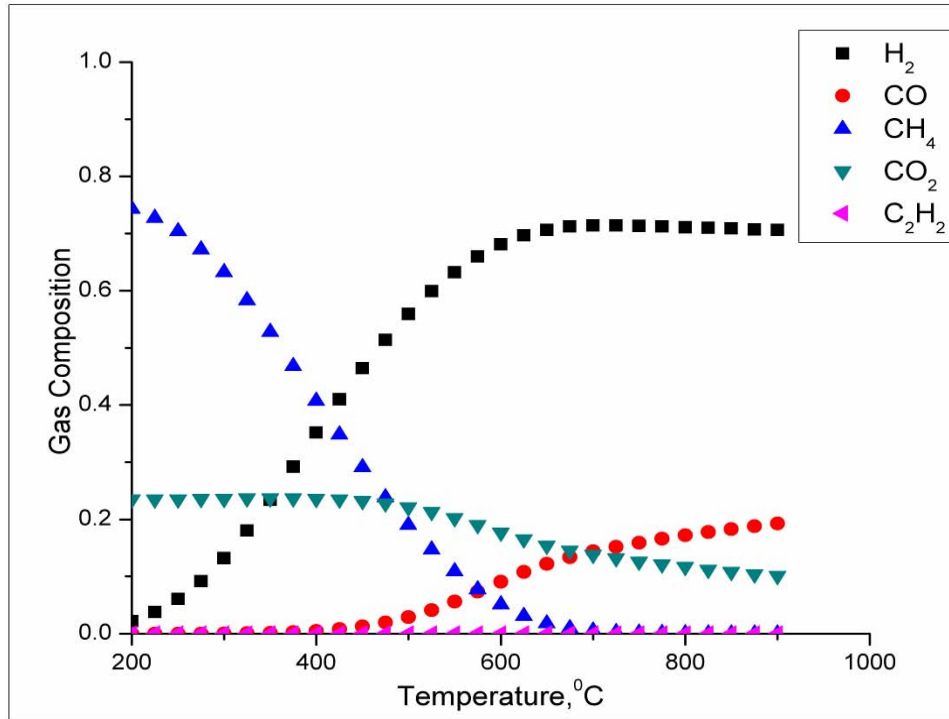


Figure 3-1. A CHEMCAD simulation of steam reforming of n-hexadecane at S/C 3

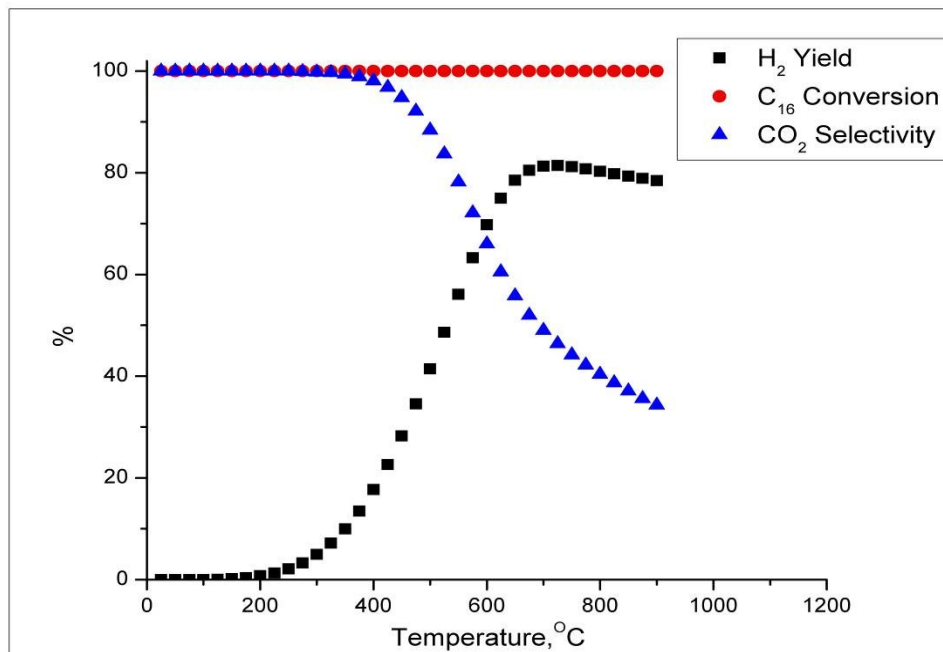


Figure 3-2. A CHEMCAD simulation on steam reforming of n-hexadecane showing the change in the hydrogen yield, n-hexadecane conversion and CO₂ selectivity with temperature

Conversion was close to 100% throughout the temperature range leading to products including methane, hydrogen, carbon dioxide and carbon monoxide. At approximately 600°C and above, hydrogen, CO, and CO₂ were the major products observed, with only small amounts of methane still remaining in the product gas. Increasing the temperature beyond 800°C started to show a decrease in hydrogen yield. This was partly due to the reverse water gas shift being dominant at the higher temperatures. At lower temperatures, the water gas shift reaction was more prevalent, leading to greater hydrogen production. Beyond this temperature, the reverse water gas shift reaction becomes increasingly favored and the amount of hydrogen produced decreases with further increase in temperature. This combined effect causes the total hydrogen produced to drop beyond 800°C.

3.1.2. Steam-to-carbon ratio (S/C)

S/C is another important operating parameter; increasing S/C increases the conversion of the fuel at a given temperature. Theoretically, a S/C ratio of 2 is needed to achieve complete conversion to hydrogen and carbon dioxide. As the S/C ratio increases, for a given temperature, conversion of methane increases. Similarly, the equilibrium conversion of the water gas shift reaction also increases with increasing S/C. Due to all these beneficial reasons, a higher S/C is normally preferred.

Having said that high S/C is beneficial from steam reforming process point of view, it should also be noted that the heat incurred in evaporating water comes at a cost. As a result, a drop in the thermal efficiency of the system is observed as more heat is spent in evaporating the additional steam than is recovered by the increase in hydrogen production. Thus, operating at the lowest possible S/C is favored. Moreover, using higher S/C is known to suppress the accumulation of carbon deposits on the catalyst surface.²⁹

It is understood that the coke accumulation on catalyst surface is an equilibrium reached between the rate of coke formation and the rate of coke gasification. Increasing S/C favors the coke gasification reaction, thus, reducing the risk of coke accumulation. Coking of catalyst causes significant deactivation and degradation in its performance. There could be physical blockage of reactants leading to tremendous increase in pressure in the reactor. A S/C of 3 is industrially very common in case of methane steam reforming. In the present study, a S/C of 3 is used throughout the study unless otherwise mentioned.

3.2. Steam reforming of Methane

3.2.1. Thermodynamics

The steam reforming of methane including water gas shift can be represented as:



While steam reforming is highly endothermic, water gas shift is moderately exothermic. The steam reforming is favored at higher temperatures as the reaction is endothermic. Moreover, since the overall reaction results in the increase in the number of moles per mole of the reactant, low pressure is favorable. However, industrially, the process is carried out at high pressure keeping in mind the process economics. On the other hand, the exothermic shift reaction is favored by low temperature, while it remains unaffected by changes in pressure. Ideally, using higher steam to carbon ratios is known to suppress coke and carbon deposition which may in turn delay the deactivation of the catalyst. However, this works against the economics as it involves the generation of steam. Commercially, steam reforming is conducted at high temperature and pressure at a steam to carbon ratio of 3 followed by a 2 step shift reaction at lower temperatures (generally 200 to 400°C) in order to maximize the hydrogen yield. For high temperature water gas shift, catalyst used industrially is iron oxide promoted with chromium oxide and copper on a mixed support composed of zinc oxide and aluminum oxide for the low temperature shift.

3.2.2. Kinetics

Many studies have concentrated on investigating the kinetics of methane steam reforming. Although there is a general conclusion on the kinetics, the activation energies vary over a wide span. Most of these discrepancies can be attributed to the different reactor configurations used in the studies which may in turn lead to different forms of heat and mass transfer limitations. Bodrov and co-workers found that the reaction rate of methane reforming on a conventional nickel/alumina catalyst depends only on the partial pressure of methane, whereas on a nickel foil, which has less diffusion restrictions, the rate depends also on the partial pressures of H₂O, H₂, and CO.³⁰ Xu and Froment studied the intrinsic kinetics of the methane steam reforming and water-gas shift reactions on a Ni/MgAl₂O₄ catalyst.³¹ They developed a detailed Langmuir-Hinshelwood model using 14 reaction steps. In general, the rate equation was proved to be:

$$r = \frac{k_i f_i(P_i, K_i)}{Z^2(P_x, C_x)} \quad 3.3$$

$$i=1,2,3$$

$$x=CH_4, CO_2, CO, H_2$$

where the k_i denote the rate coefficients of the reactions i , which incorporate temperature dependence, adsorption enthalpies, reaction activation energies, and entropies. The f_i are complex functions of the partial pressures P_x and equilibrium constants K_i . Z is an arbitrary function of P_x and the adsorption constants C_x .

3.2.3. Catalysts

Alumina supported nickel catalyst is used for steam methane reforming on a commercial scale. However, other catalysts incorporating other oxide supports such as CeO₂ and ZrO₂-supported metals and supported Pd, Pt, and Rh catalysts have also been used successfully with superior activity and stability. To improve the coking resistance of the catalyst, certain additives such as potassium and oxides of rare earth metals are successfully added. The challenge is to improve the coking resistance without significantly altering the steam reforming performance. However, these catalysts are shown to result in a decrease in the steam reforming activity. Borowiecki *et al.* studied the influence of small MoO₃ additions on the properties of nickel steam reforming catalysts.³² A Ni/Al₂O₃ catalyst containing 0.5 wt% MoO₃ was found to retain its catalytic activity in methane steam reforming as opposed to the potassium-promoted nickel catalyst. However, the beneficial effect of the molybdenum addition is still unclear since Ni/Al₂O₃ catalyst with as much as 3 wt% MoO₃ was also reported to increase the rate of carbon deposition in CO methanation by one order of magnitude. Also, it is known that the morphology and mechanism of the formation of carbon deposits in steam reforming of hydrocarbons and CO methanation are quite similar.³³

One of the important breakthroughs in catalysis has been the introduction of supports with oxygen storage capacity, such as cerium oxide. Zhang *et al.* researched on the activity of cerium oxide promoted nickel catalysts for methane steam reforming.³⁴ It showed a positive effect by decreasing the rate of carbon deposition, thus maintaining the catalytic activity during the induction period and in the constant carbon deposition region. Su and Guo also reported a significant improvement in the stability and the high

temperature steam resistance of Ni/Al₂O₃ catalysts promoted with rare earth oxides.³⁵ It is known that the formation of surface spinel species in the form of nickel aluminate (NiAl₂O₄) leads to catalyst deactivation. By adding rare earth metal oxides, formation of nickel aluminate was significantly suppressed, thereby preventing catalyst deactivation. It is believed that magnesia enhances coke gasification on the catalyst surface, thereby preserving the active sites for steam reforming.

The deactivation of Ni/Al₂O₃ catalysts by sintering during methane steam reforming at 500°C and 800°C was studied.³⁶ The authors concluded that the combined action of steam and high temperature enhanced the rate of sintering of small nickel crystallites, particularly for narrow initial crystallite size distributions and high initial dispersions. Addition of lanthanum is suggested to prevent the sintering of nickel crystallites under the reducing environment.

3.3. Steam reforming of higher hydrocarbons

3.3.1. Thermodynamics

The overall steam reforming of hydrocarbons is generally endothermic ($\Delta H^{\circ}_{298} = 1108$ kJ/mol for n-heptane). Like methane steam reforming, it is desirable to perform steam reforming of higher hydrocarbons at high temperature and low pressure. Since water gas shift is exothermic, it is inhibited at high temperature.³⁷ It is known that energy requirements for steam reforming of higher hydrocarbons change depending on the reaction conditions.³⁸ By manipulating temperature and molar ratios of steam to hydrocarbon, the overall reaction enthalpy may be positive or negative. For example, the overall process is exothermic ($\Delta H = -47.9$ kJ/mol) at a relatively low temperature of 450

°C and a steam to naphtha ratio of 2.0. On the other hand, the process becomes endothermic ($\Delta H = 102.9$ kJ/mol) at higher temperatures and higher steam to naphtha ratios (800 °C and 3.0, respectively). However, carbon deposition slowly starts to dominate with decreasing steam to carbon ratios. In practice, excess steam/carbon ratios are used to inhibit carbon deposition although process economics works against it. Moreover, undesirable side reactions including methanation begin to dominate at low steam to carbon ratios.

3.3.2. Kinetics

Rostrup-Nielsen studied the kinetics of ethane steam reforming at atmospheric pressure and 500°C over various catalysts.³⁹ A difference in the kinetics of the reaction was influenced by steam partial pressure, which was related to the catalyst composition. Magnesia-supported and alkali-promoted catalysts were found to enhance steam adsorption. For a Ni/MgO catalyst, the following rate expression was obtained:

$$r = 20p_{C_2H_6} / \left[1 + \frac{30p_{C_2H_6}p_{H_2}}{p_{H_2O}} + 1.26 \times \frac{10^{-2}p_{H_2O}}{p_{H_2}} \right]^2 \quad 3.4$$

$$r, \text{ mol/m}^2 (\text{Ni}) \text{ h}$$

$$p, \text{ Mpa}$$

In addition, a mechanism for steam reforming of hydrocarbons was proposed in the same study. It was assumed that hydrocarbon was adsorbed on a dual active site, followed by

successive α -scission of the C-C bonds. The resulting C1 species subsequently reacted with adsorbed steam to yield CO and H₂.

Tottrup investigated the kinetics of steam reforming of n-heptane on a commercial Ni/MgO catalyst at 450 to 550°C and 5 to 30 bar.⁴⁰ The rate expression obtained based on their experimental results is shown below:

$$r = k_a (p_{C_7H_{16}})^{0.6} (p_{H_2O})^{-0.1} (p_{H_2})^{0.2} \quad 3.5$$

k_a , the apparent rate constant and the apparent activation energy was 38.3 kJ/mol

Phillips *et al.* investigated the kinetics and mechanism of steam reforming of n-hexane and n-heptane over a nickel-alumina catalyst at 360-450°C and 14.6 atm.⁴¹ The reaction rate was found to be proportional to $(p_{C_6H_{14}} \text{ or } p_{C_7H_{16}})^{0.3}$ and the activation energy for the reaction was around 88 kJ/mol. Muraki and Fujitani studied the kinetics of steam reforming of n-heptane over a Rh/MgAl₂O₄ catalyst at 400-500°C.⁴² The observed initial reaction rate was expressed by a Langmuir-type equation with the adsorption equilibrium constant for n-heptane and water of 111 and 0.712 atm⁻¹ respectively. Furthermore, the reaction between n-heptane adsorbed on rhodium metal and adsorbed steam on the spinel surface was found to be the rate-determining step. CO was a primary product whereas both CO₂ and CH₄ were secondary products.

Goud *et al.* studied the steam reforming of n-hexadecane (surrogate for diesel) to evaluate the effect of temperature, steam to carbon ratio and sulfur.⁴³ They started with a first

order rate equation and showed that deactivation was dependent upon all the parameters studied. The authors also formulated a universal rate equation 3.6 for the catalysts system which was shown to be dependent on temperature, steam to carbon ratio and sulfur level.

$$k_d = 0.4780 - 0.082(S/C) - \frac{393.9}{T} - 0.038S + \frac{70(S/C)}{T} + 0.0099(S/C)S + \frac{40S}{T} - \frac{10.43(S/C)(S)}{T} \quad 3.6$$

k_d , deactivation rate constant, hr^{-1}

S/C, molar steam to carbon ratio

S, sulfur in the fuel, ppm

T, temperature, $^{\circ}\text{K}$

3.3.3. Catalysts

With increase in the molecular weight of the reacting molecules, the conventional nickel catalyst becomes less active and deactivates fairly rapidly. Use of small amounts of noble metals (Rh, Pd, Pt) are very common in catalysts designed for higher hydrocarbon reforming, although they are very expensive as compared to nickel.

The introduction of MgO to Al_2O_3 in Ni catalysts has been known to improve the catalytic properties such as activity, stability, and resistance to coking. Borowiecki investigated the effects of calcination and reduction conditions on the phase composition and the resistance to coking of the Ni/MgO-NiO- Al_2O_3 catalysts for steam reforming of n-butane.⁴⁴ Calcination and reduction temperatures were found to strongly affect the nickel crystallite sizes and the phase composition of the catalysts. A phase of solid

solution rich in NiO was observed with a rise in calcination temperatures but a fall in the degree of NiO reduction. In addition, higher reduction temperatures were found to increase the degree of NiO reduction. It was concluded that the optimum calcination and reduction temperatures were 400 and 500 °C, respectively. Furthermore, a phase of solid solution MgO-NiO (rich in MgO) and a MgO phase suppressed the rate of carbon deposition of the catalyst while that of solid solution NiO/MgO (rich in NiO) enhanced coking. Borowiecki further examined direct and indirect factors affecting the coking rate. Nickel dispersion and phase composition of the support were found to have a direct effect on the coking rate. On the other hand, other variables connected with preparation procedures such as catalyst composition and preparation conditions indirectly affected the catalyst coking rate and mechanisms. The structure of carbon deposits on Ni/Al₂O₃ and Ni/MgO catalysts during steam reforming of n-butane at 400-680°C was subsequently studied.⁴⁵ The similar carbon structures, which were true filaments, tubes, and shells, were observed on both catalysts. The dependence of temperature on the created forms and their degree of graphitization was also observed. Moreover, the arrangement of the carbon layers in the deposits was strongly affected by the shape of the nickel particles. It was suggested that rate of catalyst coking did not affect the morphology of carbon deposits formed. The introduction of small amounts of molybdenum (≤ 1.0 wt%) into the Ni-Mo catalysts has shown the increase in their resistance to coking.^{46,47} This was likely due to lower rates of carbon deposit formation caused by the addition of molybdenum as a promoter. Kepinski *et al.* investigated carbon deposition on Ni/Al₂O₃ and Ni-Mo/Al₂O₃ catalysts during steam reforming of n-butane. Ni-Mo/Al₂O₃ catalyst showed a remarkable reduction in coke deposition. As mentioned earlier, magnesia as a support has been

known to reduce catalyst coking via the enhancement of gasification by steam. The benefits of magnesia for nickel steam reforming of ethane and propane were established by Sidjabat and Trimm.⁴⁸ Ni/MgO catalysts were found to deactivate much slower than Ni/Al₂O₃ catalysts and performed even better with the presence of hydrogen. Also, the preparation method for magnesia did not strongly affect the catalytic activity and coking rate.

When dealing with heavy hydrocarbons (including diesel, jet fuel and gasoline), Ni based catalysts are known to deactivate fairly rapidly due to carbon deposition and sulfur poisoning. Consequently, noble metal based catalysts, particularly Rh-based catalysts have attracted increasing interest for developing carbon- and sulfur-resistant reforming catalysts.^{49, 50, 51, 52, 53} The kinetics of steam reforming of n-heptane at 500°C were studied by Kikuchi *et al.* on a Rh/Al₂O₃ catalyst, and by Muraki and Fujitani on Rh/MgAl₂O₄.^{54,42} Igarashi *et al.* reported that Rh/ZrO₂ showed much higher activity than Rh/Al₂O₃ during low temperature steam reforming of butane.⁵⁵ Suzuki and coworkers have studied pre-reforming of kerosene and liquefied petroleum gas using Ru supported on Al₂O₃, La₂O₃ and CeO₂-Al₂O₃.⁵⁶ Ceria-based supports such as CeO₂-Al₂O₃ and CeO₂-SiO₂ have been demonstrated to be superior to unmodified Al₂O₃, since they can further enhance catalyst activity and reduce carbon formation.⁵⁶

Steam reforming of heavier oil feedstocks such as jet fuel and diesel fuel using noble metal supported catalysts have also been studied.^{57,58,59} Ruthenium-based (Ru/Al₂O₃) catalyst has been used for steam reforming of hydrocarbons while preventing the carbon deposition.^{60, 61} Suzuki *et al.* has successfully conducted a long-term (8000 h) test of steam reforming of desulfurized kerosene using Ru/Al₂O₃-CeO₂ catalyst and reported that

the sulfur resistance was dramatically improved through the addition of CeO₂ to Al₂O₃. When the same catalyst was used for steam reforming of kerosene (with 30–55 ppm sulfur), the conversion of kerosene was decreased to 85.5% after 25 h on stream.

3.4. Catalyst Deactivation

Catalyst deactivation during catalytic fuel processing is inherently present. The loss over time of catalytic activity and/or selectivity is a serious issue in most industrial processes. Costs to industry for catalyst replacement and process shutdown can be in billions of dollars per year. Having said that, time scales for catalyst deactivation vary considerably, from few seconds to years depending on a variety of factors. Over the past three decades, extensive work is being done on understanding catalyst systems.^{62,63,64,65,66,67,68,69,70} A lot of literature addresses the mechanisms of deactivation during reforming of hydrocarbons. This area of research can help us significantly in understanding and modeling catalyst deactivation processes, designing stable catalysts, and optimizing processes to prevent or delay catalyst deactivation. Although there are different mechanisms of catalyst deactivation, some of the important mechanisms include poisoning by elements such as sulfur and chlorine, carbon deposition and metal particle sintering.

3.4.1. Carbon deposition

Due to high operating temperatures during alkane steam reforming, catalyst deactivation by coke formation cannot be avoided. As a result, understanding the mechanism of coke formation provides insight into measures that may be used to control coking during steam reforming. Studies of coke formation on supported nickel catalysts have been of interest for the last two decades.^{71,72,73,74,75,76,77,78} The different routes to carbon formation affect

the morphology of the carbon and the way it gets gasified. The most common types of carbon observed in steam reforming are whisker-like, encapsulating, and pyrolytic. Whisker-like carbon is formed at temperatures approximately greater than 450°C. Unlike whisker-like carbon, encapsulating carbon films are formed by slow polymerization of C_nH_m radicals on Ni surface at temperatures below 500°C. The catalyst is then deactivated continuously. Pyrolytic carbon is formed due to thermal cracking of hydrocarbons. It subsequently deposits on the catalyst surface and encapsulates the catalyst particles. Not surprisingly, its effects are catalyst deactivation and an increase in pressure drop. Moreover, carbon deposits via CO decomposition can be further divided into five forms, depending on their reactivity and temperature of formation: adsorbed atomic carbon ($C\alpha$), amorphous carbon ($C\beta$), vermicular carbon (Cv), bulk Ni carbide ($C\gamma$), and crystalline, graphitic carbon (Cc). Finally, in extreme cases, strong carbon filaments may build-up in pores to the extent that they stress and fracture the support material, ultimately causing disintegration of catalyst pellets and plugging of reactor voids. Some forms of carbon result in loss of catalytic activity and some do not. For example, at low temperatures (<300–375°C) condensed polymer films and at high temperatures (>650°C) graphitic carbon films encapsulate the metal surfaces of methanation and steam reforming catalysts. In the intermediate temperature range of 375–650°C, carbon filaments are formed by precipitation of dissolved carbon at the rear side of metal crystallites causing the metal particles to grow away from the support.⁷⁴ Filament growth ceases when sufficient carbon accumulates on the free surface to cause encapsulation by a carbon layer; however, encapsulation of the metal particles does not occur if H_2/CO or H_2O /hydrocarbon ratios are sufficiently high. Thus, carbon filaments

sometimes formed in CO hydrogenation or steam reforming of hydrocarbons would not necessarily cause a loss of intrinsic catalyst activity unless they are formed in sufficient quantities to cause plugging of the pores or loss of metal occurs as the carbon fibers are removed during regeneration.⁷⁹

An important principle in coke insensitive reactions (e.g. methanation, Fischer–Tropsch synthesis, steam-reforming, catalytic reforming and methanol synthesis) is that the deactivation rate depends greatly on the difference in rates of formation and gasification of carbon/coke precursors. In steam reforming filamentous carbon formation rate is a strong function of hydrocarbon structure; for example, it decreases in the order acetylenes, olefins, paraffins, i.e. in the order of decreasing reactivity, although activation energies for nickel are in the same range (125–139 kJ/mol), independent of hydrocarbon structure and about the same as those observed for formation of filamentous carbon from decomposition of CO.³³ This latter observation suggests that the reactions of CO and different hydrocarbons to filamentous carbon proceed by a common mechanism and rate determining step; probably the diffusion of carbon through the metal crystallites. The rate of carbon accumulation on the surface of the catalyst can vary greatly with catalyst structure, including metal type, metal crystallite size, promoter, and catalyst support. For example, supported Co, Fe and Ni are active above 350–400°C for filamentous carbon formation from CO and hydrocarbons; the order of decreasing activity is reportedly Fe, Co, and Ni. Pt, Ru and Rh catalysts, on the other hand, while equally or more active than Ni, Co, or Fe in steam reforming produce little or no coke or carbon. This is attributed to reduced mobility and/or solubility of carbon in the noble metals, thus retarding the nucleation process. Thus, it is not surprising that addition of noble metals to base metals

retards carbon formation; for example, addition of Pt in Ni lowers carbon deposition rate during methanation, while addition of Cu to Ni substantially lowers carbon formation in steam reforming.³³ Addition of certain metals is expected to cause changes in electronic structure in addition to reducing the ensemble size. A reduction in ensemble size is beneficial from carbon deposition point of view. It is generally well established that coking is inhibited by smaller ensemble size particles. For example, in case of nickel based catalysts, it is believed that coking is dominant only above an ensemble size of 6-7 nickel atoms. If the ensemble consists of less than 6 atoms, carbon gasification is dominant and thereby its deposition is negligible.

In addition to hydrocarbon structure and reaction conditions, extent and rate of coke formation are also a function of the acidity and pore structure of the catalyst. Generally, the rate and extent of coke formation increase with increasing acid strength and concentration. In the case of supported bifunctional metal/metal oxide catalysts, different kinds of coke are formed on the metal and the acidic oxide support, e.g. soft coke (high H/C ratio) on Pt or Pt-Re metals and hard coke (low H/C ratio) on the alumina support in catalytic reforming.⁷⁷ In this case, coke precursors may be formed on the metal via hydrogenolysis, following which they migrate to the support and undergo polymerization and cyclization reactions, after which the larger molecules are dehydrogenated on the metal and finally accumulate on the support causing loss of isomerization activity.

One of the very early studies in understanding deactivation due to coking in methane steam reforming was undertaken by Rostrup-Nielsen *et al.*⁷⁴ The coke formed may originate from different sources. However, they all involve an initial step of dehydrogenation and formation of unsaturated species which are able to migrate, either in

the gaseous phase or in the adsorbed phase, and to form dimeric or polymeric species on the acid sites of the catalyst. One of the sources of coke suggested results from gas phase reactions at high temperatures leading to carbonaceous intermediates which eventually condense on the catalyst surface. These reactions essentially involve free radicals polymerization and presence of a diluent like steam is critically important. Nonetheless, gas phase carbon can accumulate on the surface particularly in heavy feedstocks. A highly accepted mechanism to explain coking in methane steam reforming is given by Rostrup-Nielson *et al.* Hydrocarbons dissociate on the nickel surface to produce highly reactive carbon species. Most of the carbon is gasified but some is converted to less reactive carbon, probably by polymerization and rearrangement. The carbon may encapsulate the nickel particulate, may be gasified or may dissolve in the nickel crystallite. The dissolved carbon diffuses through the nickel to nucleate and precipitate at the rear of the crystallite. This process leads to formation of a carbon whisker. This is one of the few cases where carbon formation does not lead to deactivation, although it results in pressure build up in industrial applications. Rostrup-Nielson has reported data for a range of hydrocarbons which shows that olefins and aromatics can pose serious coking problems. Both as a result of reactions in the gas phase and on the catalyst, there is a tendency for coking to increase as unsaturation, molecular weight and aromaticity increases. Barbier *et al.* and Coughlin *et al.* suggest that deactivation is due to graphitization of the metal site coke which makes it catalytically inert.^{80,81} Figoli *et al.* showed that the initial deposition of coke is on the metal crystallites and that the quantity does not change much with time (within experimental error).⁸²

3.4.2. Sulfur Poisoning

The presence of sulfur also has tremendous effect on the performance of the catalyst. Sulfur forms stable compounds with all the transition metals. Many studies have examined the interaction of sulfur with monometallic surfaces and are reviewed in refs. After examining the bonding of sulfur with several transition metals, it is found that in all cases sulfur withdraws charge from the metal and induces a decrease in its local charge density. From studies using single crystal metal surfaces, it is well established that sulfur inhibits the chemisorption of small molecules (H_2 , CO, NO, C_2H_4 , etc), CO methanation, alkane hydrogenolysis, olefin hydrogenation and water gas shift reaction. Studies of sulfur poisoning in hydrogenation and CO hydrogenation reactions have been thoroughly reviewed. Much of the previous work focused on poisoning of nickel metal catalysts by H_2S , the primary sulfur poison in many important catalytic processes, and thus provides some useful case studies of poisoning. Previous adsorption studies indicate that H_2S adsorbs strongly and dissociatively on nickel metal surfaces. The thermodynamic approach to the study of the metal-sulfur bond shows that there exists a highly reproducible surface saturation state of sulfur. This state can be achieved within a relatively wide range of temperature and partial pressures of hydrogen sulfide. Bartholomew *et al.* showed that free energies of formation of surface sulfides are at least 40 kJ/mol more stable than the corresponding bulk metal.⁸³ Although there is extensive literature on catalyst improvements in presence of sulfur, scientific understanding of the role of sulfur in catalyst deactivation during steam reforming is lacking.

The early study of methane steam reforming by Rostrup-Nielsen has suggested improvements in catalyst performance to protect against deactivation by sulfur. The

process known as SPARG has been commercialized in natural gas steam reforming.⁸⁴ It utilizes the fact that sulfur actually dilutes the active metal and reduces the effective ensemble size. Adsorbed sulfur will deactivate nickel surface but will also delineate ensembles of sites where sulfur is not adsorbed. The size of these ensembles was critical in allowing steam reforming with minimal formation of coke.⁸⁵ It has also been suggested that introduction of sulfur in liquid feed allows competition for metal sites between adsorbing sulfur atoms and coke precursors. Apesteguia and Barbier have indicated that this competition occurs with the sulfur blockage of metal sites for later coking and hence prolonging the catalyst life by lowering the deactivation rate of the metal catalyzed reactions.⁸⁶ Sulfur adsorbs at the hydrogenolysis sites which are also involved in coking. It is postulated that even though platinum is temporarily blocked to metallic site reactions by sulfur, n-heptane can still adsorb to the platinum atoms adjacent to the metal-support interface but then by spillover move to the alumina surface where it undergoes the acid site cracking and isomerization.

Regeneration of sulfur poisoned catalyst is extremely difficult. At high temperatures (400-500°C), during burn-off in oxygen, the metal surface is cleaned from carbon deposits and also from sulfur; nevertheless, in the latter instance, sulfur oxides are trapped by the support alumina as sulphates.⁸⁷ These species can be reduced above 300°C to H₂S, which allows sulfur to return to metal sites. This is why it is extremely difficult to take out sulfur completely from the catalyst.

Experimental evidence on effect of variable sulfur concentrations on Pt/Al₂O₃ and Pt-Re/Al₂O₃ during normal reforming operations was presented by Bickel *et al.*⁸⁸ It was observed that cracking reactions were high at high sulfur concentrations (500 ppm) while

lower sulfur concentrations (10 ppm) suppressed cracking products. At such high concentrations of sulfur, cracking products were mainly of acid type. The phenomenon was explained by the fact that the behavior of hydrocarbons in the presence of high concentrations of sulfur involves the spillover of adsorbed species to the alumina. Similar finding of spillover was discussed by Khoobiar.⁸⁹ Bickel had stated that during normal operation of the reformer, the deactivation of the alumina due to coking is controlled by the mechanism of hydrogen spillover from the platinum surface. It involves the reaction of spillover of coke precursors from the metal surface with atomic hydrogen as both species diffuse along the alumina surface to the acid site coke islands. A fraction of the acidic coke islands are also gasified by the atomic hydrogen that has surface diffused from the platinum surface.

3.4.3. Metal particle sintering

One of the critical parameters in steam reforming is the metal crystallite size. It is easy to understand that smaller crystallites give more surface area for the reaction while sintering of metal crystallites generally results in lowering of accessible metal surface area. Smaller particles will provide a larger surface for reaction and hence improved catalyst activity. But other aspects concerning the particle size are also important. Smaller particles are known to have more steps and kinks on the surface than larger crystals. Also, smaller crystallites are reported to be more resistant to carbon formation. Steam reforming was found to involve 3-4 nickel atoms while carbon formation requires 6-7 atoms.

Sintering is one of the most dominant causes of loss in activity during reforming. Particle sintering is driven primarily by the reduction in the total surface energy. The process of sintering occurs by mainly two mechanisms; (a) crystallite migration where entire crystallites migrate over the surface of the carrier followed by coalescence and (b) Ostwald ripening, where metal transport species emitted by one crystallite travels on the support or in the gas phase and are captured by other crystallite. Steam reforming nickel based catalysts were shown to sinter in reducing environment by both the fundamental mechanisms mentioned above. However, at temperatures above 600°C, it is believed that Ostwald ripening is the dominant cause of sintering. This mechanism change also seems reasonable considering that it is expected that the energy involved in creating and moving nickel transport species at the surface of nickel particles is lower than the energy involved in nickel transport at a carrier. It is also well established that the sintering of the metal catalysts is accelerated with the presence of steam in the atmosphere around the catalyst. For nickel steam-reforming catalysts, DFT calculations show that the combined energy of formation and diffusion for Ni₂-OH complexes at Ni(1 1 1) is 40 kJ/mol lower than that for nickel adatoms, strongly indicating that the former species are dominating the surface transport of nickel at nickel surfaces when steam is present in the atmosphere.

Deactivation due to sulfur and coking can be challenging especially in heavier fuels like diesel and jet fuel. Deactivation is mainly due to two primary reasons: high molecular weight hydrocarbons present in these fuels and high levels of sulfur (especially in jet fuel). Investigators have explored different possibilities to improve catalyst performance by different means. Use of more than one metal, modifying the support structure (basic

oxide supports or promoters), effect of nickel crystallite size, effect of alloying and sulfur passivation are some of the means of improving catalyst performance investigated.

The first bimetallic system to be reported, more than 25 years ago, was Pt-Re, used in naphtha reforming. The modifications proposed in the literature for explaining the role of rhenium include the stability of platinum crystallites against sintering using rhenium as an anchor, formation of a catalytically active rhenium compound with alumina, alloying of rhenium with platinum and interaction of alloy with sulfur.⁹⁰ They attribute the improvement to the formation of physical barriers by rhenium-sulfur. Rhenium-sulfur makes it difficult for molecular fragments to diffuse to platinum sites and further dehydrogenate there to form high molecular weight carbonaceous deposits. One of the explanations given is that the rhenium-sulfur bond sterically hinders graphitization of the carbon layer on metal sites. A highly favored explanation recalls the expected changes in electronic structure of the metal component when a bimetallic catalyst has been formed.⁹¹ Some authors have pointed out that the beneficial effect of the second metal could be primarily due to changes in the extent and mechanism of the hydrogenation / dehydrogenation / hydrogenolysis reactions. It is well known that hydrogenolysis is a reaction which needs relatively large metal atom ensembles. Sulfur dilutes the metal sites on the surface of the catalyst, which leads to smaller metal atom ensembles.

3.4.4. Catalyst deactivation in higher hydrocarbons / transportation fuels

Apart from high sulfur content, logistic fuels also contain appreciable amounts of aromatics and naphthenes which are known to be precursors for coking during reforming, particularly substituted naphthalenes. There is sparse literature on conversion of

naphthalenes to hydrogen. One study on steam reforming of 1-methylnaphthalene is by Delahay *et al.*⁹² Three main reactions occur during steam reforming of 1MN: dealkylation (DA), selective ring opening (OCN) yielding benzene and toluene and degradation of ring (DCN). The relative activities of different metals towards the reactions are as follows: dealkylation: Pt>Rh>Ni, OCN: Rh~Ni>Pt, DCN: Ni>Rh>Pt.

Kataria studied the steam reforming of individual components believed to represent the major constituents of jet fuel. A nickel based catalyst promoted by rhodium was used for their studies. N-hexadecane which represented the paraffins was easy to reform and gave hydrogen yields higher than 75% with no detectable deactivation in the first 10 h. Toluene exhibited activation in the initial few hours of steam reforming after which the hydrogen yield was constant. Similar catalyst activation was repeatedly observed by McCoy *et al.*⁹³ during toluene steam reforming and was viewed as a function of the aromatic species. Hydrogen yield during tetralin reforming was stable although the value was lower than that in case of n-hexadecane. In case of methylnaphthalene, the initial activity was close to 55% while it dropped to close to zero within 2 h on stream which basically points to the coking ability of the component.

Catalyst deactivation in case of heavy fuel reforming is poorly understood, particularly sulfur poisoning. It is well known that sulfur poisoning hinders catalyst activity; however, lack of adequate information on sulfur species present on the deactivated catalyst is a major drawback. In particular, surface analysis techniques such as XPS coupled with TEM and EDS studies could help us immensely in decoding the deactivation mechanism during reforming. Such studies were used earlier on model catalyst materials but its extension to real catalysts has not been explored. Present study is an attempt to conduct

such analysis on real catalysts and this study will provide new insights into the deactivation mechanisms of steam reforming catalysts and initiate new research opportunities in this area.

Chapter 4

Analysis of deactivation mechanism on NM4 catalyst

4.1. Introduction

The use of logistic fuel for hydrogen generation may be an attractive short term option to produce hydrogen for the fuel cell industry. This solution looks viable and environmentally responsible. Steam reforming is one choice at present due to its technological maturity. Moreover, it yields high hydrogen concentration in the exit stream. Deactivation of the catalyst is the main problem, especially for reforming of logistic fuels. This is because the logistic fuel contains a mixture of high molecular weight hydrocarbons including paraffins, naphthenes, and aromatics. In addition, it also contains small amounts of organic sulfur compounds.

The first part of the research was focused on understanding deactivation and its mechanisms during steam reforming of diesel on NM4 catalyst. Because of the desire to generate scientifically rigorous data, a mixture of hydrocarbons was used as a model of diesel throughout these studies.

Figure 4.1 shows a gas chromatogram of a diesel fuel obtained from the local BP gas station. The peaks were identified using mass spectroscopy and marked accordingly in

the chart. It contains a very high proportion of normal and substituted paraffins and small amounts of organic sulfur compounds. For the deactivation studies, n-hexadecane was used as the surrogate to represent the hydrocarbon part of the diesel. Although different organosulfur compounds are present in logistic fuels, thiophene was chosen as the surrogate to represent sulfur compounds in diesel, since previous results indicate that catalyst performance is relatively independent of the nature of the sulfur-containing component.

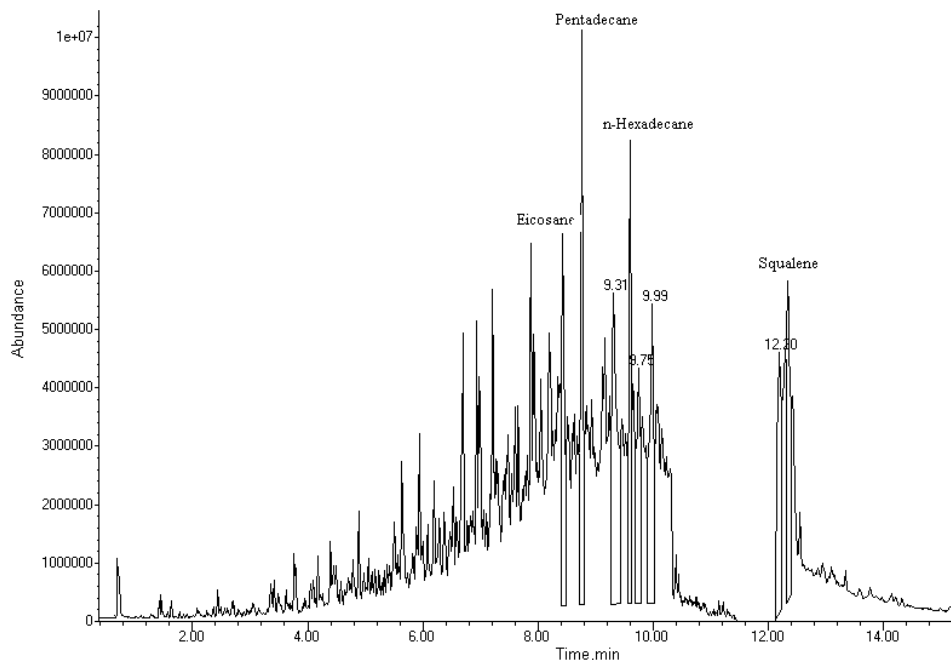


Figure 4-1. Gas chromatograph of diesel performed on Hewlett Packard 6890/5973 GC/MS

As mentioned earlier, the main objective in this part of the research was to elucidate the mechanisms for deactivation of the catalyst NM4 during steam reforming of model diesel

fuel. In this study, three other catalysts containing some combination of Ni and/or Rh were prepared (details in the experimental section).

4.2. Steam reforming of n-hexadecane

4.2.1. Activity and deactivation

Catalysts were tested for steam reforming of n-hexadecane at 800°C, atmospheric pressure and S/C of 3. The effect of sulfur was investigated by doping n-hexadecane with thiophene at 1000 ppm by weight. H₂ yields were used to demonstrate the activity of the catalysts and the deactivation brought on by the presence of sulfur in the fuel. Figure 4.2 compares the amount of H₂ produced relative to that obtained at the beginning of an experiment as a function of time on stream during the steam reforming carried out on NM4, where the initial yield was estimated by a straight line fitting of yield over a period of 10 h. Since the total deactivation is the critical measure, relative yield is used to eliminate any experimental complications associated with slight differences in catalyst weight placed in the reactor, flow rate of the feed, or flow patterns in the reactor associated with the packing of the catalyst. When there was no sulfur in the feed, the hydrogen production remained essentially stable for 10 hr of time on stream. The addition of 1000 ppm thiophene resulted in hydrogen production decrease by about 50% over 10 hrs, relative to the initial value. For all catalyst formulations as shown in figures 4.2, 4.3, 4.4, 4.5, the addition of thiophene in the feed increased substantially the total amount of deactivation observed over 10 h of reforming, except for the catalyst (2.5RhNi)/a. This particular catalyst did not incur substantial deactivation in the 10 h steam reforming reaction and moreover, the relative yields of hydrogen did not change

much over the period of 10 h. However, it is speculated that this behavior would match with that of other catalysts at longer times on stream.

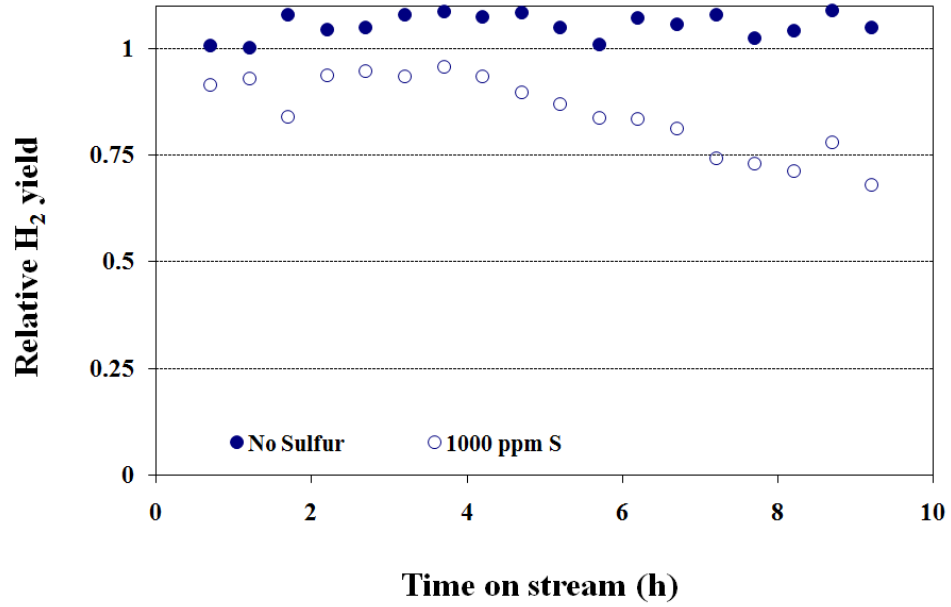


Figure 4-2. Relative H₂ yields of catalyst NM4 during steam reforming of sulfur-free and sulfur-laden n-hexadecane at 800°C, S/C 3 and 1 atm

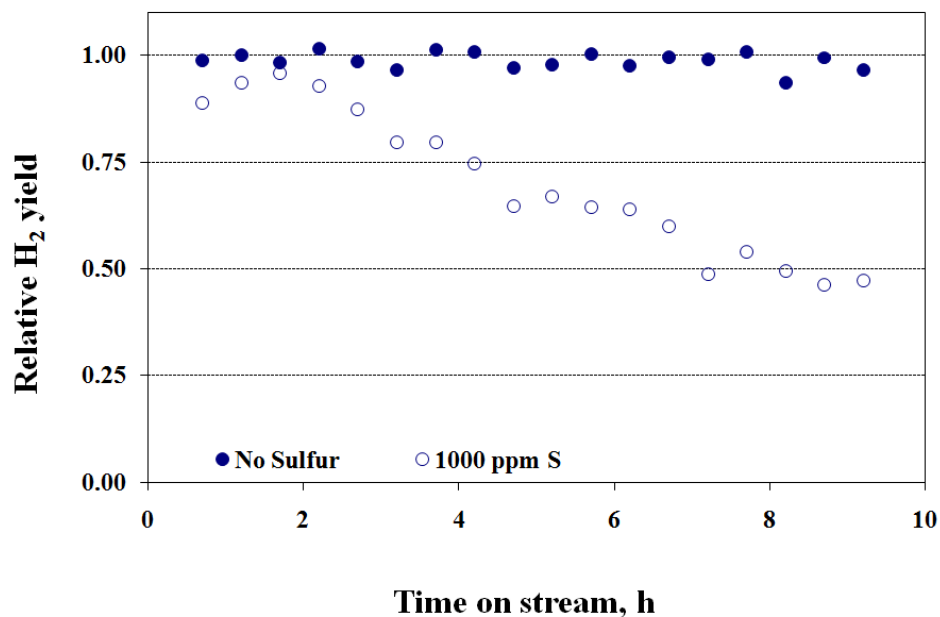


Figure 4-3. Relative H₂ yields of catalyst Ni/a during steam reforming of sulfur-free and sulfur-laden n-hexadecane at 800°C, S/C 3 and 1 atm

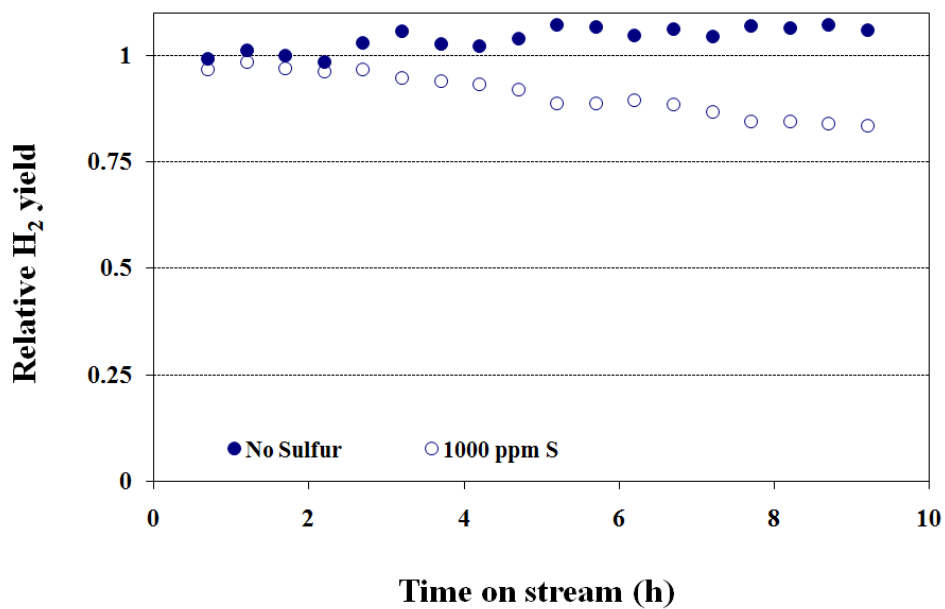


Figure 4-4. Relative H₂ yields of catalyst Rh/a during steam reforming of sulfur-free and sulfur-laden n-hexadecane at 800°C, S/C 3 and 1 atm

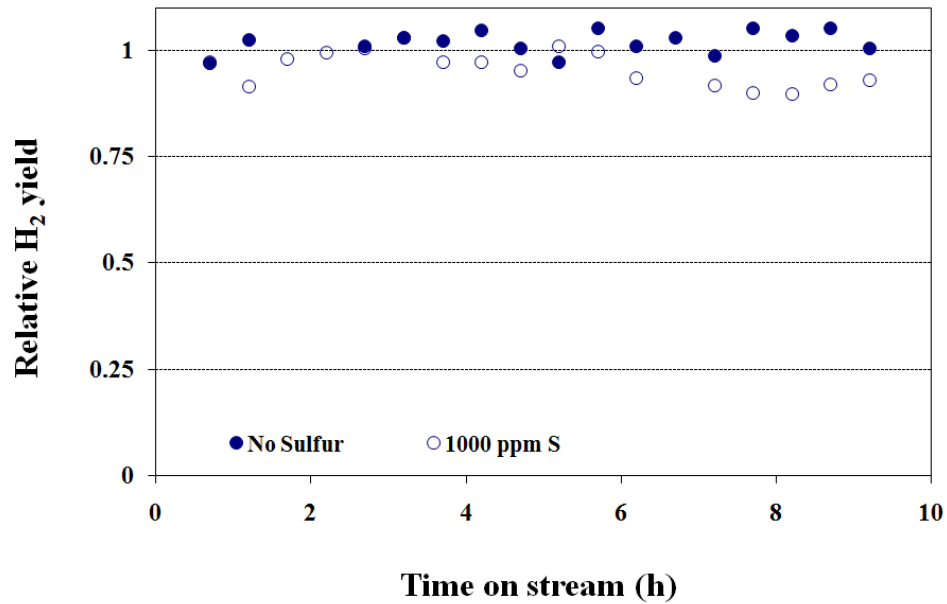


Figure 4-5. Relative H₂ yields of catalyst (2.5RhNi)/a during steam reforming of sulfur-free and sulfur-laden n-hexadecane at 800°C, S/C 3 and 1 atm

To compare the relative activities of each of the catalysts towards the steam reforming of n-hexadecane, initial rate in terms of hydrogen yield and the rate of deactivation are plotted and are shown in figures 4.6 and 4.7. In general, the catalysts containing both Ni and Rh exhibited better activity than monometallic catalysts. When sulfur was present, the activity of all catalysts was significantly decreased relative to the non-sulfur fuel.

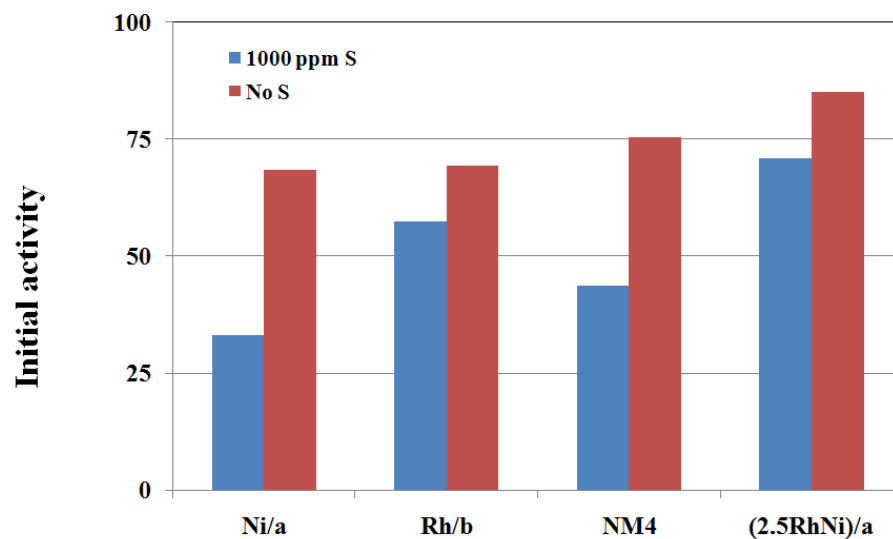


Figure 4-6. Initial activity in terms of hydrogen yield evaluated by straight line fitting of reaction data for different catalyst formulations during steam reforming of sulfur-free and sulfur-laden n-hexadecane at 800°C, S/C 3 and 1 atm

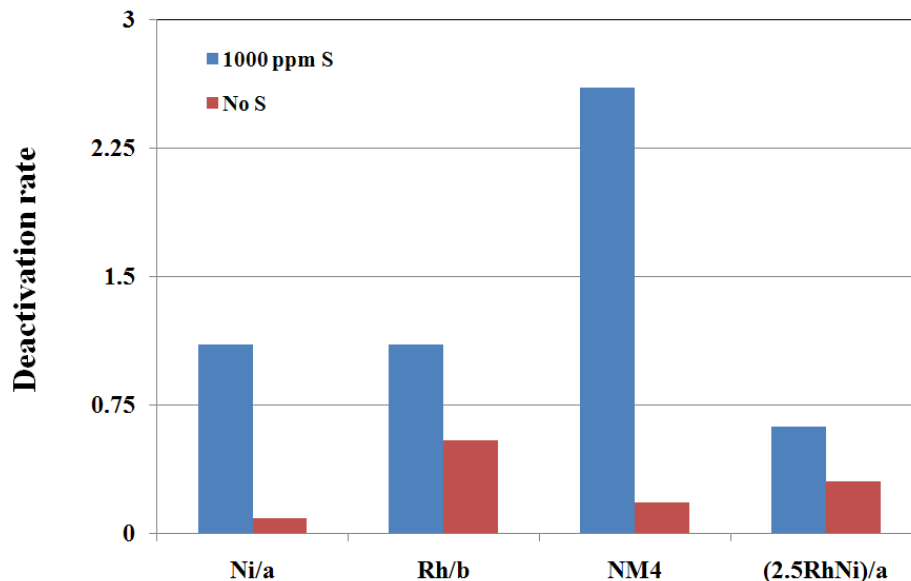


Figure 4-7. Deactivation rate in terms of hydrogen yield per hour evaluated by straight line fitting of reaction data for different catalyst formulations during steam reforming of sulfur-free and sulfur-laden n-hexadecane at 800°C, S/C 3 and 1 atm

Figure 4.8 gives the product composition on water free basis during the steam reforming of n-hexadecane on NM4 catalyst. Figure 4.9 provides information on the composition of the product gases in terms of H_2/CO , H_2/CO_2 and CO_2/CO ratios. In the absence of sulfur, the yields for most of the gases including hydrogen, carbon dioxide and carbon dioxide reached thermodynamic equilibrium. It is important to notice that hydrogen mole fraction was significantly lowered in the presence of sulfur in the fuel during the course of 10 h on stream. This may point to the fact that the reaction pathways to form H_2 , CO and CO_2 are significantly altered by catalyst deactivation. It is also important to notice that the sum of mole fractions becomes substantially less than 1 at longer times. This is because

at longer times, the reactions are generally characterized by presence of cracked products (C_2+). The same is explained in detail in the subsequent section on cracking.

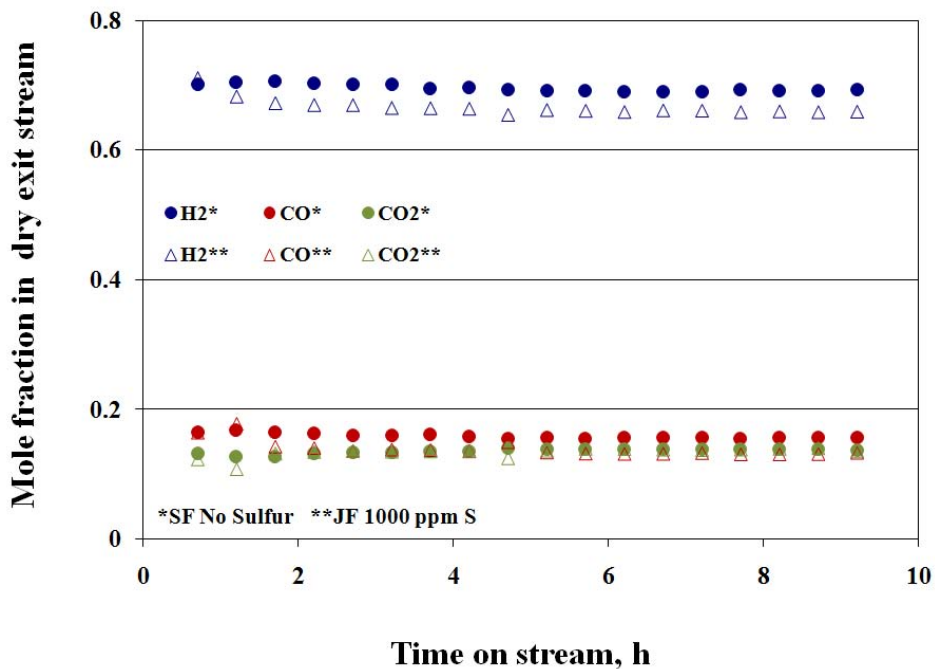


Figure 4-8. Dry product gas composition over 10 h during steam reforming of sulfur-free and sulfur-laden n-hexadecane at 800°C, S/C 3 and 1 atm

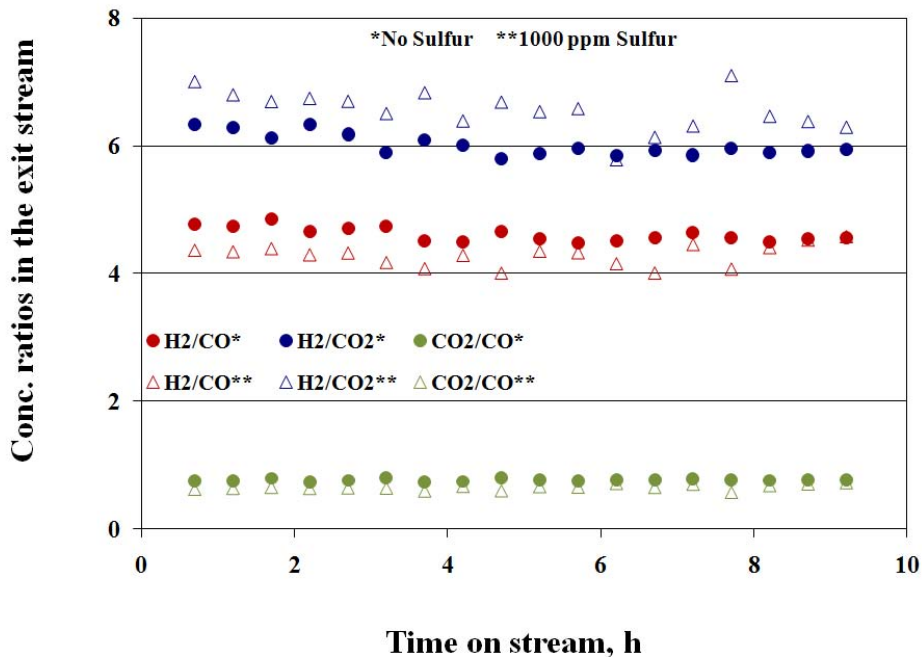


Figure 4-9. H_2/CO , H_2/CO_2 and CO_2/CO in the dry product gas over 10 h during steam reforming of sulfur-free and sulfur-laden n-hexadecane at 800°C , S/C 3 and 1 atm

4.2.2. Extent of cracking

Cracking was monitored during steam reforming by measuring the C_2+ in the exit stream (ethene, ethane, propane, propene, butane). Extent of cracking was defined as the percentage of C_2+ in the dry product gases. For all the catalyst formulations, reforming of sulfur-free fuel did not result in the formation of any significant cracked products. On the contrary, cracked products were observed from reforming in the presence of sulfur as shown in Figure 4.10. In the case of catalysts containing 2.5% Rh, cracked products in the product stream were relatively lower. A more close observation at the NM4 data shows that for the first 3 h, cracked products were not as much as seen at the later part of the progress of reaction. In case of Ni/a catalyst, the cracked products started at a

significantly higher level indicating the reduced effect (or the absence) of Rh as is the case. With 0.5% Rh addition to Ni/a catalyst, the cracked products are reduced for the first 3 h after which the effect of Rh is nullified and cracked products show up in high quantities, a behavior seen throughout in case of Ni/a. This slight increase in the mole fraction of cracked products at the end of the 10 h on stream period can be viewed as emanating from both, the GC calibration at low concentrations and slight experimental fluctuations. This slight decrease should not be seen as the characteristic of a particular reaction.

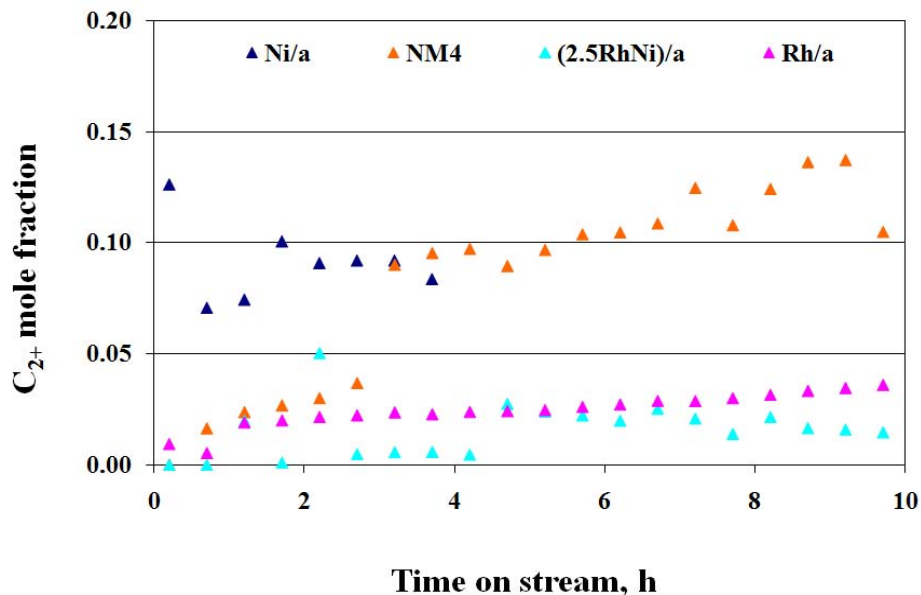


Figure 4-10. Extent of cracking in the dry product gas over 10 h during steam reforming of sulfur-free and sulfur-laden n-hexadecane at 800°C, S/C 3 and 1 atm

4.2.3. Hydrogen sulfide in the product stream

H₂S was monitored using the GC system, since thiophene was primarily decomposed into H₂S. Total exit sulfur was estimated relative to the amount of sulfur present in the fuel. A 100% value would mean that all the sulfur present in the fuel was detected as hydrogen sulfide in the product stream. In such a case, there would presumably be no residual sulfur either trapped on the catalyst surface or in the liquid products collected. This is an ideal case and is seldom seen in steam reforming due to the strong affinity of metals for sulfur abstraction.

Figure 4.11 represents total H₂S detected in the product stream during the 10 h experiment, relative to the amount of sulfur in the feed. It can be seen that the sulfur balance was not closed, which means that some of the sulfur was either retained by the catalyst or was converted to some other species not detected by our analytical procedure. This basically means that two sulfur sinks were important from analytical point of view; one is the catalyst itself and the other the liquid products. The highest sulfur balance was observed for the bimetallic catalysts. No analysis of sulfur was completed for the liquid products due to lack of liquid analytical system.

Nickel gave slightly better sulfur yields than rhodium. A better sulfur yield means that sulfur was effectively converted to hydrogen sulfide and is not trapped on the catalyst surface. Therefore, a better sulfur yield can lead to higher hydrogen yield as the catalyst surface was supposedly free of sulfur poisoning. Except for (2.5RhNi)/a, the postulation was valid in case of other catalysts. Despite poor sulfur yield, (2.5RhNi)/a gave better hydrogen yield than NM4 and the same was hard to explain, solely based on sulfur

yields. It is possible that some of the sulfur might have gone into the effluent liquid product and that might explain reduced hydrogen sulfur yield in case of better performing (2.5RhNi)/a. In other words, for estimating overall sulfur yields, both gas phase and liquid phase sulfur should be taken into consideration. In the present study, only gas phase hydrogen sulfide was considered for estimating sulfur yields.

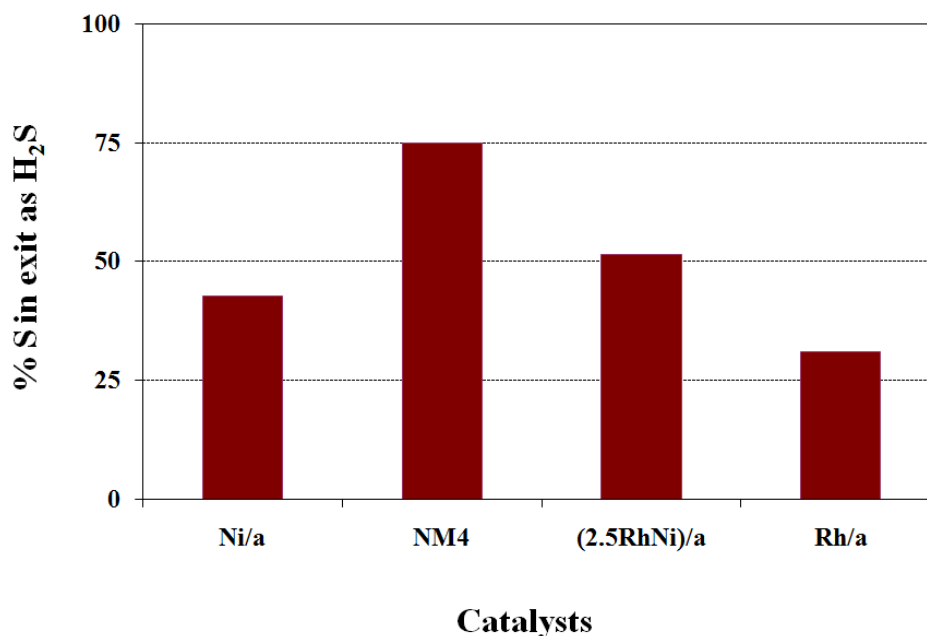


Figure 4-11. Total % sulfur out over 10 h during steam reforming of sulfur-free and sulfur-laden n-hexadecane at 800°C, S/C 3 and 1 atm

4.3. Characterization of fresh catalysts

Fresh catalysts were characterized using XRD and TPR. STEM coupled with EDS was used to elucidate the structural morphology of NM4.

4.3.1. Phase structure and Ni crystallite size

All the fresh reduced catalysts were characterized to get an insight into the phases present after catalyst reduction. XRD was also useful in estimating the crystallite sizes of the different phases using the Scherrer equation. Since the catalysts were reduced, both Ni and Rh were expected to be present in the reduced form. As it can be seen in the XRD patterns in Figure 4.12, Ni /a catalyst shows a very sharp peak which means that the nickel crystallites were relatively large in size. Addition of Rh to the Ni drastically reduces the Ni crystallite size. One of the important observations made was that of Rh peak at 41° . This peak was clearly visible in case of monometallic Rh catalyst but was not observed in the case of bimetallic catalysts. This result was confirmed using TPR.

TPR of all the four catalysts were performed to give insights into oxidation states and phases, shown in figure 4.13. Catalysts containing Ni exhibited a high temperature peak in the range $780-800^\circ\text{C}$. This is normally attributed to the reduction of Ni aluminate (NiAl_2O_4), a surface spinel species formed by the diffusion of NiO into the support alumina.^{94,95} Formation of NiAl_2O_4 occurs at calcination temperatures higher than 700°C with NiO diffusing into the surface of support. There were no low temperature peaks found around $400-450^\circ\text{C}$, which indicates that the catalyst surface was deprived of any free NiO dispersed on the support. Since XRD profiles shown in the figure refer to the reduced catalysts, the peaks for Ni aluminate (Ni^{2+}) were not seen.

Reduction peak for Rh was not observed in TPR of both the bimetallic catalysts. This suggested that Rh might have undergone some kind of strong interaction with the base metal Ni and/or support alumina. This was said to be possible due to the high temperature

calcinations and is observed in three way automotive catalysts. From the mechanistic point of view, this can alter the way reactants take part in the reaction. These observations are in agreement with that of TPR, shown in the later part of this section.

TPR of fresh catalyst Rh/Al₂O₃ showed a peak at approximately 115°C which is assigned to the reduction of Rh₂O₃. But none of the Rh-Ni/Al₂O₃ catalysts exhibited this peak. This indicates that Rh was not present as Rh₂O₃ but as some other species. As mentioned earlier, Rh is also known to undergo strong interaction with support alumina at high calcination temperatures in the presence of air to form Rh aluminates. There is no clear explanation as to why Rh aluminate is formed in the case of bimetallic catalysts and is not observed in monometallic Rh catalyst. In Rh/Al₂O₃, a small bump at around 700 °C was observed and we assigned this peak to reduction of such a species. The fact that the peak at 115 °C disappears in Rh-Ni/Al₂O₃ strengthens our belief that Rh aluminate could be formed at such severe temperatures.

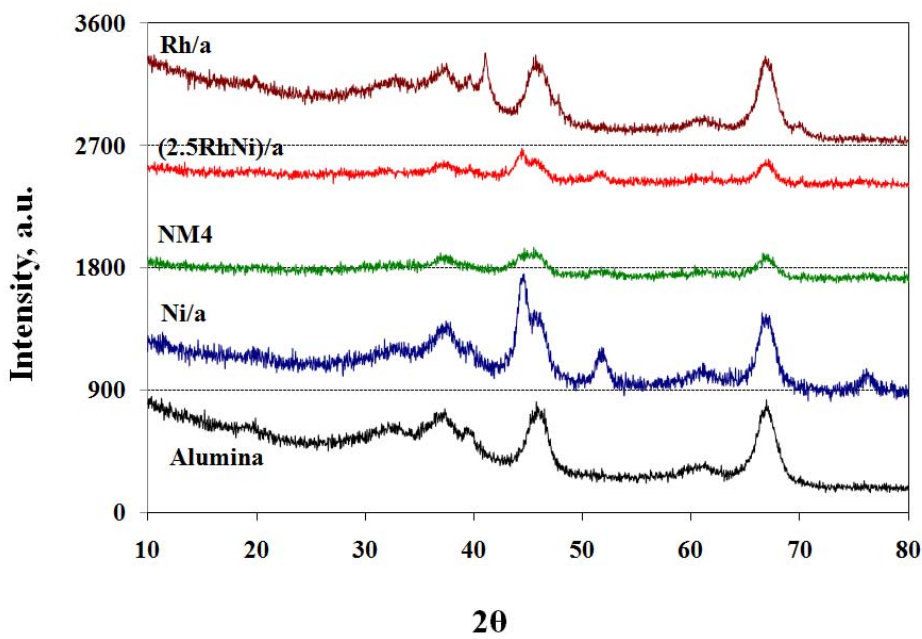


Figure 4-12. XRD profiles of fresh catalysts calcined in air at 800°C and reduced in 5%H₂/N₂ at 800°C

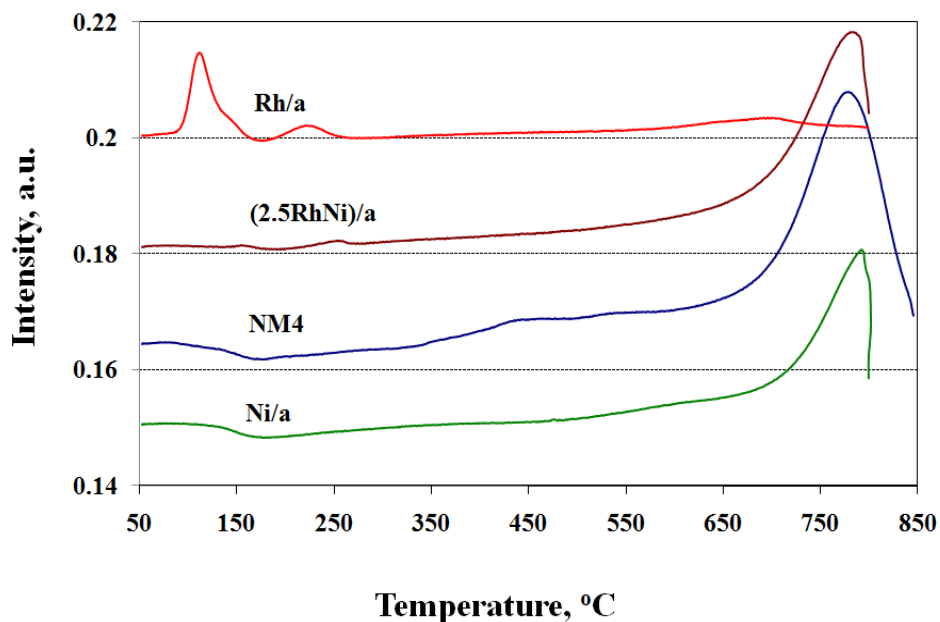


Figure 4-13. TPR profiles of fresh catalysts calcined in air at 800°C

4.3.2. Microscopic structure and composition

Figure 4.14a shows the STEM image of fresh reduced NM4 catalyst while figure 4.14b magnifies a small portion of the same image. It is clearly seen that the fresh catalyst is made of two kinds of particles; larger particles of diameter ranging from 10-20 nm (particle A) and smaller particles of size less than 4 nm (particle B). EDS analysis at these locations, shown in figure 4.14c, reveals that particle A was predominantly Ni while particle B was mainly Rh. For comparison purpose, the baseline of EDS of particle A has been shifted along the intensity axis. The observed size of these particles can be

attributed to the relative resistance to sintering at high temperature. Rh, being a noble metal, is more resistant to sintering and thus remains as small crystallites. EDS patterns of these two particles also showed peaks corresponding to Al. These peaks may either arise from the support in the vicinity or from an alloy species between the metal and the support. The alloying of Ni with alumina to form aluminate is well known, and the formation of Rh aluminate at the high calcination temperatures used in the current study has also been previously reported.^{96,97} Although Rh aluminate is clearly seen in the experiments, its formation is speculated based on the high calcination temperatures, especially in catalysts containing Ni.

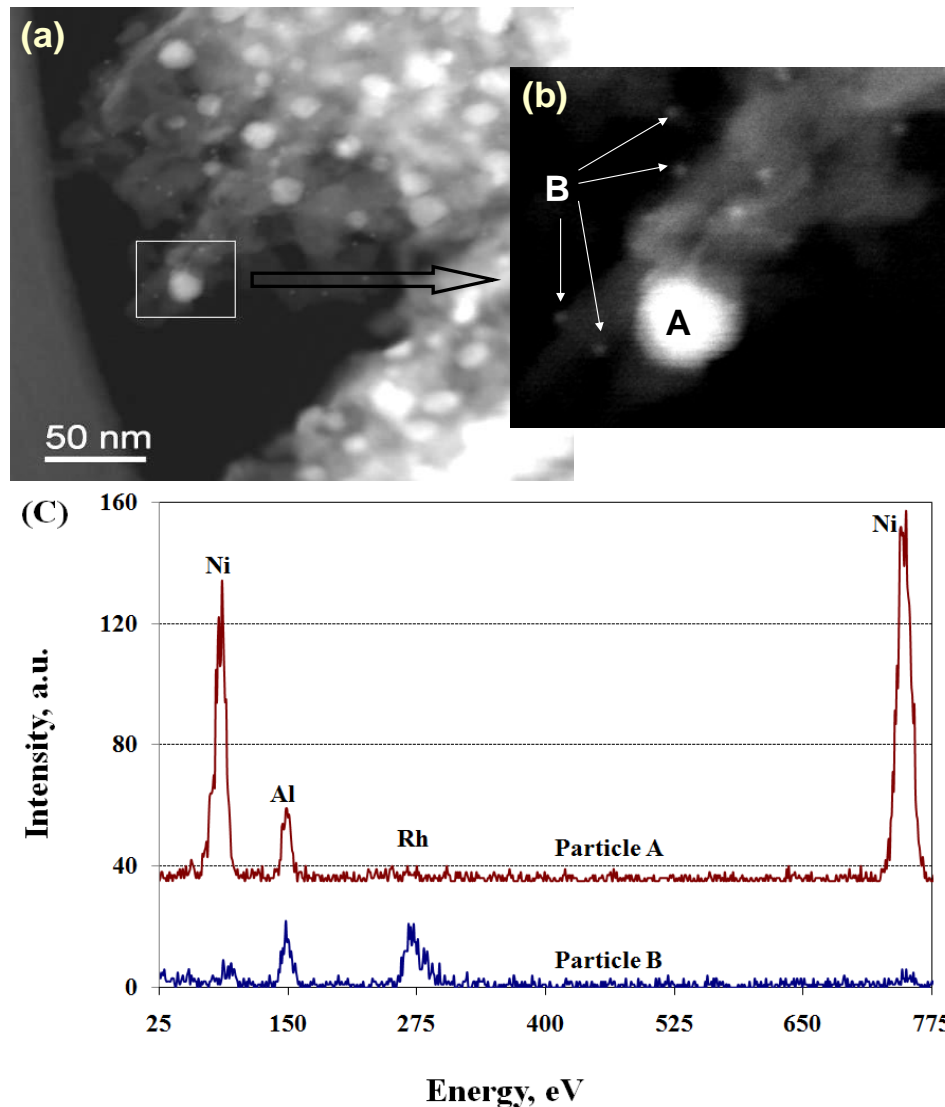


Figure 4-14. EDS analysis of fresh NM4, calcined in air at 800°C and reduced in 5% H_2/N_2 at 800°C. (a) STEM image, (b) Magnification of box in image a, and (c) EDS signature of particles A and B, as seen in b

4.4. Characterization of used catalysts

Catalysts used during steam reforming were recovered after activity testing for 10 h and characterized using XRD, TPR and XPS. NM4 was also characterized using STEM coupled with EDS for the presence of sulfur on the crystallites of Ni and Rh.

4.4.1. Phase structure and Ni crystallite size

Figure 4.15 compares the XRD patterns (with baseline shifted) of used catalysts after steam reforming of sulfur-laden n-hexadecane with that of alumina support. A nearly identical set of XRD patterns was observed for the catalysts used with sulfur-free hexadecane. The peaks for support alumina can be seen unchanged for different catalyst formulations. It was also seen that these peaks remain intact even after reaction, indicating the stability of the support during reaction at high temperatures. The peak at 44° corresponds to Ni^0 , observed for all Ni-containing catalysts, which indicates that Ni was present in the reduced state during reaction. The peak at 41° , corresponding to Rh^0 , was observed for the monometallic Rh catalyst $\text{Rh}/\text{Al}_2\text{O}_3$, but not observed for bimetallic $\text{Rh-Ni}/\text{Al}_2\text{O}_3$ catalysts. This means that Rh species of the bimetallic catalyst was not reduced during steam reforming. This was interesting as the metallic Rh^0 peak was expected to be formed in the reducing environment present during steam reforming. It is unlikely that exposure of the used catalyst to air resulted in the oxidation of Rh^0 back to Rh^{+3} , as this would also have been observed for the monometallic Rh as well. Having said that, oxidation in air cannot be ruled out. Presence of Ni may have some catalytic effect to cause or not cause oxidation of Rh in Rh-containing catalysts.

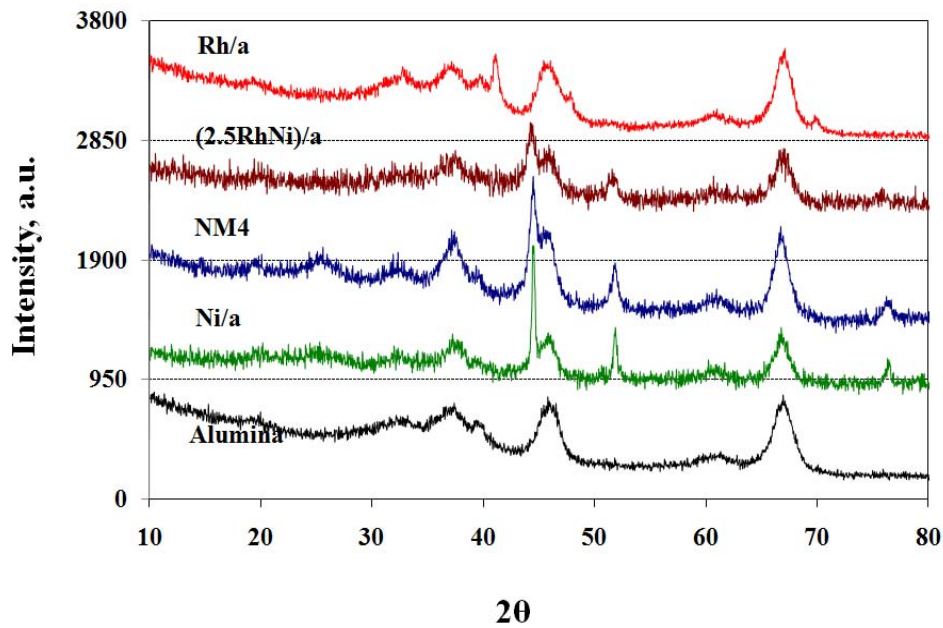


Figure 4-15. XRD patterns of used catalysts, after steam reforming of sulfur-laden n-hexadecane at 800°C, S/C 3 and 1 atm

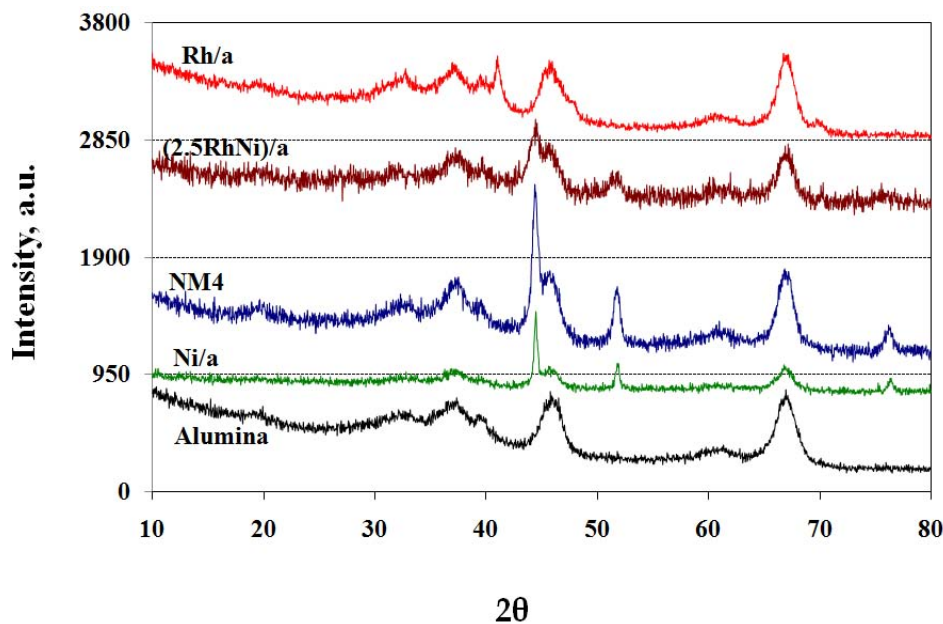


Figure 4-16. XRD patterns of used catalysts, after steam reforming of sulfur-free n-hexadecane at 800°C, S/C 3 and 1 atm

Figure 4.17 shows the XRD patterns of used catalyst NM4 recovered at different TOS to study the effect of time on the phases and crystallite sizes. One of the important observations made was that of nickel particle size. The peak at 44° which corresponds to Ni was seen to get sharper and finer with increasing time on stream. This can be attributed to the increasing particle size of Ni. The Ni particle size was seen to be increasing during the 10 h on stream.

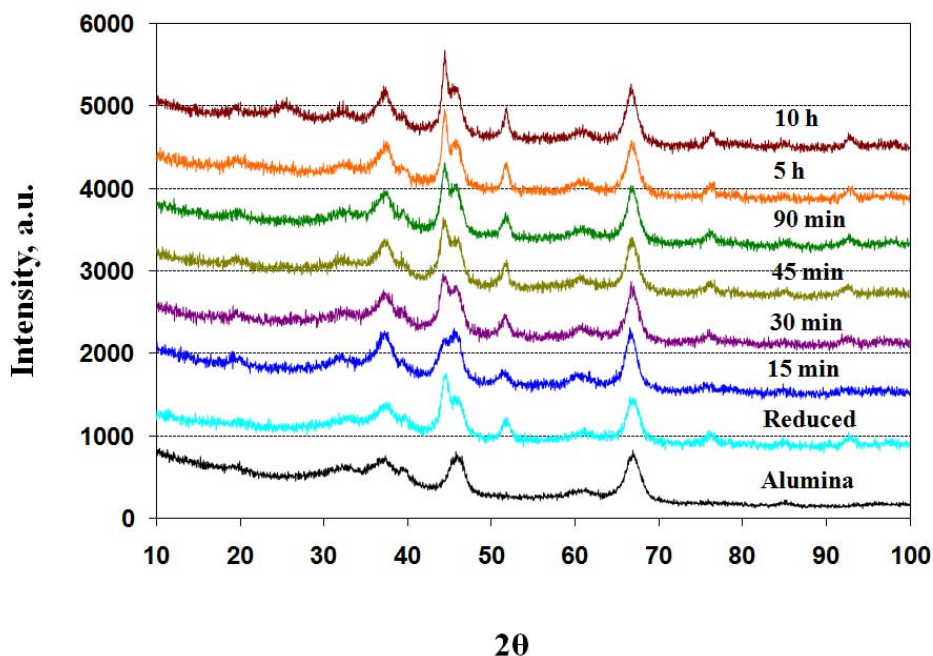


Figure 4-17. XRD patterns of used catalyst NM4 at different TOS, after steam reforming of sulfur-laden n-hexadecane at 800°C , S/C 3 and 1 atm

HRTEM images shown in Figure 4.18 indicated significant Ni particle growth during steam reforming, with the increase dependent on the catalyst composition and choice of

fuel. Sulfur-free reactions on Ni/Al₂O₃ resulted in Ni particle sizes in the range of 70-100 nm; when Rh was added to the catalyst, the size of Ni particles only increased to 25-35 nm. When sulfur was present in the feed, Ni particles grew to about 45 – 55 nm for the Ni-only catalyst while still smaller Ni particles were observed in Rh-Ni catalysts.

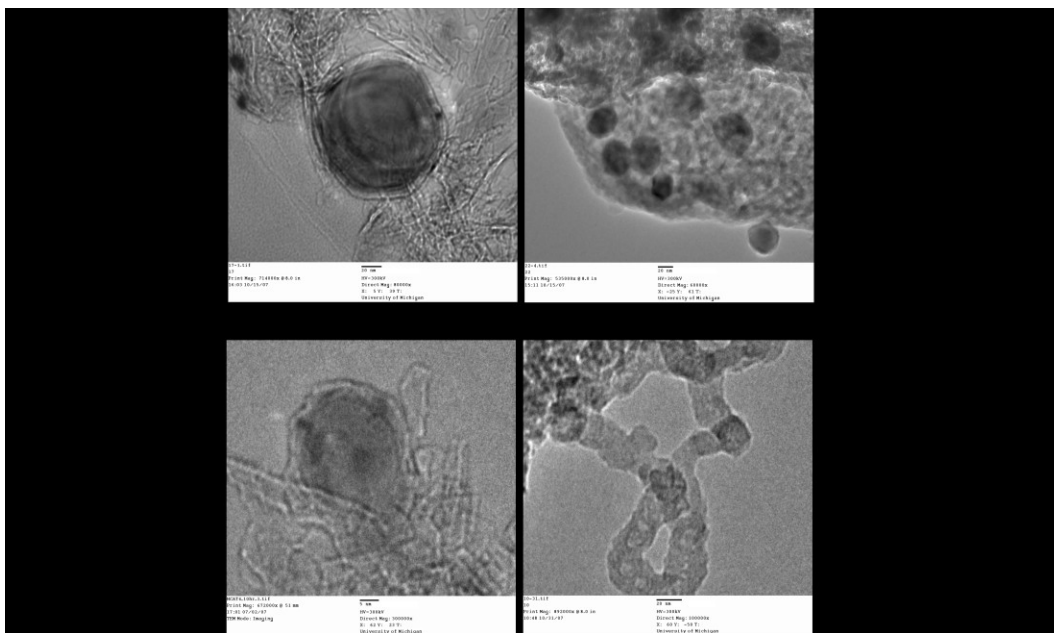


Figure 4-18. HRTEM images of used catalysts, after steam reforming of sulfur-free and sulfur-laden n-hexadecane at 800°C, S/C 3 and 1 atm

4.4.2. Sulfur adsorption studies

EDS was employed to study the bulk and surface composition of used catalysts. Figure 4.19 shows the STEM image of used NM4 after reforming sulfur-doped hexadecane. To investigate the bulk composition of particle A, the center of particle A was analyzed (position 1). To give information of the surface, the edge of particle A was analyzed

(position 2). Particle B (position 3) was only studied as a bulk particle since these particles were too small to permit a location specific scan. Figure 4.21 gives EDS signatures (baseline shifted) at all three positions. Position 1 was predominantly Ni and showed no detectable peak for sulfur. Position 2 (edge), which represents the surface of the Ni particle, showed a clear peak at 230 eV that was assigned to the presence of sulfur. Position 3 revealed a peak at 270 eV, indicative of rhodium, and no significant peak at 230 eV, suggesting that sulfur generally was not adsorbed onto Rh. One may argue that presence of sulfur on the surface of nickel crystallite should be reflected by a peak at 230 eV in position 2 EDS profile. It should be noted that position 2 predominantly scans the bulk of the particle. Presence of sulfur on the surface should only be expected to come as a tiny peak which may or may not be detectable, considering the intensity of nickel peak. Thus, sulfur was predominantly present on the Ni surface and no bulk sulfide was observed. This is in agreement with the results obtained by Bartholomew and Rostrup-Nielsen⁹⁸, who concluded that adsorbed sulfur was more stable than the bulk sulfide and that the surface nickel–sulfur bonds are a factor of three more stable than bulk nickel–sulfur bonds.

Elemental mapping was also performed on the used catalysts to more fully define the locations for sulfur adsorption. Figure 4.20 illustrates this result for the used NM4; similar data is available for used (2.5RhNi)/a. The location of sulfur aligns well with that of Ni particles. However, a small amount of sulfur is also found at locations other than Ni particles, although it is not known if these correspond to Rh particles or the alumina support. The high concentration of sulfur on the nickel particles indicates preferential adsorption, suggesting that Ni acts as a sacrificial site to take up sulfur while protecting

Rh, which remains active for steam reforming. A similar postulate was made by Strohm *et al.*, though no direct evidence was provided at that time.⁹⁹

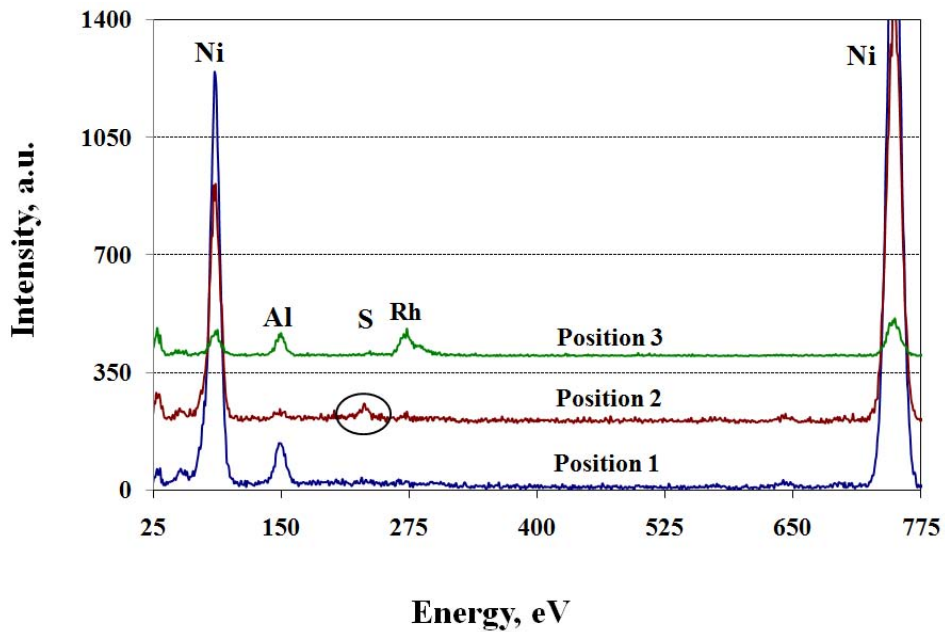
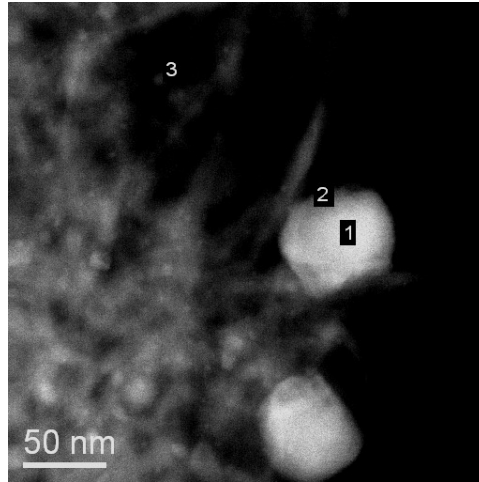


Figure 4-19. EDS analysis of used NM4 after steam reforming of sulfur-laden n-hexadecane at 800°C, 1 atm, S/C=3 and 1000 ppm sulfur (a) STEM image, and (b) EDS signature at positions 1, 2 and 3

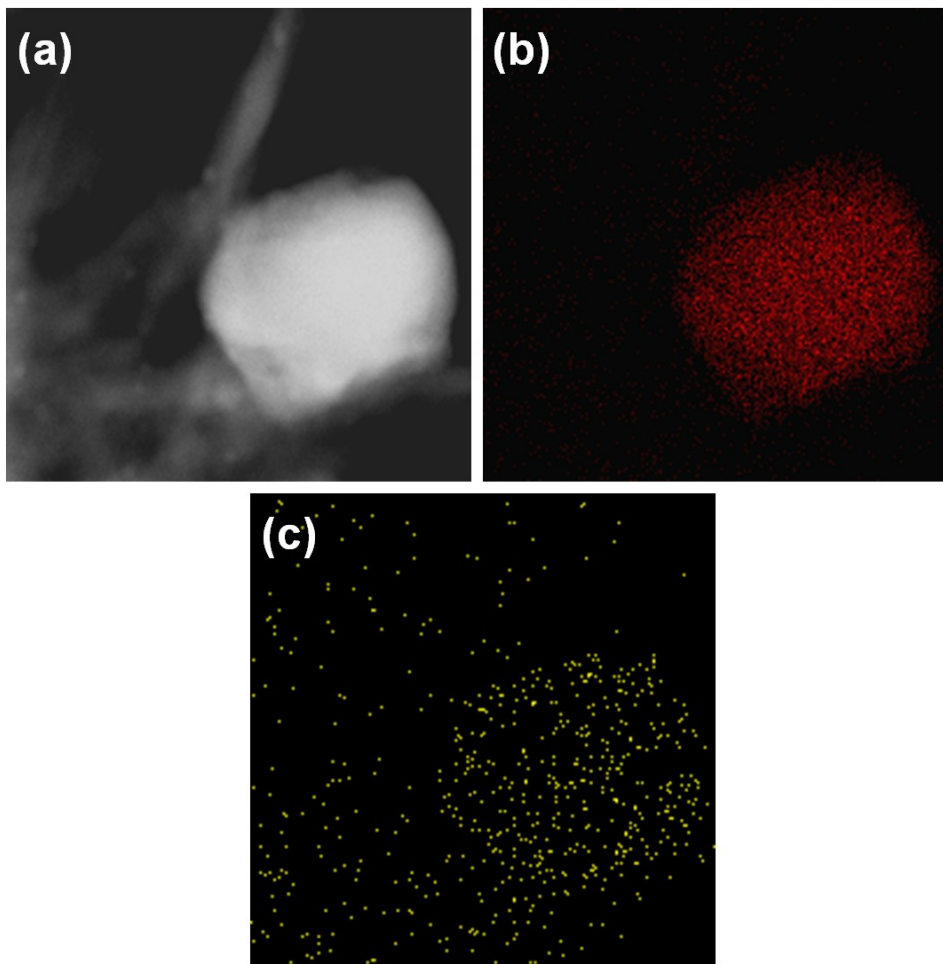


Figure 4-20. Elemental mapping analysis of used NM4 after steam reforming of sulfur-laden n-hexadecane at 800°C, 1 atm, S/C=3 and 1000 ppm sulfur (a) STEM image, (b) nickel mapping, and (c) sulfur mapping

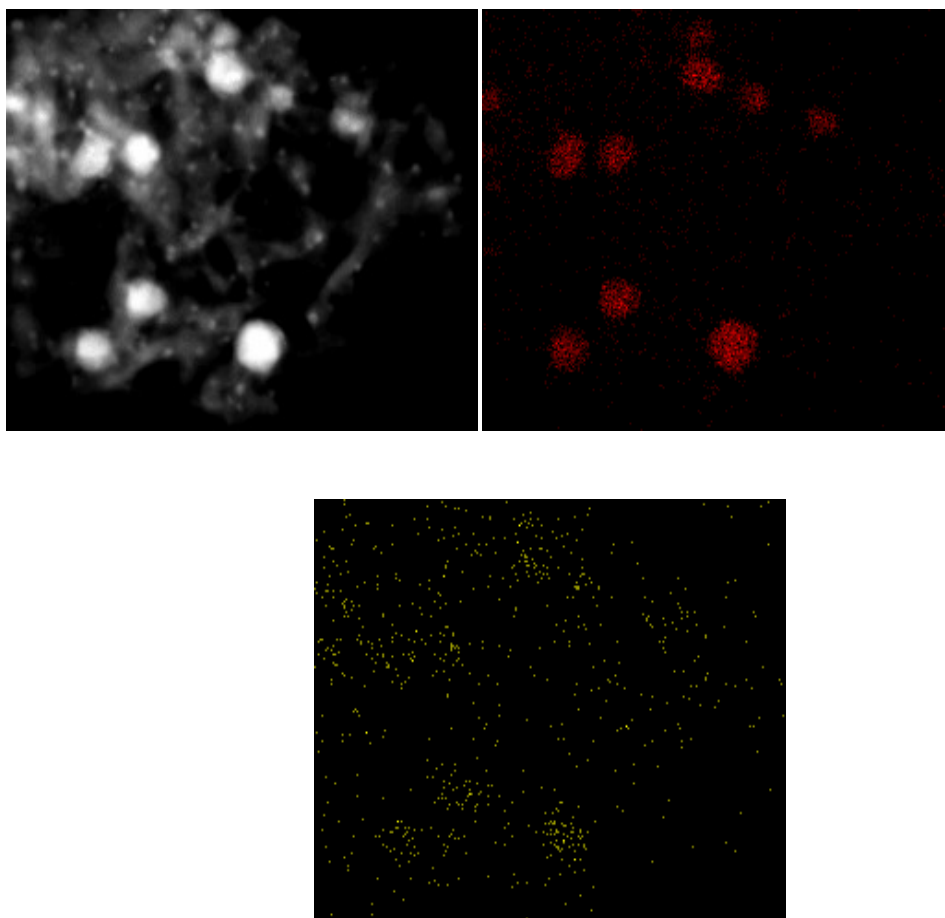


Figure 4-21. Elemental mapping analysis of used (2.5RhNi)/a after steam reforming of sulfur-laden n-hexadecane at 800°C, 1 atm, S/C=3 and 1000 ppm sulfur (a) STEM image, (b) nickel mapping, and (c) sulfur mapping

4.4.3. Carbon deposition studies

Deactivation occurs both through sulfur deposition and coke formation. TPO of the used catalyst was employed to understand both the quantity and quality of coke formed on the catalyst. Figure 4.22 shows the TPO profiles of used NM4 from reforming experiments completed with both sulfur-free and sulfur laden feed. Varying peak maxima observed within a sample indicate that there are coke deposits in the catalyst having different reactivity with oxygen. In the current case, a low temperature peak can be seen at around

180°C while two high temperature peaks are observed at 570°C and 770°C for the catalyst that was used with sulfur-containing fuel. The low temperature peak is typically assigned to coke deposited in the vicinity of metal particles while the high temperature peaks are attributed to the carbon residues in close contact with the support.¹⁰⁰

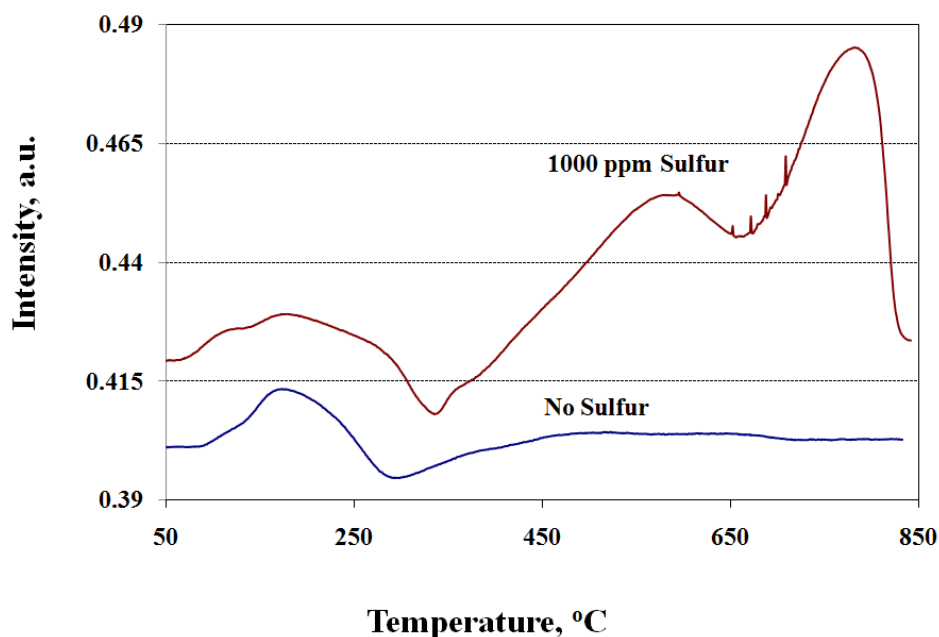


Figure 4-22. TPO of used catalyst NM4 after steam reforming of sulfur-free and sulfur-laden n-hexadecane at 800°C, S/C 3 and 1 atm

Based on these assumptions, the area under the high temperature peaks (using valley to valley baseline) was used to estimate the amount of the carbon deposited on the catalyst support during the reaction. This area was calibrated based on CO₂ produced in the exit gas during the TPO experiment; the resulting CO₂ yield was converted to carbon deposition assuming that all carbon was burned off the catalyst surface and then normalized against the catalyst weight and is shown as a function of catalyst composition in figure 4.23. Minimal carbon deposition was observed in the case of sulfur-free runs.

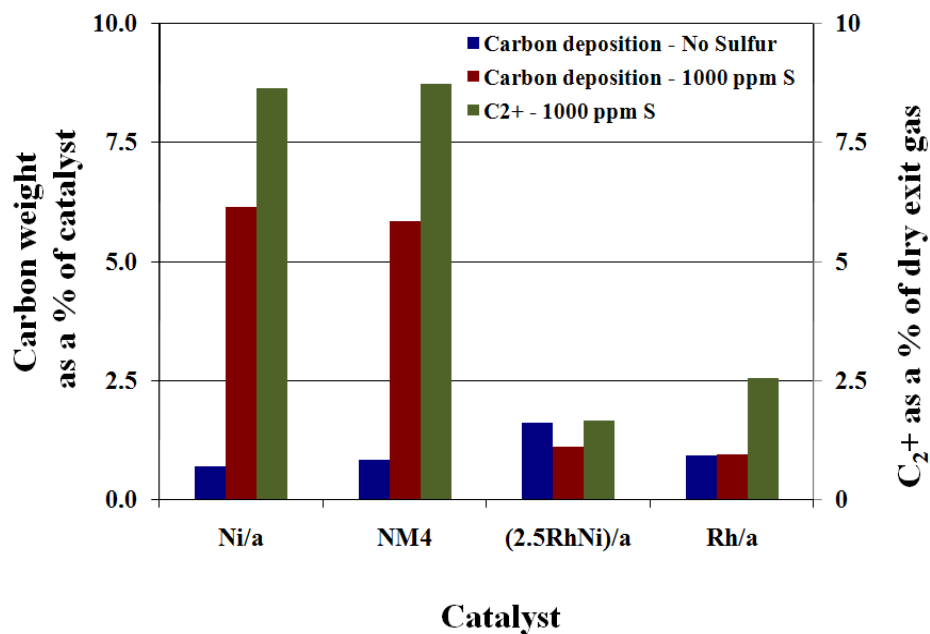


Figure 4-23. Carbon deposition on the catalyst (based on integration of TPO, as described in text) and C₂+ in dry exit gas during steam reforming n-hexadecane at 800°C, 1 atm, S/C=3.

During sulfur-doped runs, excessive carbon deposition was seen when the Rh loading of the catalyst was relatively low. Because the carbon was burned off the catalyst during the high temperature portion of the TPO, it can be attributed to depositions in close vicinity of the support. The carbon formation can also be compared with the gas composition produced during the steam reforming reaction, as C₂+ products (% dry basis) in the effluent stream. A close relation between the amount of cracked products in the reformat and the amount of carbon deposition on the support during the course of steam reforming was observed. In the presence of sulfur, catalysts Ni/Al₂O₃ and NM4 had high carbon deposition, in addition to high C₂+ production while catalysts containing 2.5 wt % Rh showed relatively low carbon deposition.

The carbon deposition was confirmed using STEM images coupled with carbon mapping for NM4 and (2.5RhNi)/a catalysts, shown as figure 4.24. While carbon is seen extensively throughout the surface for catalyst with only 0.5% Rh, much less carbon is observed for the high Rh material. In both cases, carbon is distributed fairly uniformly throughout the sample. One of the explanation is that hydrocarbon adsorbed on the sulfur poisoned Ni surface may migrate to the alumina support, where it can undergo acid site cracking, as proposed previously by Bickle and Khoobiar.¹⁰¹ According to the authors, when sulfur in the fuel was higher than 500 ppm, hydrocarbon that adsorbed on the sulfur poisoned metal site was transferred to the nearby support surface where it underwent acid site cracking. Although there is no clear evidence to support this speculation, subsequent data obtained using XPS helps in understanding the morphology of carbon species deposited on the catalyst.

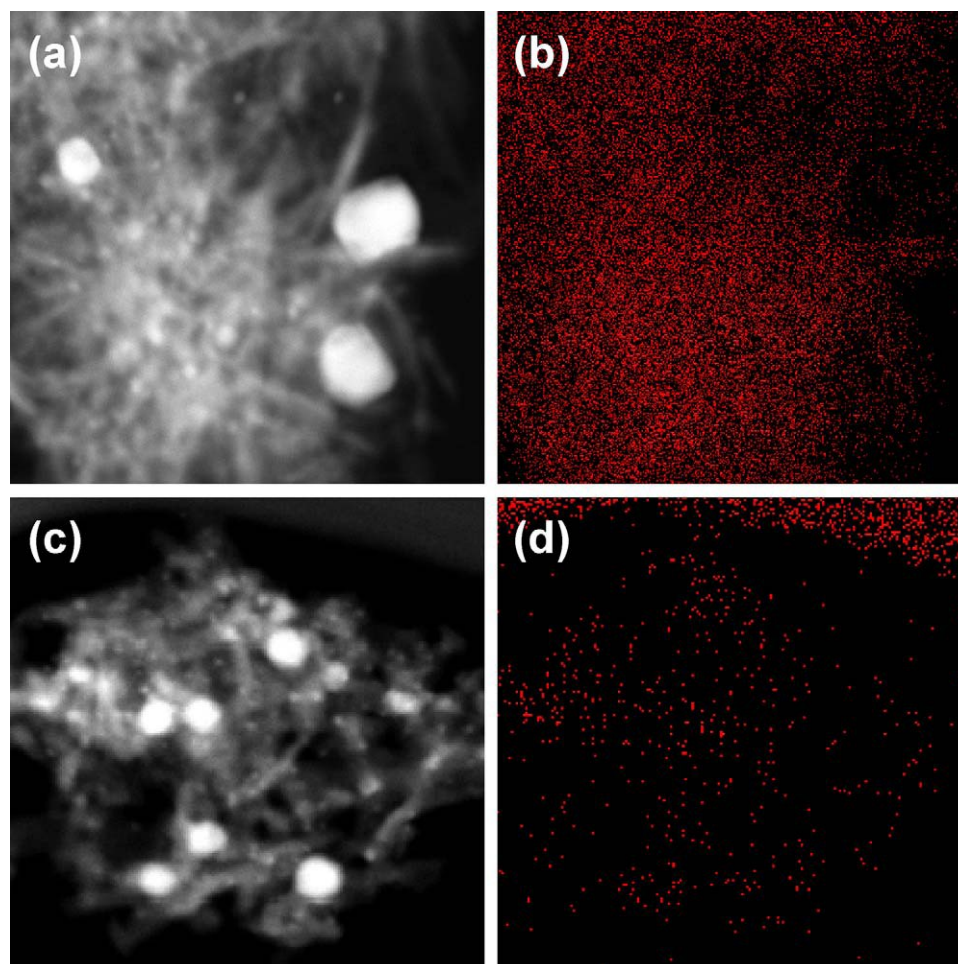


Figure 4-24. Carbon mapping of used catalysts, after steam reforming of sulfur-laden n-hexadecane at 800°C, 1 atm, S/C=3 and 1000 ppm sulfur (a) STEM image and (b) carbon mapping of NM4, and (c) STEM image and (d) carbon mapping of (2.5RhNi)/a.

C1s XPS of the used catalysts, shown in figure 4.25a, provides further information on carbon deposition during steam reforming. The baseline for intensity is shifted for comparison purpose. A survey scan was first determined and core analysis was done for elements of interest. All catalysts used for reforming of sulfur-free feeds showed only one peak at around 284.7 eV (shown only for the Ni/a catalyst in figure 4.25a). This peak is

attributed to the hydrocarbonaceous and/or graphitic type of carbon¹⁰² and was present irrespective of the catalyst formulation. Ni/Al₂O₃ and NM4 catalysts, when used for reforming of sulfur-laden feeds, displayed a peak at 286.3 eV, attributed to a polymeric and/or aromatic type of carbon species and a second peak at about 283.5 eV.¹⁰³ This small component at the lower binding energy corresponds to isolated carbon atoms and small non-polymerized fragments on support acid sites. Catalysts containing higher Rh content only contained a single peak at 284.7 eV, indicating that higher amounts of Rh inhibited the formation of aromatic/polymeric type of carbon when sulfur was present. Recall that the Ni/Al₂O₃ and NM4 catalysts deactivated more rapidly than the catalysts containing higher percentages of Rh, suggesting that formation of aromatic/polymeric carbon was a primary deactivation mechanism. S 2p XPS was also done on the used 3J1 to determine the presence of sulfur on the surface of catalyst but no detectable peaks were observed in the region of interest (166-169 eV). This is also a confirmation that the surface of catalyst was excessively covered with carbon which masks the sulfur adsorbed on the catalyst surface. It may also be possible that the amount of sulfur adsorbed was below the detectable limit of the instrument.

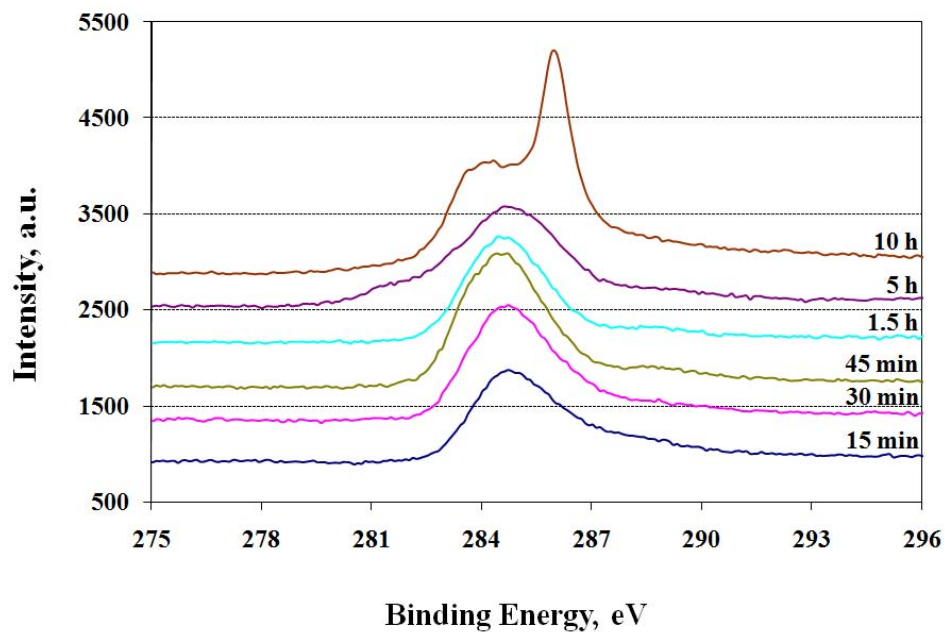
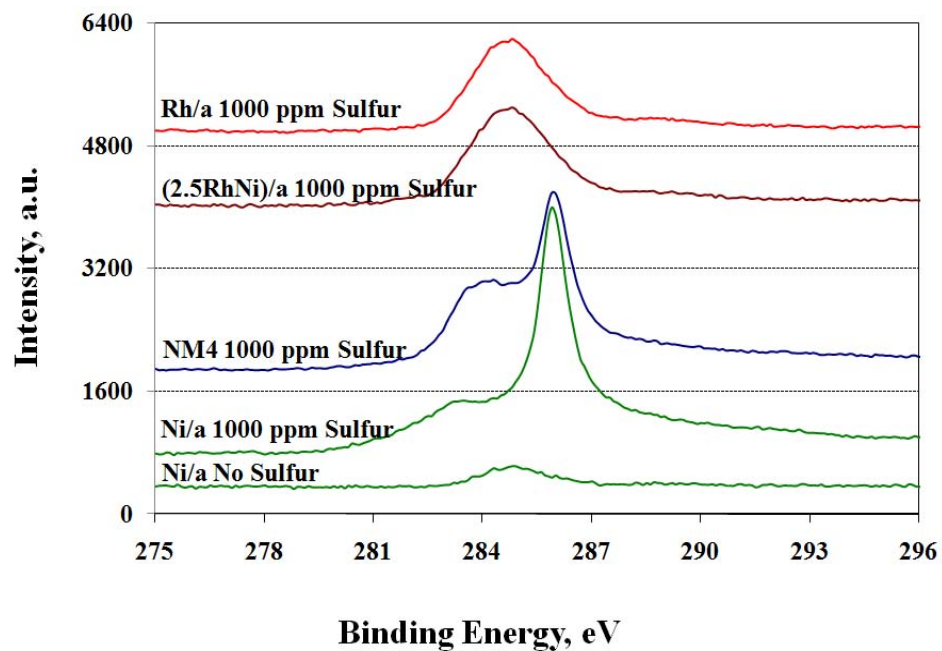


Figure 4-25. C 1s XPS of used catalysts, after steam reforming of n-hexadecane at 800°C, 1 atm and S/C=3 (a) sulfur-free and sulfur laden runs, and (b) sulfur-laden run on NM4 taken as a function of time on stream

It was previously suggested that aromatization of alkene intermediates occurs by Diels-Alder reaction, as verified by Parera *et al.*¹⁰⁴ To demonstrate this phenomenon, analysis of the C1s peaks was done at different stages of the reaction starting from 15 min to 10 h time on stream. Figure 4.25b shows the evolution of these peaks (baseline shifted) as a function of time on stream for reforming of sulfur laden fuel by NM4 catalyst. It was interesting to see that the aromatic carbon peak was only formed after 5 h on stream, indicating the formation of these species only after longer time on stream. This suggests that the rate of the Diels-Alder reaction leading to aromatic/polymeric carbon formation increases with time on stream, either because of the increase of the concentration of the coke precursors on the catalyst surface or deactivation of the gasification reactions.

Carbon was also deposited in the form of whiskers after steam reforming of sulfur-doped fuel on catalyst NM4. The same was not observed in case of sulfur free runs. Figure 4.26 shows the STEM image of used NM4 after steam reforming of sulfur doped fuel. Position 1 shows the nickel particle while position 2 shows carbon whisker that precipitated out of the nickel crystallite. Formation of carbon whiskers in case of conventional steam reforming catalysts is well known. Hydrocarbons dissociate on the nickel surface to produce highly reactive carbon species. Most of the carbon is gasified but some is converted to less reactive carbon, probably by polymerization and rearrangement. The carbon may encapsulate the nickel particulate, may be gasified or may dissolve in the nickel crystallite. The dissolved carbon diffuses through the nickel to nucleate and precipitate at the rear of the crystallite. This process leads to formation of a carbon whisker. This is one of the few cases where carbon formation does not lead to deactivation, although it results in pressure build up in industrial applications. The same

is seen in the present study of steam reforming of sulfur doped fuel on nickel containing catalysts. Carbon whiskers were not observed in sulfur free runs. Formation of carbon whiskers leads to clogging and thereby causing pressure drop across the catalyst bed, leading to fouling and eventual deactivation.

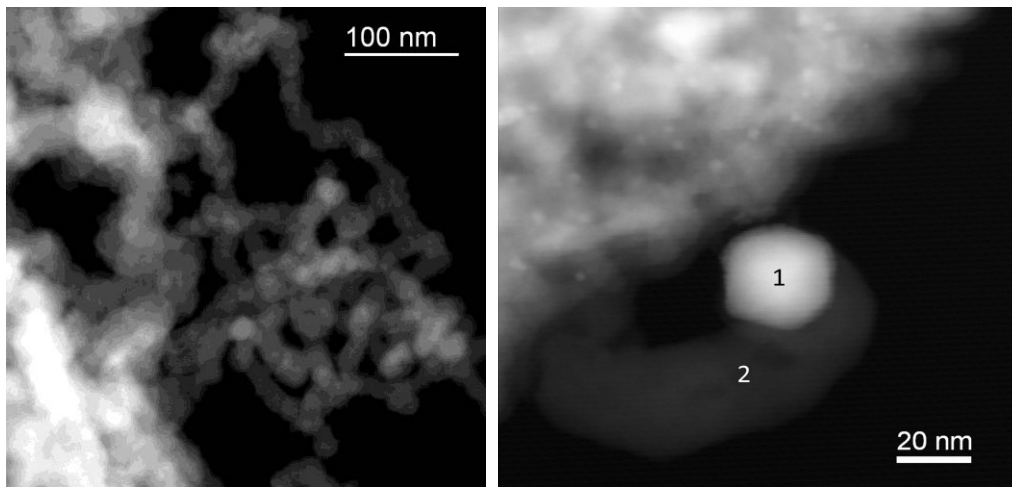


Figure 4-26. STEM image of used NM4 catalyst showing presence of carbon whiskers after steam reforming of sulfur-laden n-hexadecane at 800°C, 1 atm and S/C=3

Chapter 5

Analysis of deactivation mechanism on 3J1

5.1.Introduction

As mentioned in the earlier section, the use of logistic fuel for hydrogen generation can be an attractive short term alternative to drive the fuel cell industry. The previous chapter was focused on understanding deactivation during steam reforming of diesel surrogate on a bimetallic catalyst (NM4 containing Rh and Ni). In the present chapter, an attempt has been made to understand deactivation on a ternary catalyst (3J1 containing Rh, Pd and Ni) during steam reforming of jet fuel. Jet fuel is more difficult fuel than diesel for reforming, mostly due to high content of coke precursors, and specifically the presence of methyl naphthalenes. Moreover, the sulfur content in jet fuel is often more than 1000 ppm, which is about 2 orders of magnitude more than in diesel.

At the start of the project, jet fuel was not available and therefore a simulated fuel was used to study deactivation. In the later part of the study, Jet A was used. Although a comparison has been made between the performances of the two liquid fuels, catalyst characterization was accomplished only in case of catalysts tested with Jet A.

Jet fuel (Jet A) was obtained from the local aviation center. This ‘as received’ fuel

contained 183 ppm sulfur by weight. For deactivation studies, sulfur was externally added in the form of thiophene to increase the sulfur level to 1000 ppm by weight. Since jet fuel was not available at the start of the project, kerosene was initially used to identify the key components present in the fuel. Analysis was completed using HP 6890/5973 GC/MS.

Figure 5.1 shows a GC-MS chromatogram of kerosene. The peaks were identified and marked accordingly in the chart. Kerosene contains a very high proportion of normal and substituted paraffins, ranging from C₁₃ to C₁₈. Along with the paraffins, various types of monocyclic and bicyclic aromatic compounds were also present in a significant amount. Substituted benzenes, especially toluene and naphthalene, were the dominant species amongst the aromatic compounds.

In an attempt to represent this complex mixture, a feed containing 70% hexadecane, 15% toluene, 10% tetralin and 5% methylnaphthalene, by weight, was used. For the deactivation studies, thiophene was chosen as the surrogate to represent sulfur compounds in diesel.

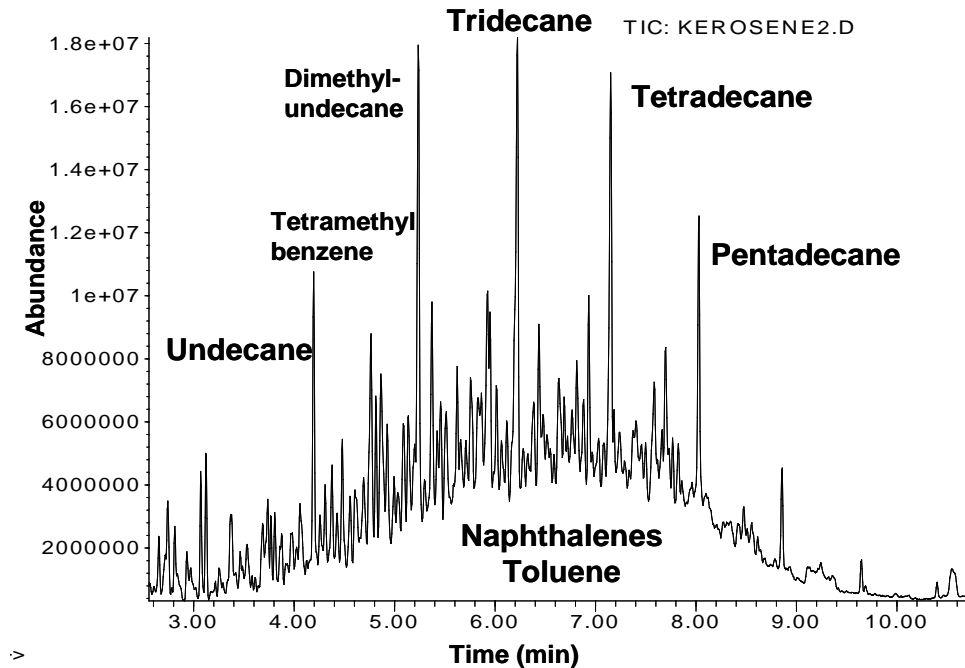


Figure 5-1. Gas chromatograph of kerosene performed on Hewlett Packard 6890/5973 GC/M

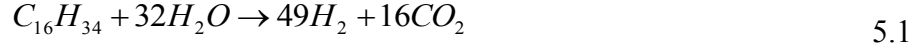
5.2. Selection of process parameters to study deactivation

Process parameters, temperature, pressure and steam to carbon ratio were kept the same as used in the earlier study. Steam reforming was conducted at 800°C, 1 atm and a steam to carbon ratio of 3, unless otherwise mentioned.

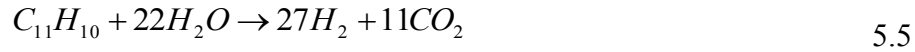
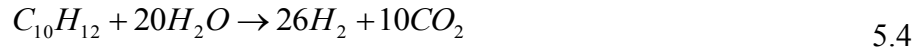
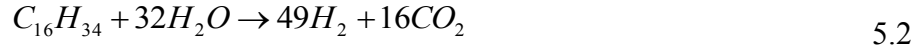
5.3. Hydrogen yield

Hydrogen yield was used as a quantitative measure of catalyst performance and a means of comparison amongst various catalysts. It was defined as the percentage ratio of the flow rate of hydrogen obtained in the product stream to the flow rate of hydrogen one would expect if all of the fuel were converted to hydrogen and carbon dioxide. Since the exact composition of jet fuel was unknown, complete steam reforming of jet fuel was

approximated by assuming that the hydrocarbon part could be represented by the simulated fuel.



The steam reforming of simulated fuel consisted of the following four reactions.



One mole of simulated fuel would yield 49.9 moles of hydrogen if all the fuel was converted to carbon dioxide and hydrogen. Thus, hydrogen yield for simulated fuel steam reforming would be the percentage ratio of molar flow rate of hydrogen in the product gas to 49.9 times the molar flow rate of simulated fuel fed in.

$$H_2 \text{ yield} = \frac{F_{H_2, out}}{49.9 F_{nHex, in}} \times 100 \quad 5.6$$

5.4. Steam reforming of Simulated fuel and Jet A

5.4.1. Activity and deactivation

Catalysts were tested for steam reforming of both simulated fuel and jet fuel at 800°C, atmospheric pressure, and S/C of 3. The effect of sulfur was investigated by doping the fuels with thiophene to 1000 ppm by weight. Since jet fuel already had 183 ppm sulfur, an additional 817 ppm was added in the form of thiophene. H₂ yields were used to demonstrate the activity of the catalysts toward steam reforming of both simulated fuel and jet fuel with 1000 ppm S. Figure 5.2 compares the amount of H₂ produced relative to that obtained at the beginning of an experiment as a function of time on stream during the steam reforming carried out on Ni/b. The initial yield was estimated by a straight line fitting of yield over a period of 10 h. In general, the catalysts Ni/b, Pd/b and Ni-Pd/b (not containing Rh) deactivated fairly rapidly even in the absence of sulfur. Moreover, these catalysts not containing Rh deactivated more in the presence of the sulfur. In short, Rh containing catalysts gave better yields with lesser deactivation over a period of 10 h. For all catalyst formulations shown in figures 5.2-5.8, the addition of thiophene in the feed generally increased the total amount of deactivation observed over 10 h of steam reforming. However, in case of Ni-Rh/b and (PdRh)/b catalysts, the relative yield of hydrogen over 10 h on stream did not change much with the addition of sulfur. It is, however, important to make the reader aware that both, the relative hydrogen yield and the actual initial yield shown in figure 5.9, should be taken into consideration to better understand the performance of a given catalyst.

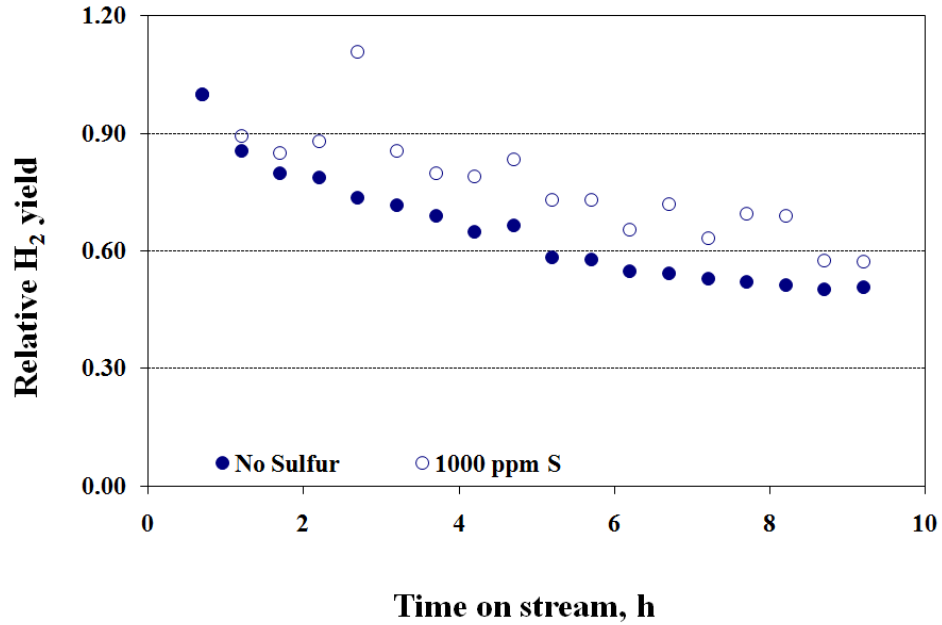


Figure 5-2. Relative H₂ yields of catalyst Ni/b during steam reforming of Simulated fuel No sulfur and Jet fuel 1000 ppm sulfur at 800°C, S/C3 and 1 atm

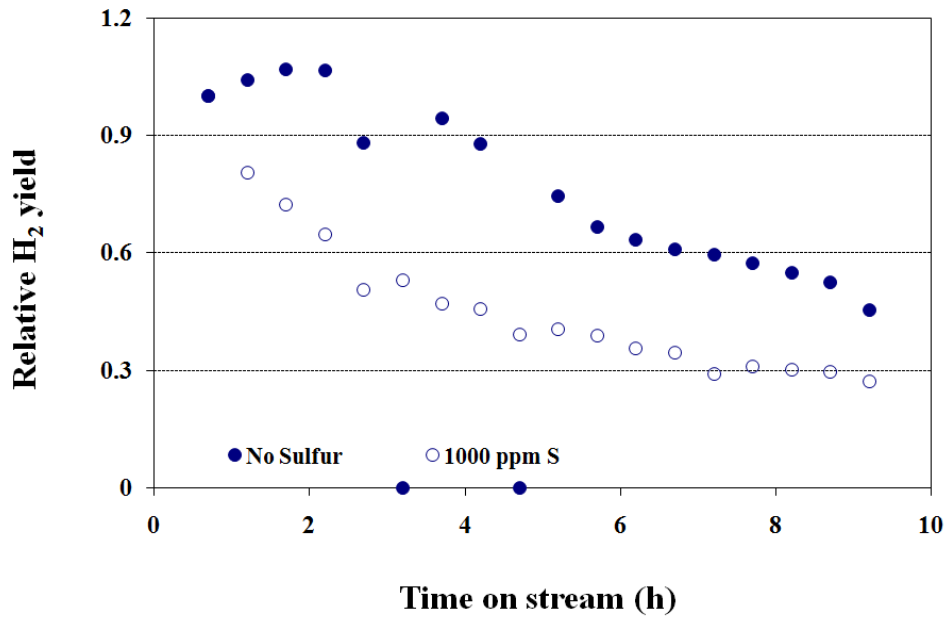


Figure 5-3. Relative H₂ yields of catalyst Pd/b during steam reforming of Simulated fuel No sulfur and Jet fuel 1000 ppm sulfur at 800°C, S/C3 and 1 atm

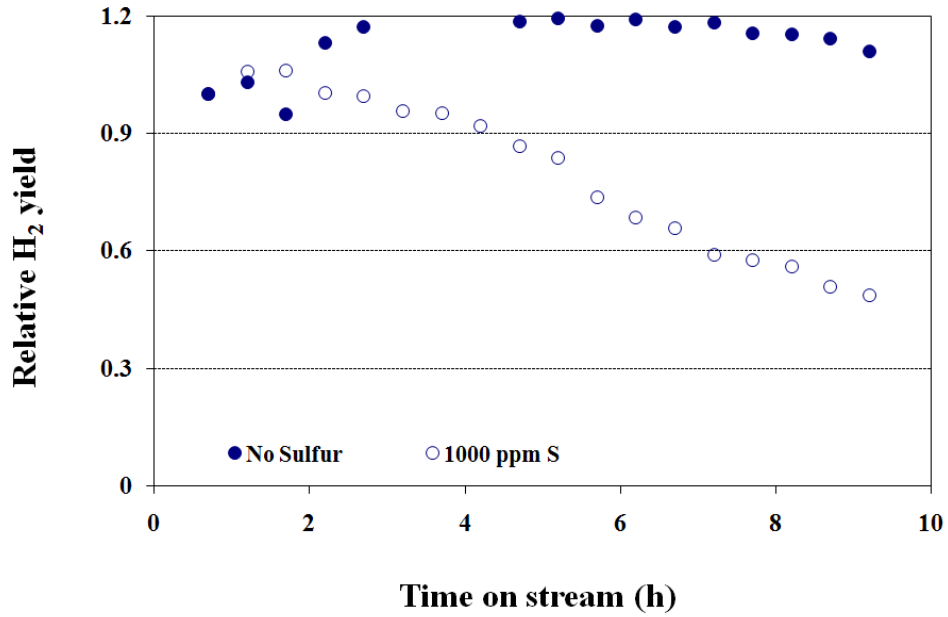


Figure 5-4. Relative H₂ yields of catalyst Rh/b during steam reforming of Simulated fuel No sulfur and Jet fuel 1000 ppm sulfur at 800°C, S/C3 and 1 atm

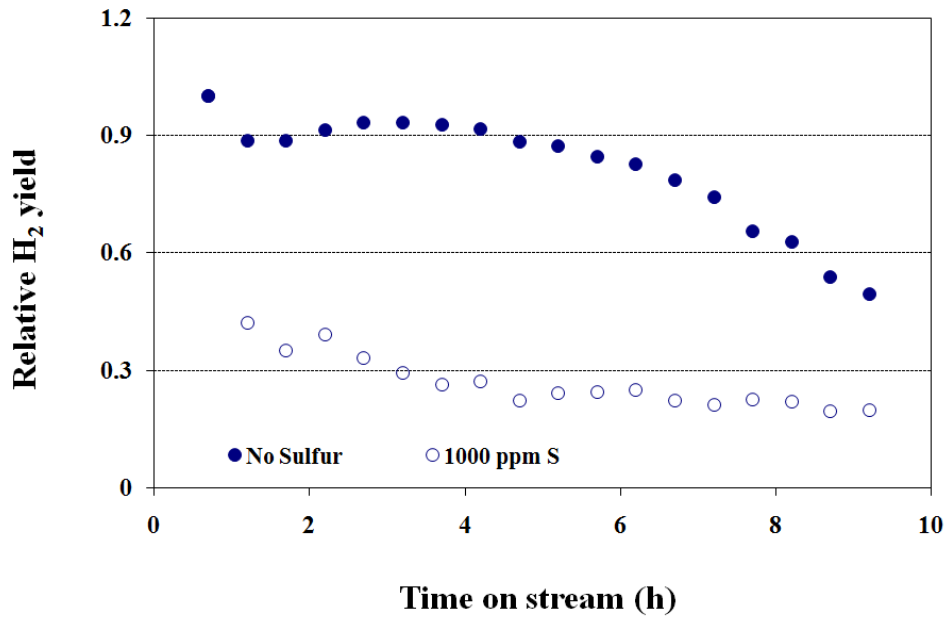


Figure 5-5. Relative H₂ yields of catalyst Ni-Pd/b during steam reforming of Simulated fuel No sulfur and Jet fuel 1000 ppm sulfur at 800°C, S/C3 and 1 atm

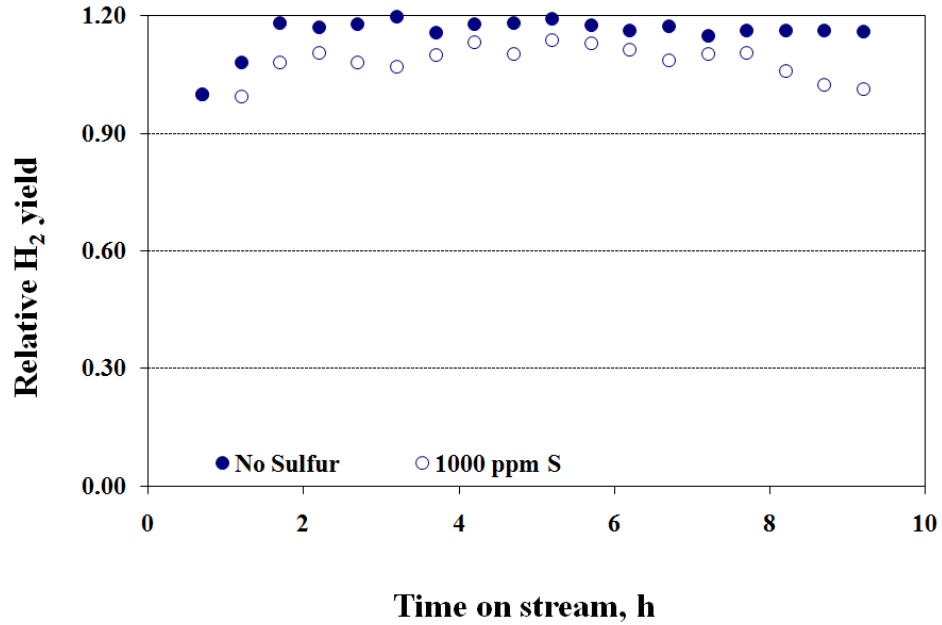


Figure 5-6. Relative H₂ yields of catalyst Ni-Rh/b during steam reforming of Simulated fuel No sulfur and Jet fuel 1000 ppm sulfur at 800°C, S/C3 and 1 atm

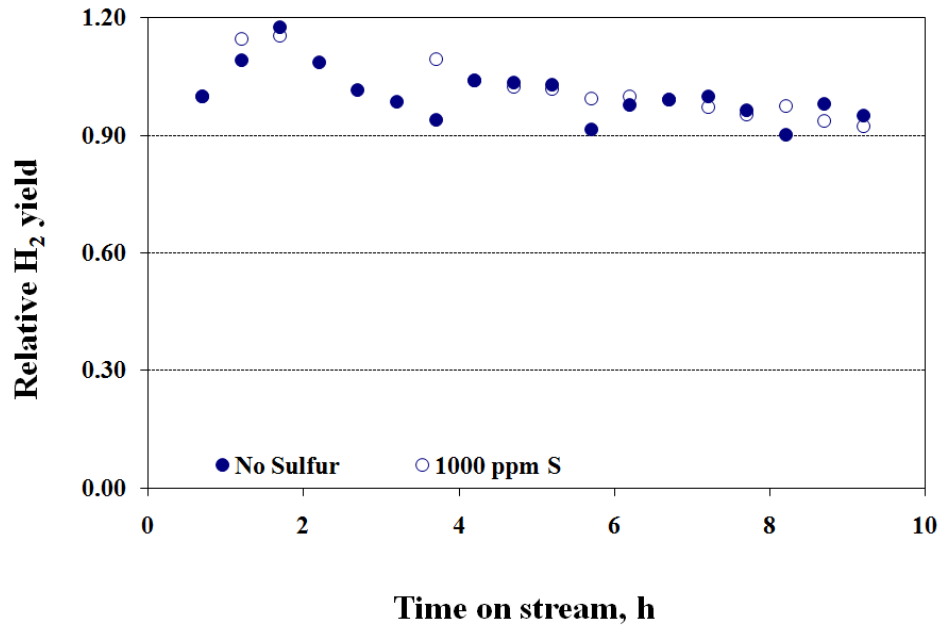


Figure 5-7. Relative H₂ yields of catalyst (PdRh)/b during steam reforming of Simulated fuel No sulfur and Jet fuel 1000 ppm sulfur at 800°C, S/C3 and 1 atm

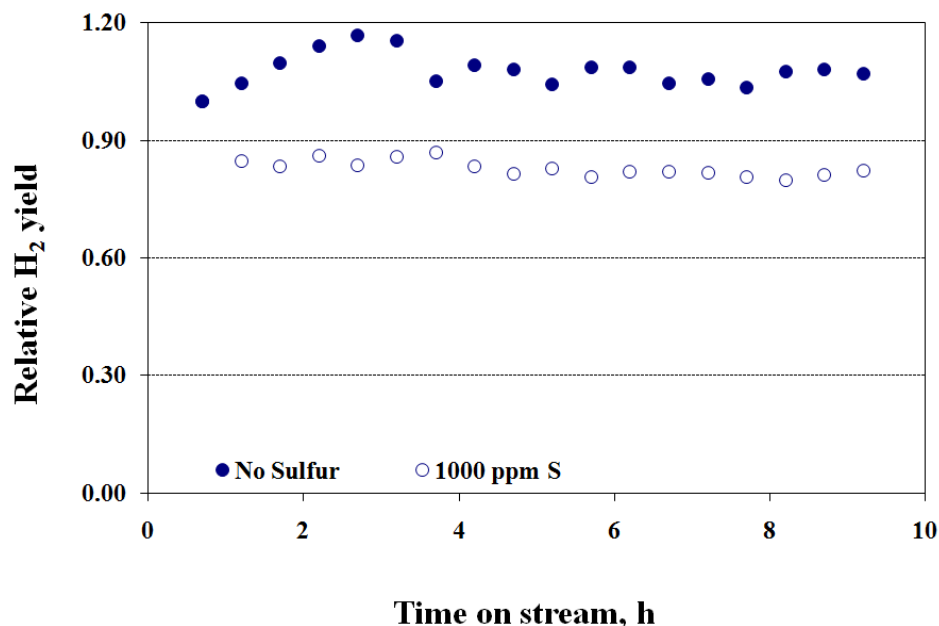


Figure 5-8. Relative H₂ yields of catalyst 3J1 during steam reforming of SF No S and JF 1000 ppm S at 800°C and 1 atm.

To compare the relative activities of each of the catalysts towards steam reforming, kinetic parameters, mainly initial reaction rate and the rate of deactivation, were evaluated in the manner described earlier. Table 5.9 summarizes the catalyst performance in terms of initial activity for all formulations. In general, the catalysts containing Rh exhibited better activity than other catalysts. Deactivation was relatively higher in case of Pd containing catalysts. Catalysts started at a high initial activity before declining during the 10 h period of reaction.

In case of rhodium containing catalysts (except Rh/b), jet fuel reforming gave slightly better initial activity than the simulated counterpart. Although the composition of simulated fuel was modeled on jet fuel, the compositions differ by more than the

presence of sulfur. The presence of certain coke precursors like methylnaphthalenes can have a large effect on the degradation of catalysts due to carbon deposition, as was previously demonstrated by Kataria et al. The slightly lower yields in the case of sulfur laden jet fuel reforming on multicomponent catalysts containing rhodium can be attributed to the presence of such precursors which can have far more detrimental effect than sulfur poisoning. It can also be argued that the over longer times on stream, the sulfur laden fuel will reach a lower hydrogen yield than the sulfur free run. This is evident from the fact that sulfur laden fuel deactivates at a higher rate than sulfur free fuel.

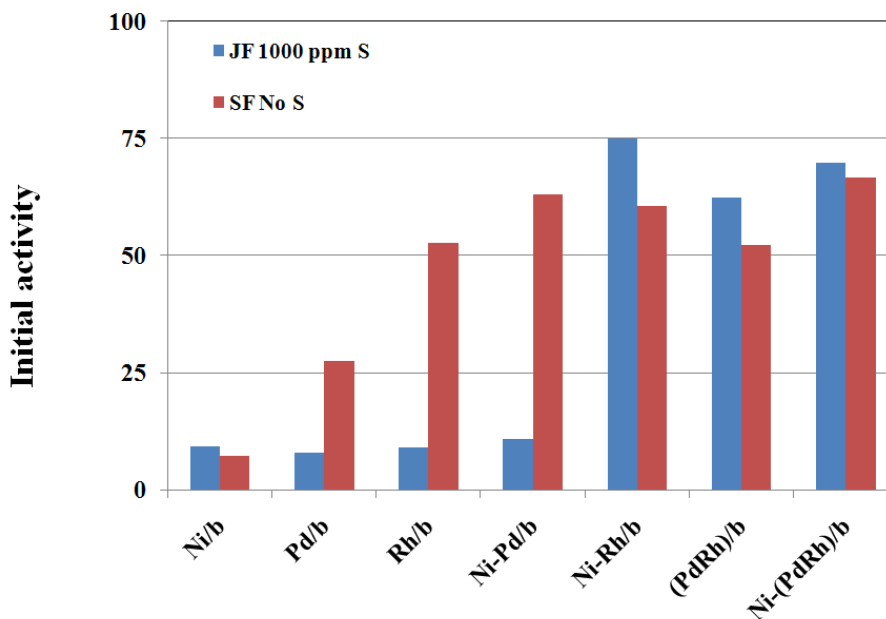


Figure 5-9. Initial activity in terms of hydrogen yield evaluated by straight line fitting of reaction data for different catalyst formulations during steam reforming of Simulated fuel No sulfur and Jet fuel 1000 ppm sulfur at 800°C, S/C3 and 1 atm

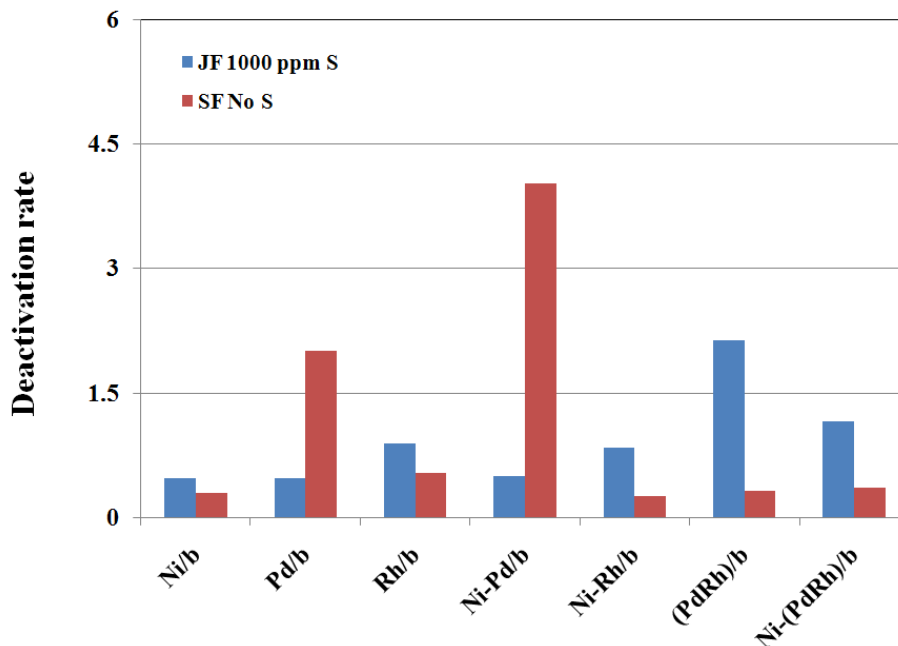


Figure 5-10. Deactivation rate in terms of hydrogen yield per hour evaluated by straight line fitting of reaction data of different catalyst formulations during steam reforming of Simulated fuel No sulfur and Jet fuel 1000 ppm sulfur at 800°C, S/C3 and 1 atm

Figure 5.11 and 5.12 gives the product composition on water free basis during the steam reforming of SF No S and JF 1000 ppm S on 3J1 catalyst. The values of hydrogen mole fraction were slightly lowered in the presence of sulfur in the fuel during the course of 10 h reforming. The stability of the product composition, coupled with the previously observed deactivation, makes it reasonable to postulate that the mechanism of reaction did not change with the addition of sulfur.

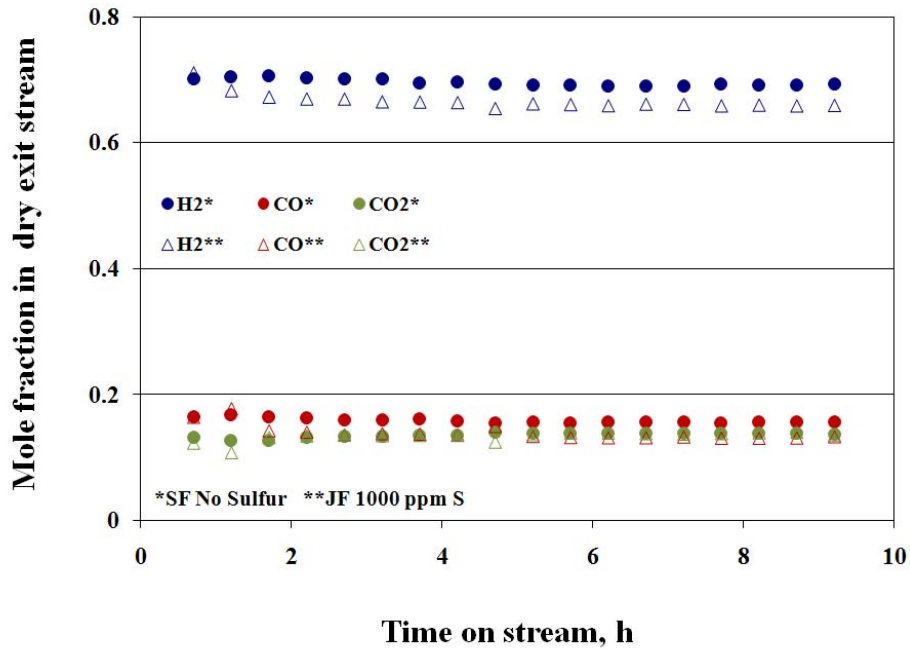


Figure 5-11. Dry product gas composition over 10 h during steam reforming of Simulated fuel No sulfur and Jet fuel 1000 ppm sulfur at 800°C, S/C3 and 1 atm

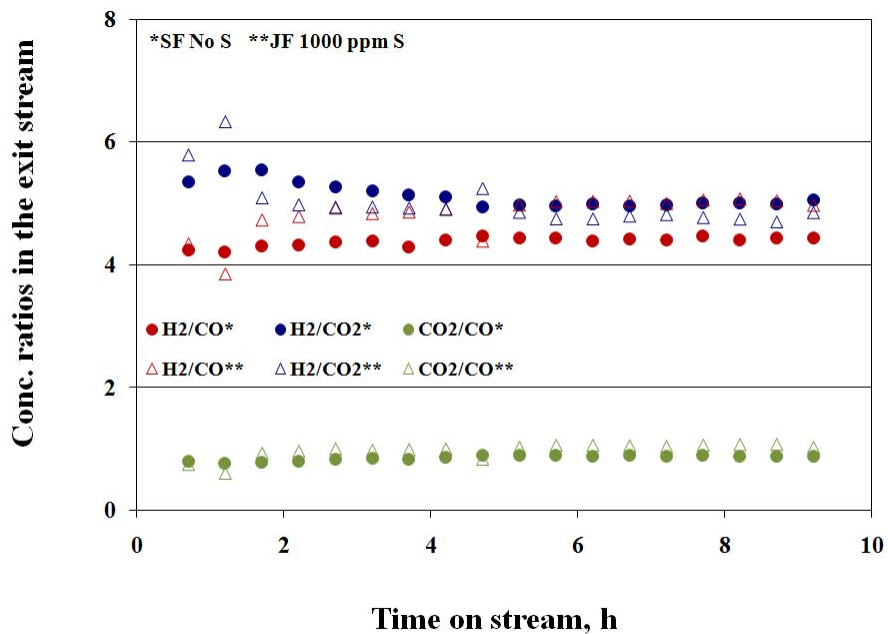


Figure 5-12. H₂/CO, H₂/CO₂ and CO₂/CO in the dry product gas over 10 h during steam reforming of Simulated fuel No sulfur and Jet fuel 1000 ppm sulfur at 800°C, S/C3 and 1 atm

5.4.2. Extent of cracking

Unlike in the case of n-hexadecane steam reforming, cracking was observed during steam reforming of sulfur free fuel, although the extent of cracking was more in sulfur laden fuel, as can be seen in figure 5.14. It was interesting to note the excessive cracking during steam reforming on Pd/b catalyst. In general, cracking was greater in case of non-Rh catalysts than Rh-containing catalyst, which had a positive effect on steam reforming attributed to the enhanced reforming of cracked products to hydrogen and carbon oxides. All the monometallic catalysts promoted excessive cracking in the presence of sulfur.

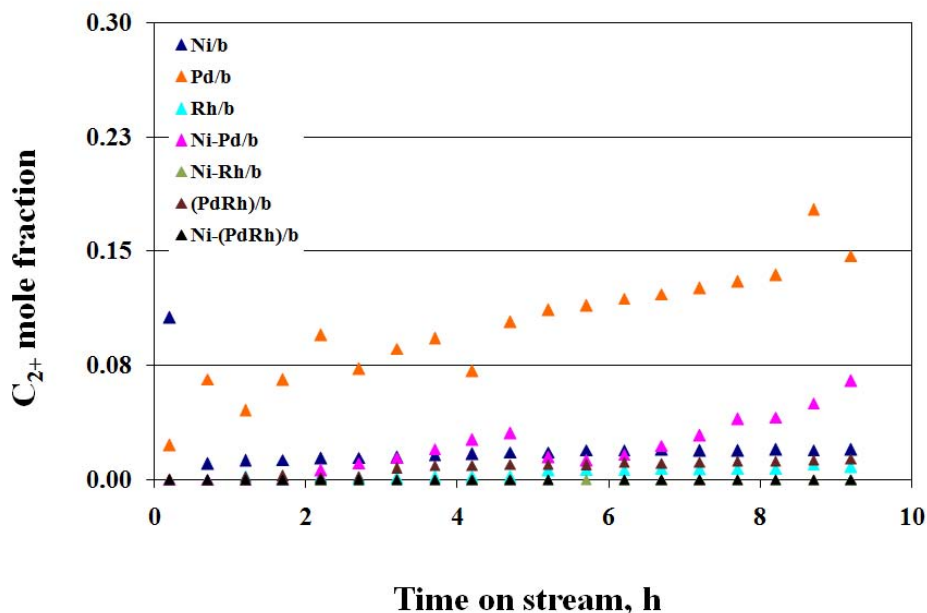


Figure 5-13. Extent of cracking in the dry product gas over 10 h during steam reforming of Simulated fuel No sulfur at 800°C, S/C3 and 1 atm

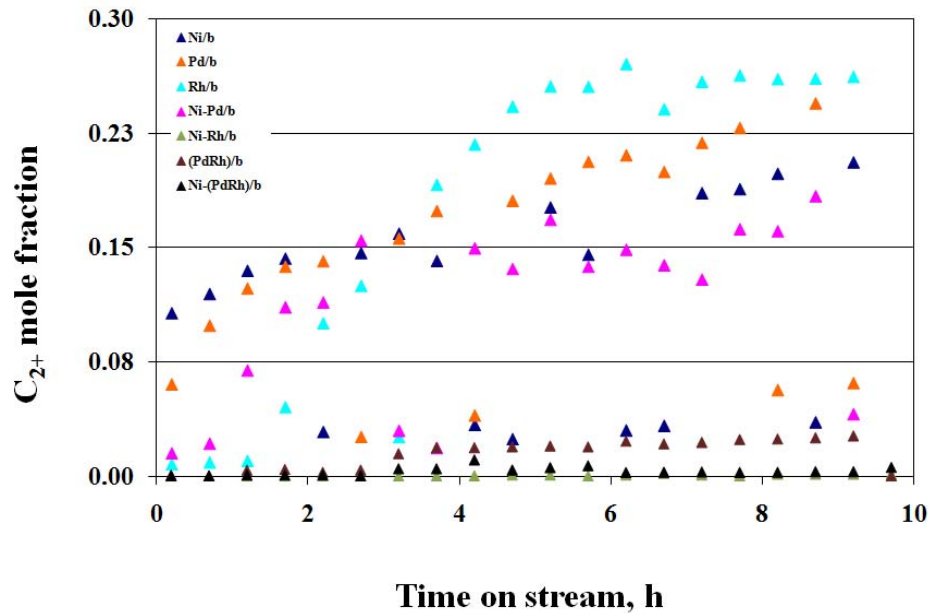


Figure 5-14. Extent of cracking in the dry product gas over 10 h during steam reforming of Jet fuel 1000 ppm sulfur at 800°C, S/C3 and 1 atm

5.4.3. Hydrogen sulfide in the product stream

Sulfur sorption onto the catalysts can occur during steam reforming and can be estimated through a mass balance comparing the amount of sulfur detected in the effluent gas relative to the amount of sulfur in the feed. Figure 5.15 represents total H₂S detected in the product stream during the 10 h experiment, relative to the amount of sulfur in the feed. As seen in the case of NM4 study, sulfur balance was not closed, which means that some of the sulfur was either retained by the catalyst or was converted to some other species not detected by our analytical procedure. The highest sulfur balance was observed for the bimetallic catalysts. It is important to note that the sulfur yields coincided with the yields of hydrogen. This means that the catalysts which were active and stable gave

highest sulfur yields while those which were inferior in performance gave lower sulfur yields. The catalysts 3J1 and Ni-Rh/b were probed using TEM/EDS to detect for the presence of sulfur trapped on the catalyst during reforming. They are presented in the subsequent sections.

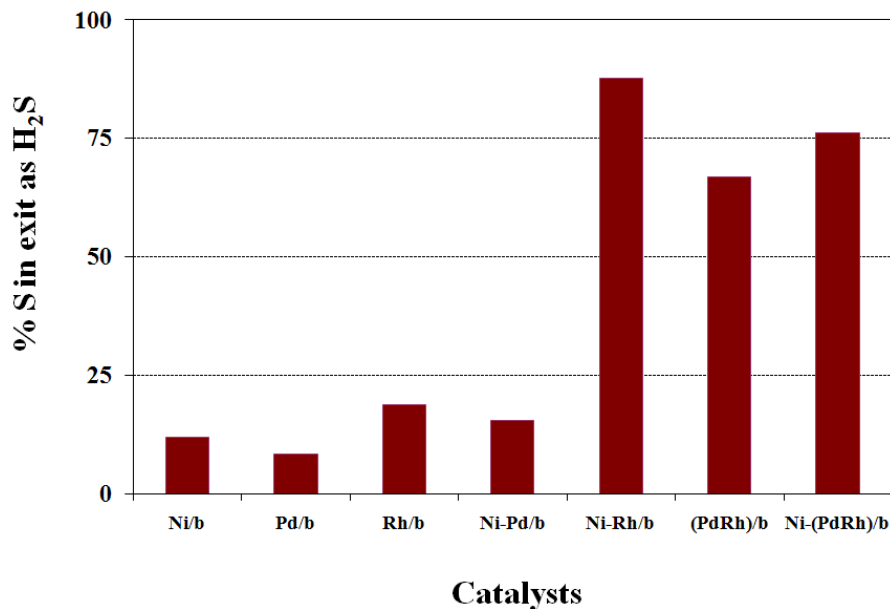


Figure 5-15. Total % sulfur out over 10 h during steam reforming of Jet fuel 1000 ppm sulfur at 800°C, S/C3 and 1 atm

5.4.4. Long time study on 3J1

The progress of hydrogen and sulfur yield with time on stream was analyzed for the case of 3J1 catalyst. This sulfur yield was estimated based on the effluent hydrogen sulfide in the dry gas stream. The same can be seen in figure 5.16. Sulfur yield starts off from a very low value indicating sorption of sulfur at the start up. The driving force for adsorption was highest at the start when the surface of catalyst had no sulfur. Sulfur yield

quickly attained the maximum value after the initial 2 h period. After the catalyst became saturated with sulfur, it was anticipated that the yield of sulfur would stay at maximum. Instead, this value decreased in parallel with that of the hydrogen yield. This observation can be explained by the detection of unreacted organic sulfur (thiophene) in the liquid effluent.

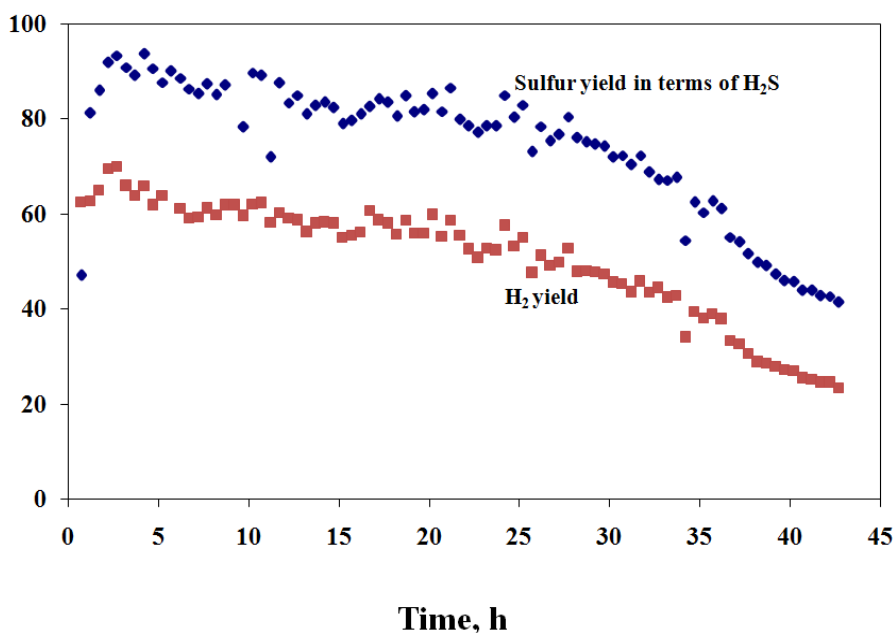


Figure 5-16. Hydrogen and sulfur yield over 10 h during steam reforming of Jet fuel 1000 ppm sulfur at 800°C, S/C3 and 1 atm

The gas chromatograph peak corresponding to thiophene (present in equilibrium in vapor phase) was seen at a retention time of 10 min during a typical gas chromatographic run. Although the GC was not calibrated for thiophene, it can be seen that the intensity of this peak increases with the progress of reaction. Refer to figure 5.17 for the same. In case of Ni/b catalyst, the peak of unreacted thiophene was seen right after the first 2 h of

reaction. In case of 3J1 catalyst, the unreacted thiophene was seen only after 37 h on stream. The observed deactivation in this case can be reasonably attributed to reduced conversion of hydrocarbon which, in turn, may be directly correlated to reduced thiophene conversion to hydrogen sulfide.

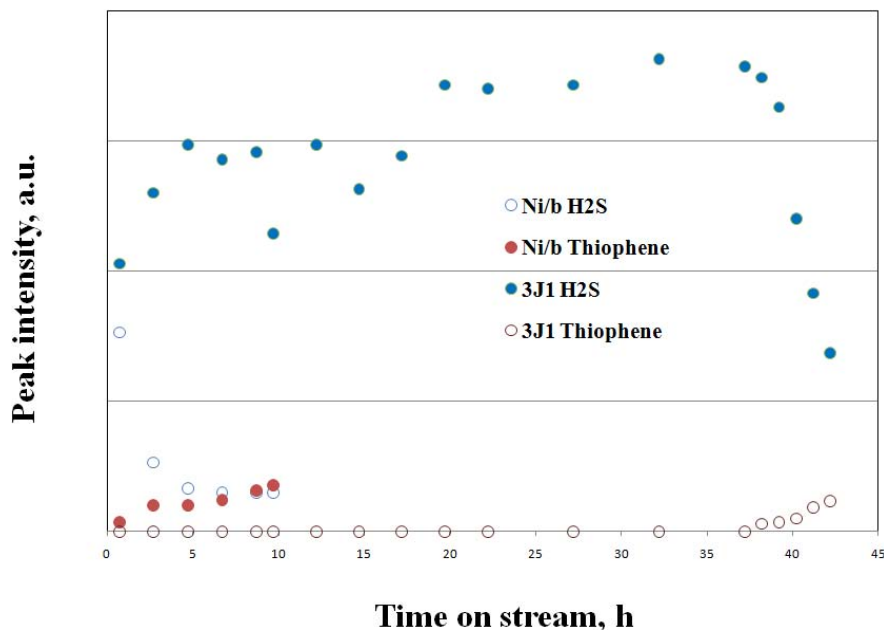


Figure 5-17. Evolution of H₂S and thiophene peak with time on stream during steam reforming of Jet fuel on Ni/b and 3J1 at 1000 ppm sulfur, 800°C, S/C3 and 1 atm

5.5. Characterization of fresh catalysts

5.5.1. Phase structure using XRD, TPR and XPS

XRD is an analytical technique that can be used to detect phase changes that might have occurred during reforming. As can be seen in the XRD patterns, all Ni-containing catalysts show a very sharp peak at 44° , indicating the presence of large nickel crystallites. Addition of a noble metal like Rh or Pd to the Ni drastically reduces the Ni crystallite size, as seen in table 5.18, where the size of nickel crystallites was estimated using XRD data and Scherrer equation. Although this is a rough estimation of the average particle size, it provides an indication of the reduction in nickel particle size with the addition of rhodium and palladium. The possibility of alloying of metals with metals or metals with the support cannot be ruled out. There is not much change in the peaks arising from the support.

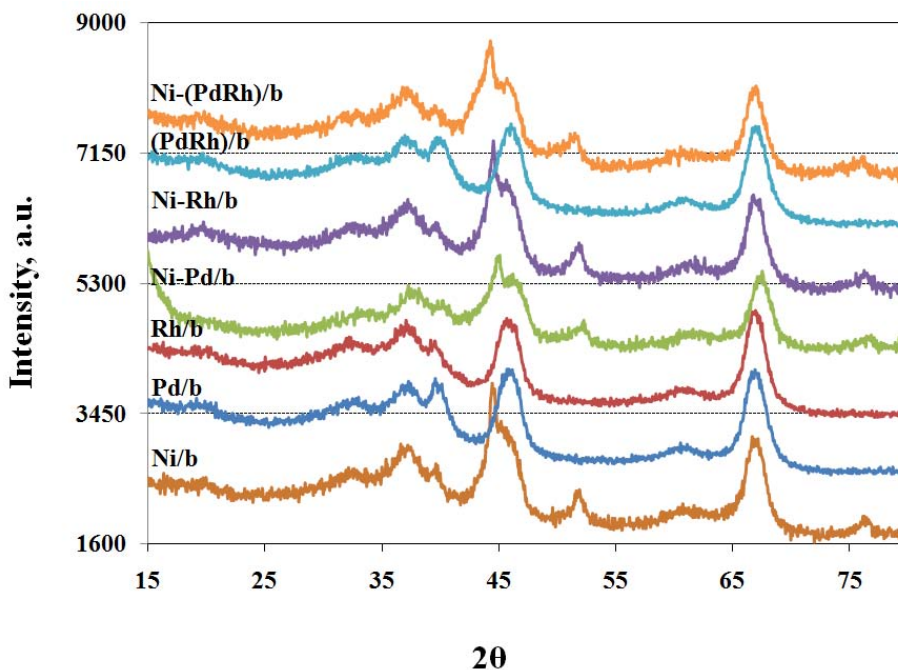


Figure 5-18. XRD profiles of fresh reduced catalysts

Table 5-1. Nickel crystallite sizes estimated by Scherrer equation

Catalyst name	Alumina crystallite size, nm	Nickel crystallite size, nm
Ni/b	5	8
Pd/b	5	-
Rh/b	5	-
Ni-Pd/b	5	5
Ni-Rh/b	5	5
(RhPd)/b	5	-
Ni-(RhPd)/b or 3J1	4	4

TPR of all the calcined catalysts were performed to give insights into oxidation states, and are shown in figure 5.19. All the nickel containing catalysts showed a peak at around 450 °C and its position did not change much with the addition of noble metals. This suggests that the interaction of NiO with the support was equally strong in all the nickel containing catalysts and the addition of noble metals did not significantly effect the degree of interaction. Only in case of Ni/b catalyst, a shoulder with peak maximum at 525 °C was observed. According to the literature, the reduction of NiO species interacting with alumina support occurs at about 550 °C, while the reduction of highly dispersed non-stoichiometric amorphous nickel aluminate spinels and diluted NiAl₂O₄-like phase happens at higher temperatures.^{94,95} Formation of NiAl₂O₄ occurs at calcination temperatures higher than 700°C with NiO diffusing into the surface of support. Thus, these two peaks, at 450°C and 525°C, are assigned to the NiO interacting with components of the support. The low temperature peak at 250°C was assigned to loosely dispersed NiO on the surface of support. The shoulder at 550°C disappeared with the

addition of noble metals and is replaced by a bump at around 750°C. This can be assigned to the strong interaction of nickel with the support or to the formation of nickel aluminate at high calcination temperatures. It should be recalled that in case of earlier study pertaining to NM4, there was a high temperature peak around 780°C assigned to nickel aluminate species. In the present series of catalysts, nickel was present in the form of NiO dispersed on the support.

In case of Rh/b, the peak at approximately 100°C is assigned to the reduction of Rh₂O₃. The second peak at around 225°C is suspected to be due to a strong interaction of the noble metal with the support. This had previously been observed for automotive catalysts prepared with high calcination temperatures.

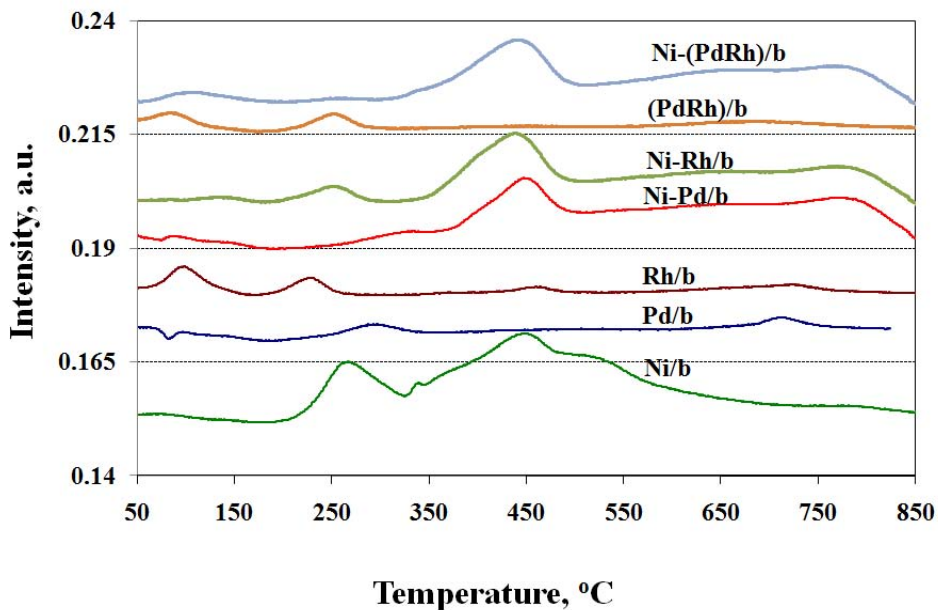


Figure 5-19. TPR profiles of fresh calcined catalysts

XPS of the fresh catalysts was performed to further understand the phase patterns and oxidation states of the as-prepared catalysts. Both calcined and reduced catalysts were characterized. Al 2p XPS of the fresh calcined and reduced catalysts are shown in figures 5.20 and 5.21. They are characterized by an intense peak at 74.7 eV which is assigned to the Al³⁺ peak arising from the alumina support. A close observation at the nickel containing catalysts reveals the presence of a broad and less intense peak at a binding energy of 68.7. This peak was not present in case of catalysts not containing nickel. The peak disappeared on reduction as seen in the subsequent figure. It is suspected that the peak is due to the strong interaction of Ni with the alumina support. Comparing this with the TPR results shown earlier, this peak can be attributed to the reduction peak at high temperatures seen in case of nickel containing catalysts. It is reasonable to assign this peak to nickel aluminate species.

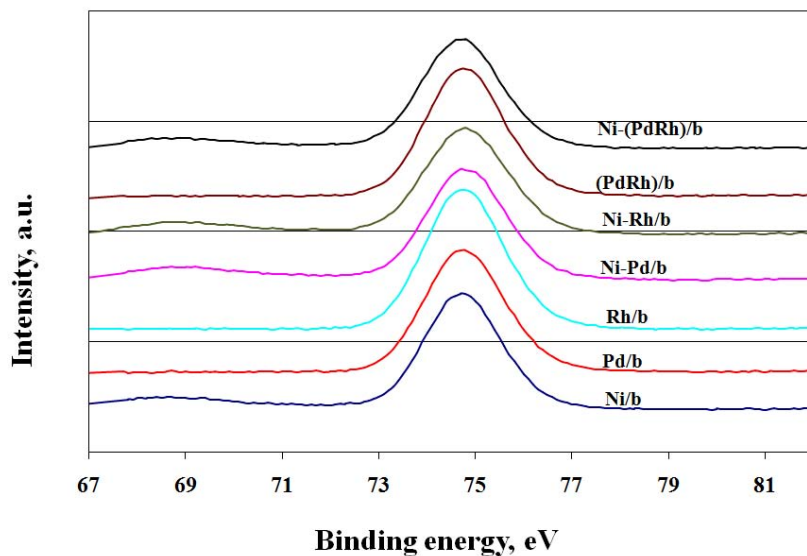


Figure 5-20. Al 2p XPS profiles of fresh calcined catalysts

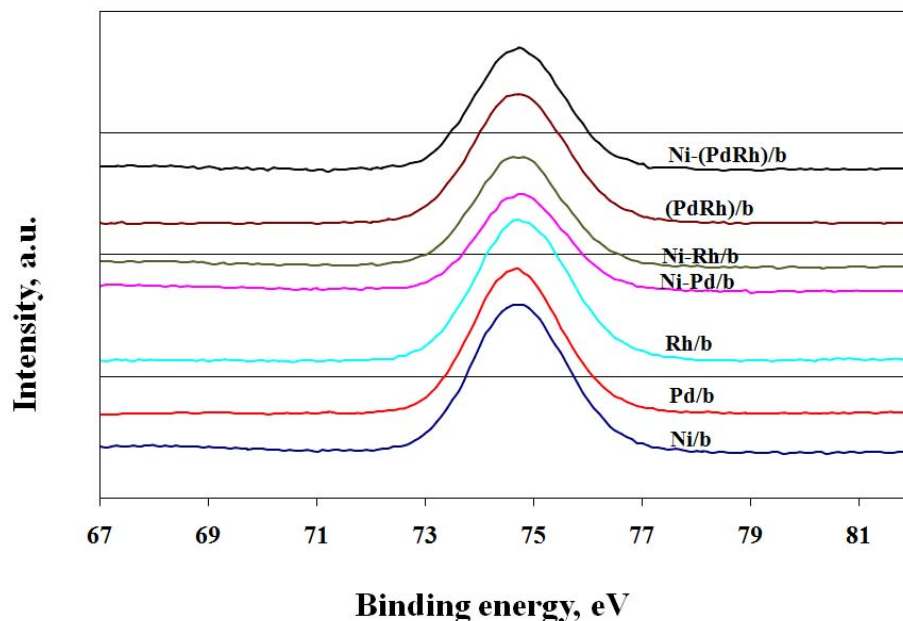


Figure 5-21. Al 2p XPS profiles of fresh reduced catalysts

Figure 5.22 presents Ni 2p XPS of calcined catalysts while figure 5.23 shows the results for reduced catalysts. After calcination, the Ni 2p spectra for all samples have a strong peak at a binding energy of 856.2 eV, consistent with the Ni²⁺ oxidation state. A small shoulder peak at a binding energy of 852.5 eV corresponds to Ni⁰ oxidation state. This may indicate that some of the nickel was present in the reduced state and was unexpected. After reduction, the peak at binding energy 852.5 eV was seen at a much higher intensity. The peak at 856.2 eV was also observed and attributed to the oxidation of Ni after exposure to air. Similar results were obtained by previous researchers. Kugai and co-workers observed nearly complete oxidation of surface Ni⁰ back to Ni²⁺ after reduction and air exposure for 3 min, and our findings show the presence of both the oxidation states in roughly equal amounts. However, we cannot rule out that the extent of Ni

reduction was not complete during the reduction step, leading to the peak observed at 856.2 eV.

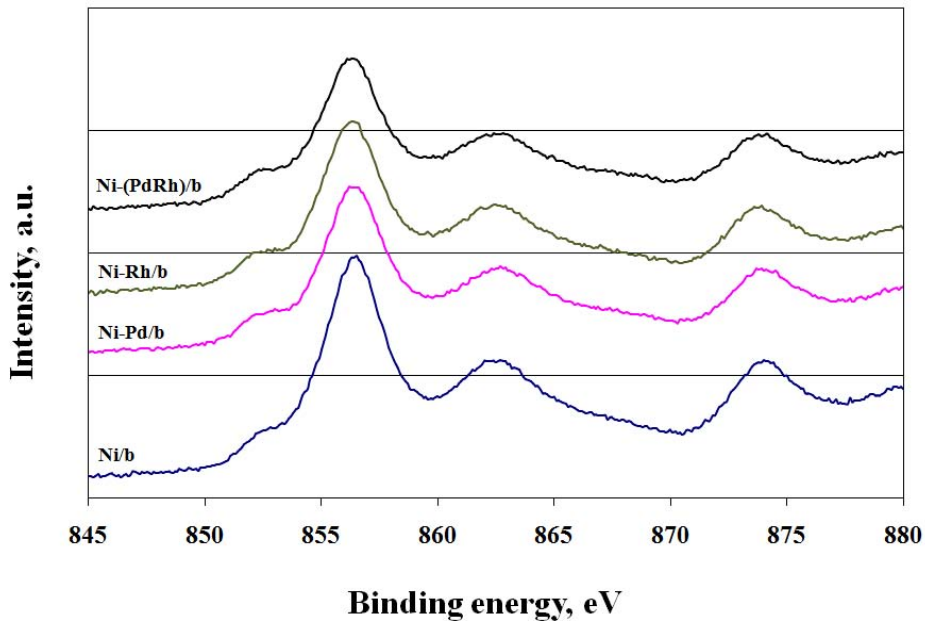


Figure 5-22. Ni 2p XPS profiles of fresh calcined catalysts

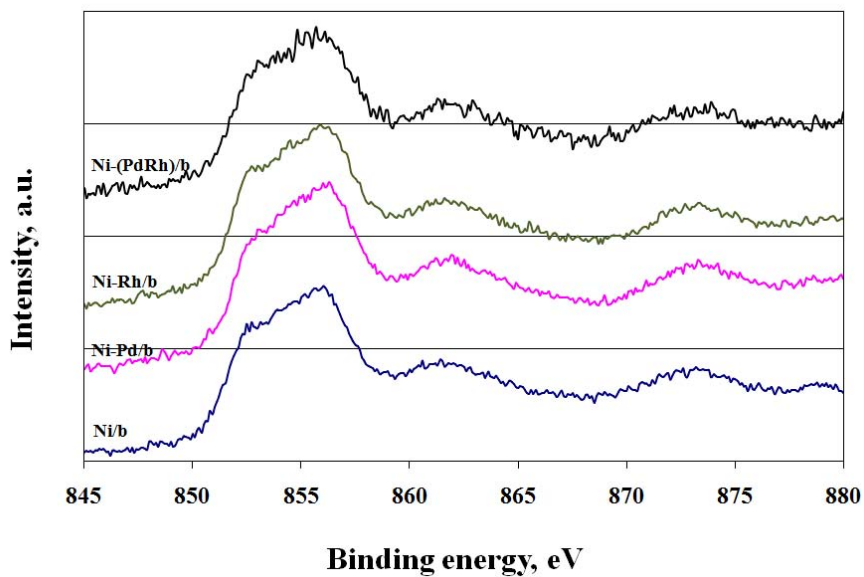


Figure 5-23. Ni 2p XPS profiles of fresh reduced catalysts

Figures 5.24 and 5.25 present the Rh 3d XPS profiles for calcined and reduced catalysts respectively. The calcined catalysts shows the peak at a binding energy of 309.0 eV which is due to the Rh^{3+} while the reduced catalysts shows the peak at a binding energy of 307.2 eV which is assigned to metallic Rh^0 . It should be noted that unlike in case of Ni catalysts, Rh was present in the reduced form even after exposure to air. Similar results were observed in case of Pd but were not shown here.

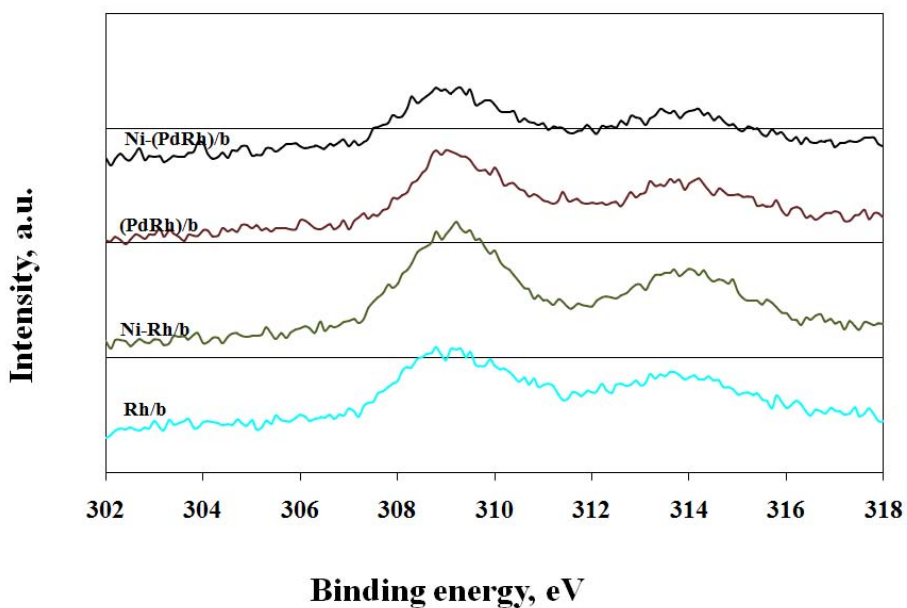


Figure 5-24. Rh 3d XPS profiles of fresh calcined catalysts

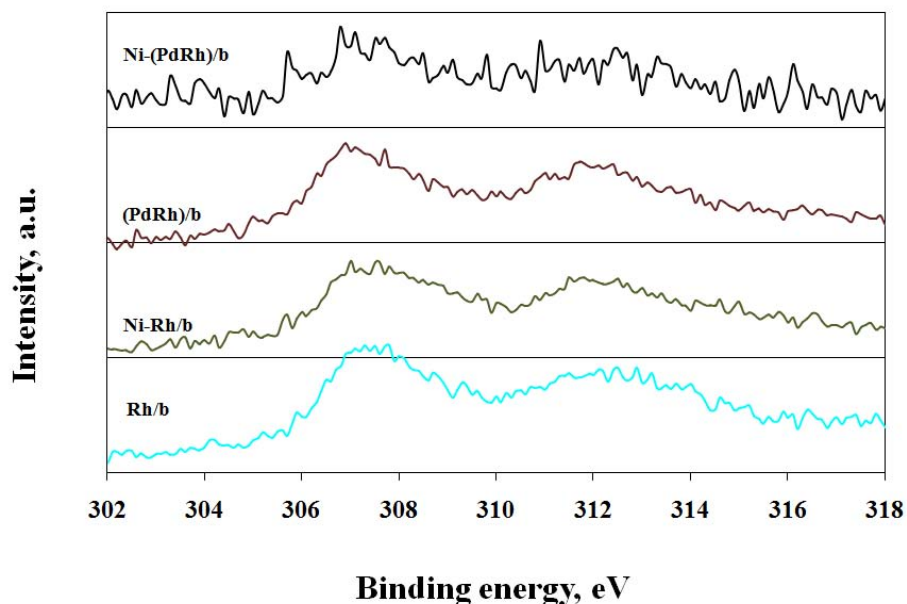


Figure 5-25. Rh 3d XPS profiles of fresh reduced catalysts

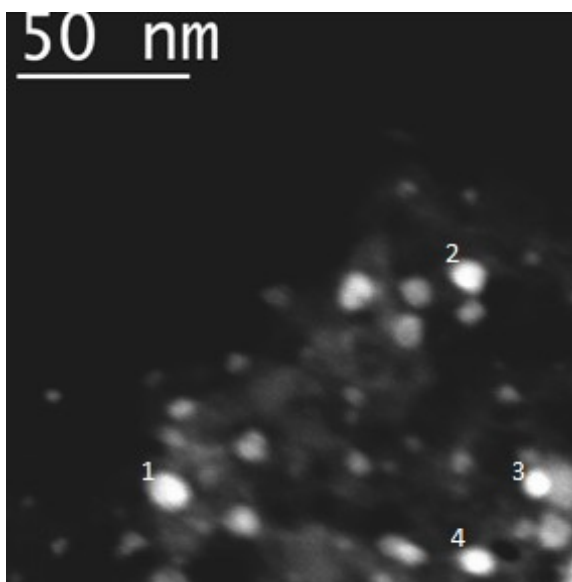
5.5.2. Microscopic structure and composition using STEM-EDS

Figure 5.26a shows the STEM image of fresh reduced 3J1 catalyst while figure 5.26b and 5.26c presents the EDS profiles of particles shown in the image. Table 5.2 gives the peak positions for different elements in EDS spectra of catalysts.

Table 5-2. EDS peak position assignments

Element	Energy (eV)
Ni	80, 750
Al	150
S	230
Rh	275, 2010
Pd	275, 2120

The particle size varies from 20 nm to particles which are as small as few nanometers. In general, the particles can be grouped into two size groups, large particles in the range of 8-20 nm and a smaller size group ranging from few nm to as large as 8 nm. To know more about the composition, EDS analysis was performed at different locations and are shown in subsequent figures. It was important to understand the proximity of each of the metals relative to the others. Position 1, 2, 3 and 4 are representative of the large particles found in fresh reduced 3J1 catalyst. Ni was characterized by peaks at 80 and 750 eV while Pd was characterized by peaks at around 270 and 2120 eV. The large particles show the presence of both Ni and Pd and no Rh. While all of the Ni particles contained Pd, it is clear that the relative amount of Pd in the large particles varied. Ni was present as large particles in the range of 8-20 nm with or without the presence of Pd.



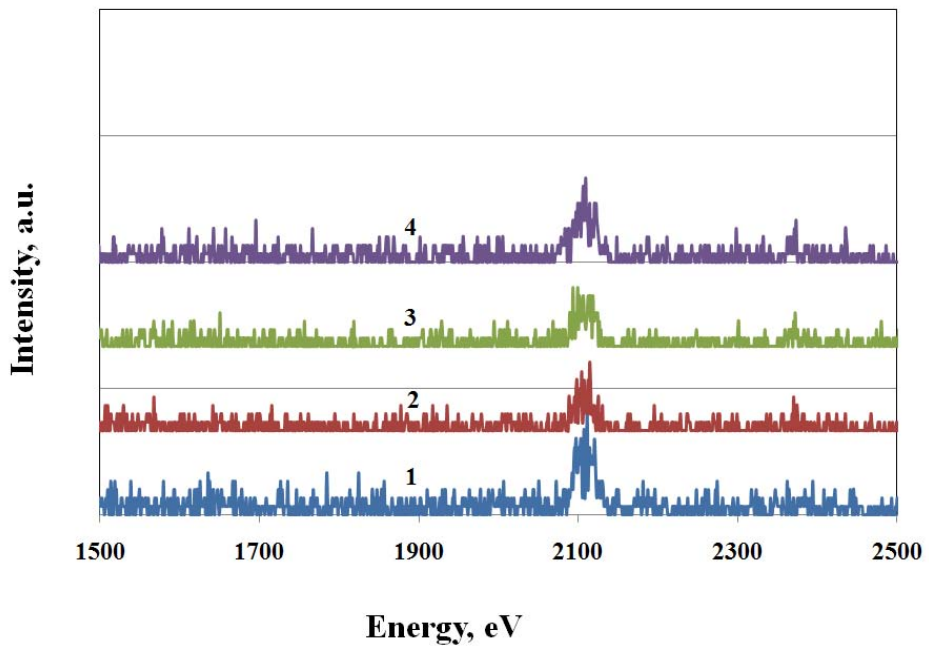
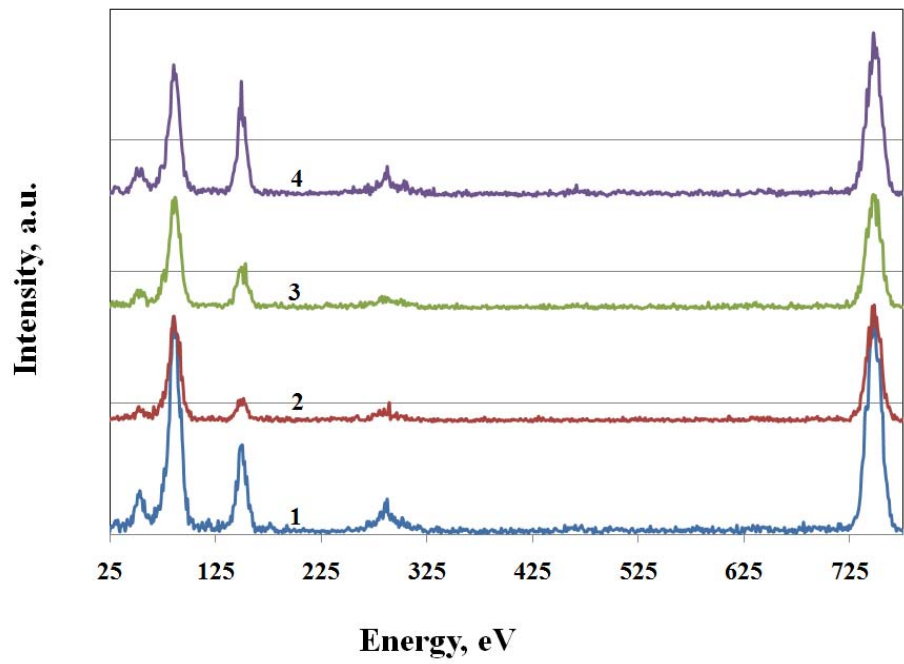
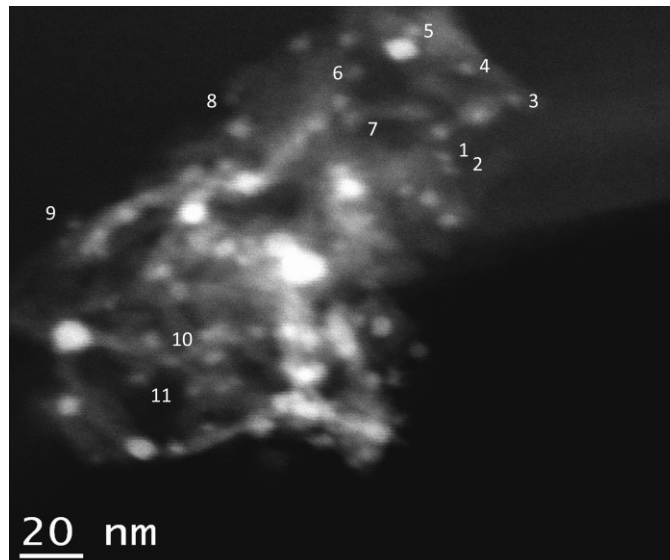


Figure 5-26. EDS analysis of fresh reduced 3J1 catalyst (a) STEM image and (b and c) EDS of particles shown in (a).

Figure 5.27 presents the TEM/EDS data for small particles found in 3J1 catalysts. The characteristic peak for Rh is seen at 270 eV. Since the characteristic peak for Rh overlaps with that of Pd, the high energy peaks are useful in distinguishing between the two noble metals. The high energy peak for Pd is observed at 2120 eV while that of Rh is seen at 2000 eV. It can be seen in figure 4.24 that small particles essentially contain Rh while traces of Ni and Pd can be observed in some cases. Since Rh is extremely resistant to sintering, it is usually seen as small crystallites with or without the presence of Ni and/or Pd.



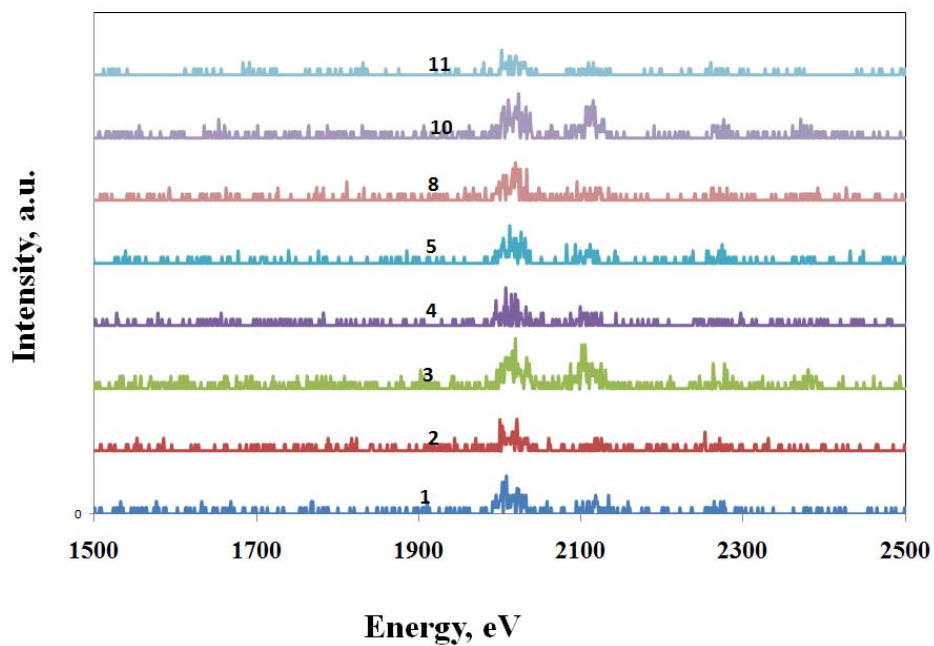
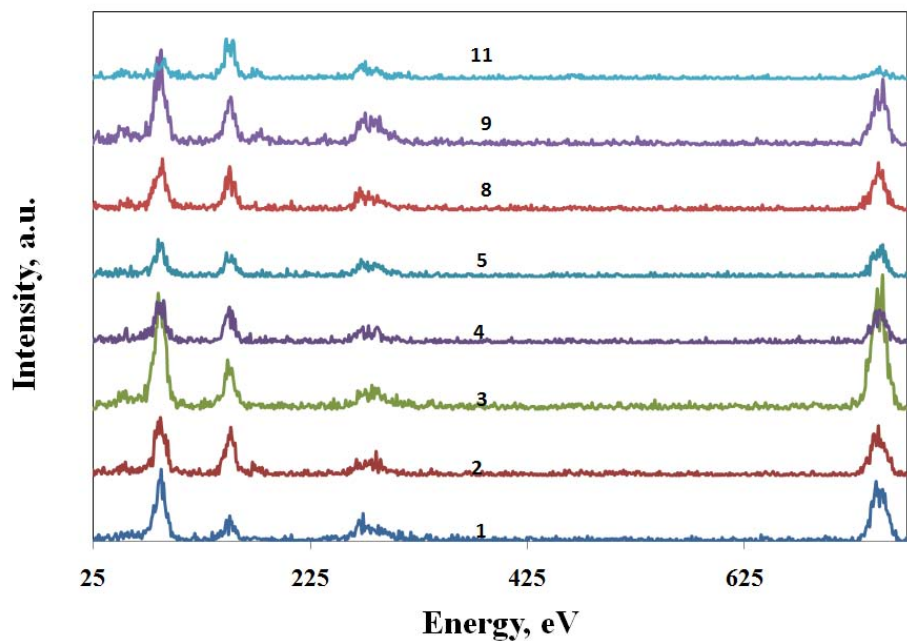
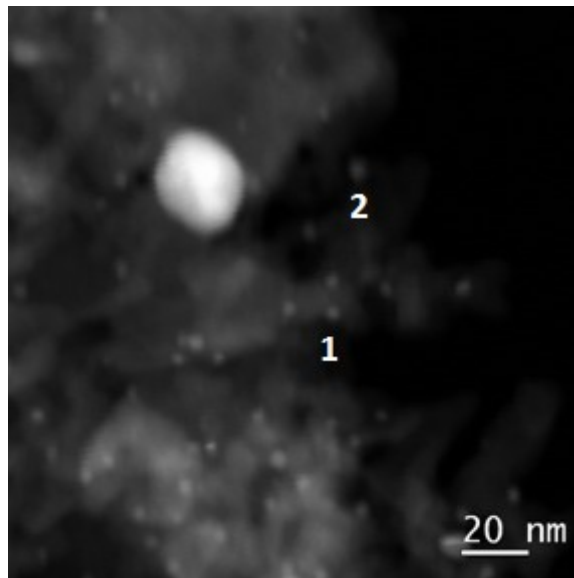


Figure 5-27. EDS analysis of small particles in fresh reduced 3J1 (a) STEM image and (b and c) EDS of particles shown in (a).

Figure 5.28 shows similar results for Ni-Rh/b fresh reduced catalyst. As seen previously with the 3J1 catalyst, there are essentially two groups of particles, a group of small crystallites in the range of few nm to 4 nm with a group of larger particles in the range of 8-20 nm. EDS of small particles shows that they are composed of mainly Rh with small amounts of Ni. Large particles are made of Ni and deprived of any Rh.



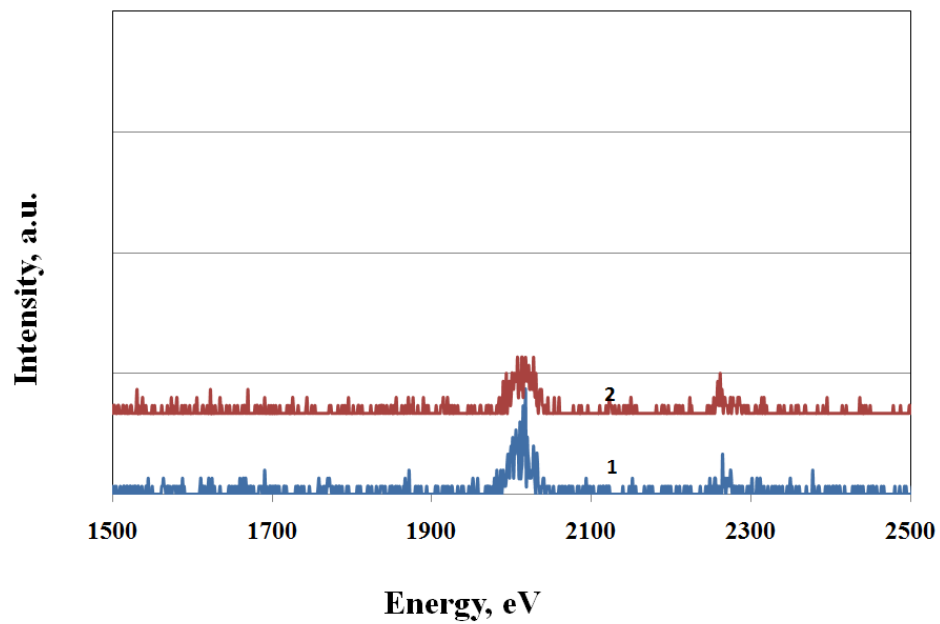
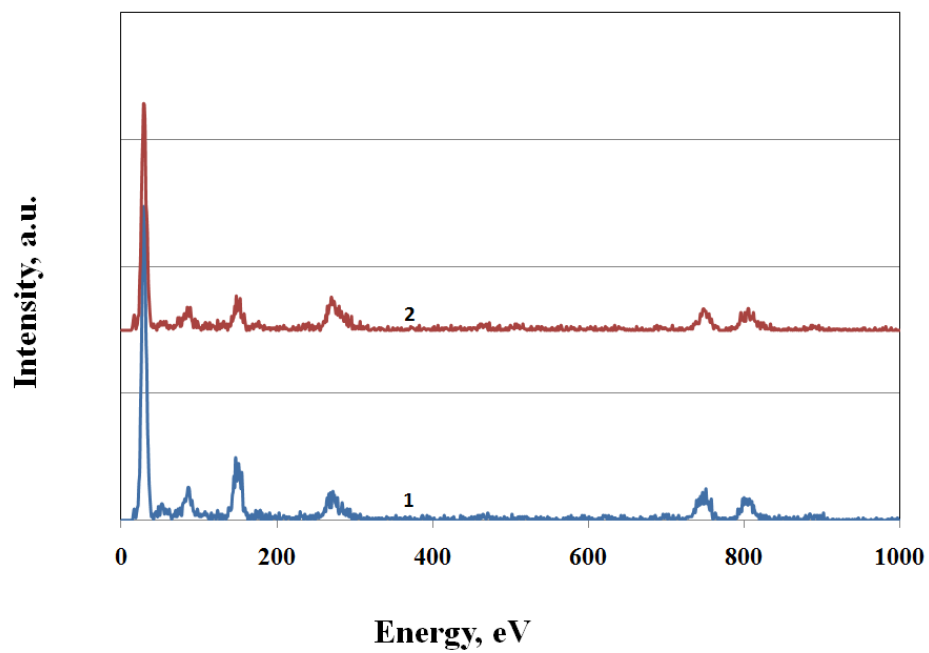
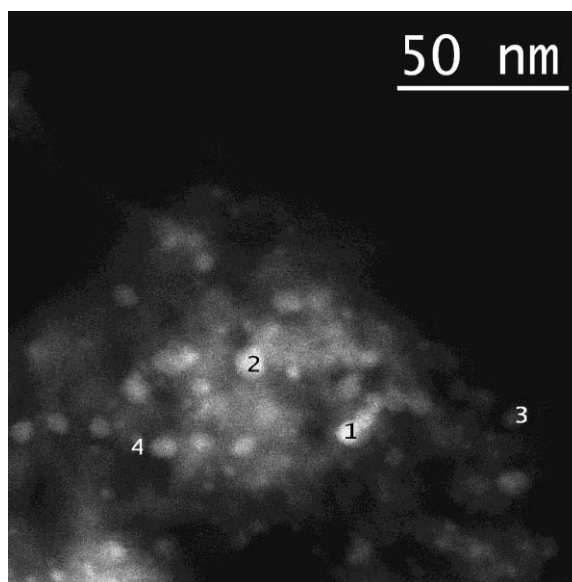


Figure 5-28. EDS analysis of small particles in fresh reduced Ni-Rh/b (a) STEM image and (b and c) EDS of particles shown in (a)

Figure 5.29 present the STEM image and EDS of particles seen in reduced (PdRh)/b catalyst. The particles were significantly smaller and were found to be in the range of few nanometers to 10 nm. Although the image is not clear, the qualitative information obtained in the form of EDS is in agreement with that of 3J1. The large particles were mainly Pd without any traces of Rh. This can be seen by the presence of peak at around 2120 eV in the EDS profiles, indicating the presence of Pd, and the absence of a peak at 2000 eV, indicating the absence of Rh.



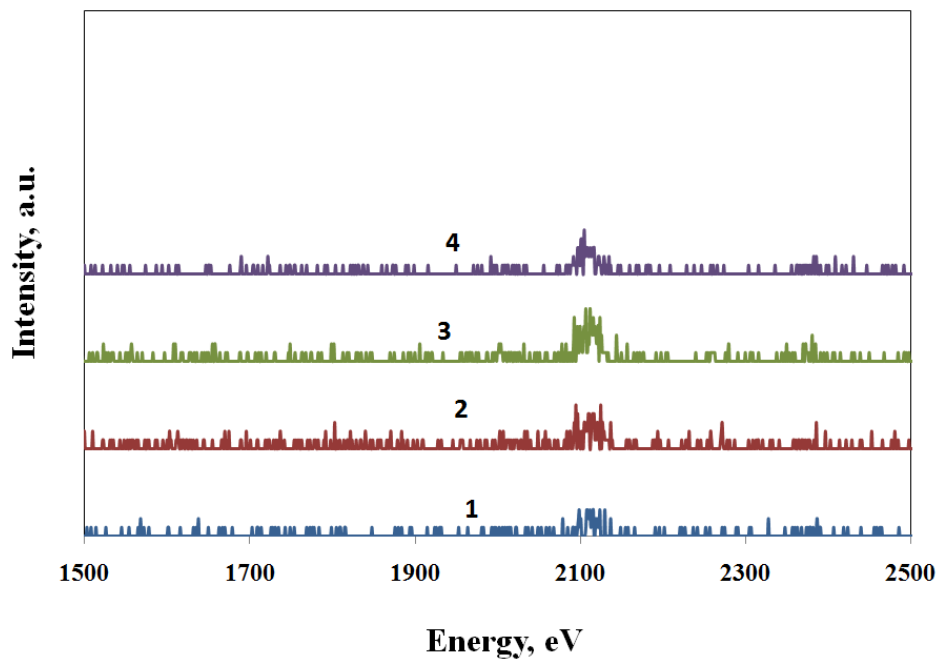
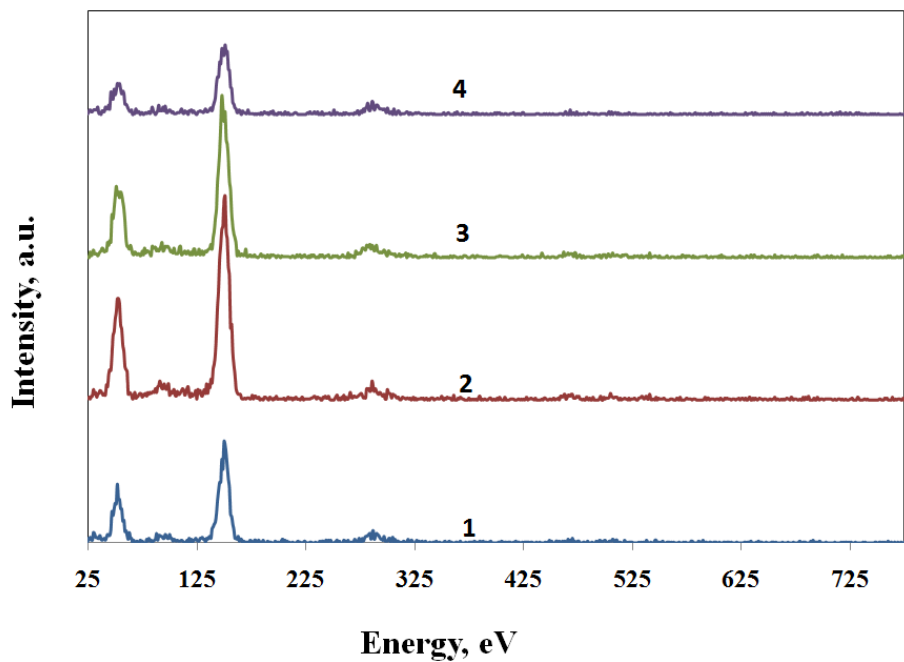


Figure 5-29. EDS analysis of big particles in fresh reduced (PdRh)/b (a) STEM image and (b and c) EDS of particles shown in (a)

5.6. Characterization of used catalysts

Catalysts used during steam reforming were recovered after activity testing for 10 h and characterized using XRD, TPR and XPS. The purpose of these tests was to investigate the observable changes in the used catalyst and compare them with the fresh ones. For comparison with fresh catalysts, data for fresh catalysts are shown alongside those for used catalysts.

5.6.1. Phase structure and crystallite growth using XRD, XPS and TPR

Figure 5.30 presents the XRD patterns of used catalysts after steam reforming of JF containing 1000 ppm S. It also shows the profiles for fresh catalysts for comparison purposes. The peak at 44° corresponds to Ni^0 , observed for all Ni-containing catalysts, which indicates that Ni was present in the reduced state during reaction. In the absence of noble metals, Ni crystallite size was as high as 50 nm (estimated using Scherrer equation) while the presence of noble metals generally limited the growth. In case of Ni-Rh/b, the crystallite size was estimated to be 12 nm while in case of 3J1, it was 10 nm. It should be emphasized here that these are estimated average values of crystallite sizes and may involve significant errors. They should be used only for qualitative analysis. The peak at 41° , corresponding to Rh^0 , was never observed in any of the Rh containing catalysts. It is therefore reasonable to postulate that Rh was present as some alloy species at the reaction conditions. Pd was seen in the reduced form in both monometallic and bimetallic (PdRh)/b catalysts, represented by peaks at 39° although it was not observed in Ni-Pd/b.

The results are in agreement with TPR profiles shown in figure 5.31. During TPR experiments, the nickel containing catalysts exhibited a peak at around 430°C that was

assigned to NiO strongly interacting with the support alumina. A high temperature bump was also seen at around 800°C which was assigned to the reduction of nickel aluminate. In case of Ni/b, the peak appears at still higher temperature and only a part of the peak can be seen in the figure. This indicates that the interaction of Ni with the support is stronger for the Ni-only catalyst than in case of other nickel containing catalysts. Nickel aluminate is formed by surface diffusion of nickel into the support species and is detrimental to the steam reforming activity of the catalysts. The incorporation of noble metals (Pd, Rh) decreases the formation of the aluminate, thereby enhancing catalyst stability.

In case of Ni/b and Ni-Pd/b catalysts, there is an additional peak at around 340 °C which is probably due to the reduction of NiO interacting loosely with the support. Moreover, the reducibility of Ni in Ni/b is reduced significantly after reaction which is evident from the decreased area under the peak. In presence of noble metals, the reducibility has increased and has a positive effect on the reaction.

One of the interesting observations was the disappearance of peaks due to reduction of Rh in rhodium containing catalysts. These peaks, which mostly appeared at temperatures lower than 200 °C in fresh catalysts, were not seen in case of used catalysts. It should be recalled that the used catalysts were first oxidized to burn off any carbon deposited on the surface during steam reforming.

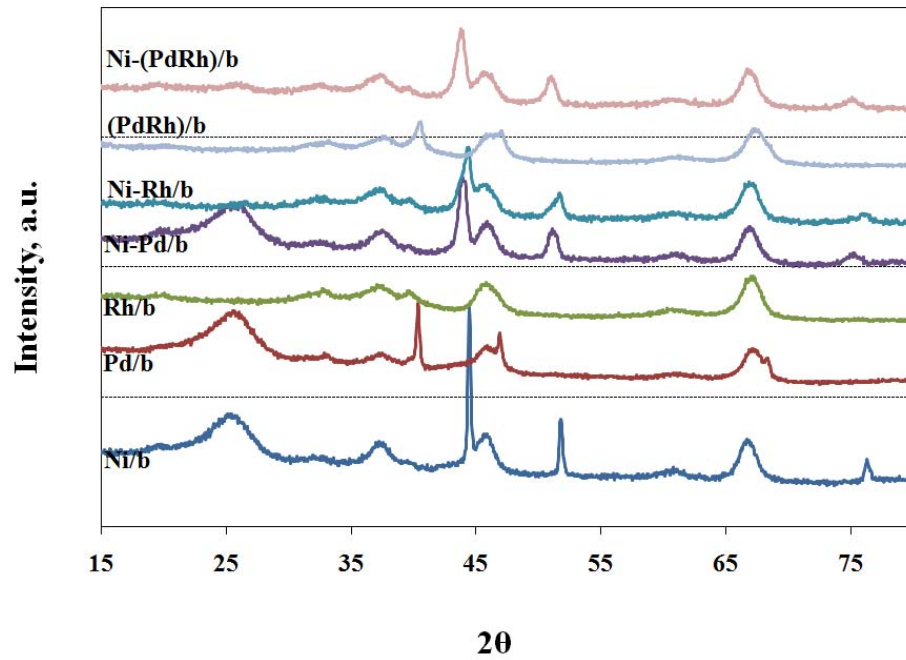
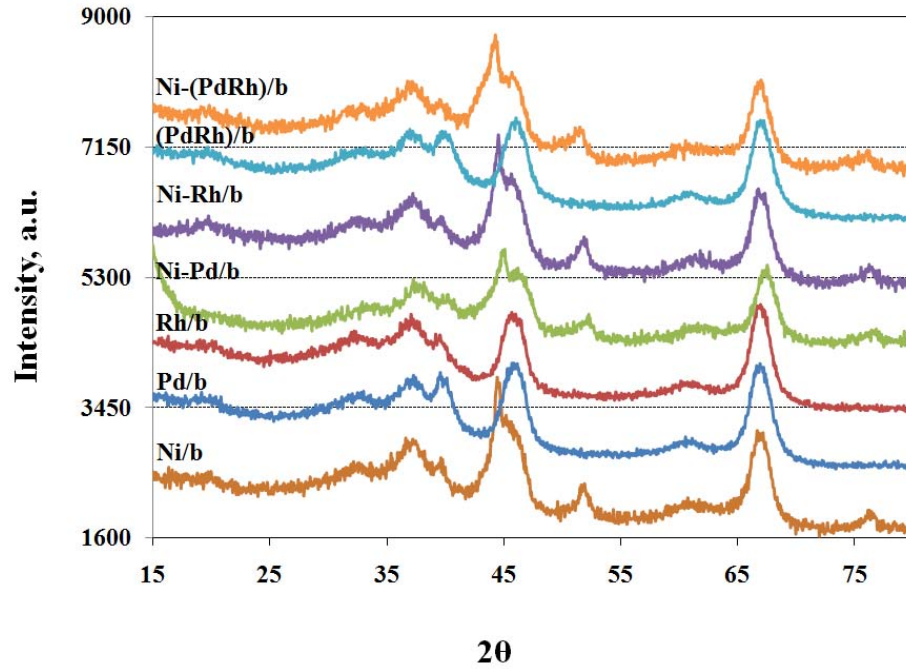


Figure 5-30. XRD profiles of (a) fresh catalysts and (b) used catalysts after steam reforming of Jet fuel 1000 ppm sulfur at 800°C, S/C=3 and 1 atm

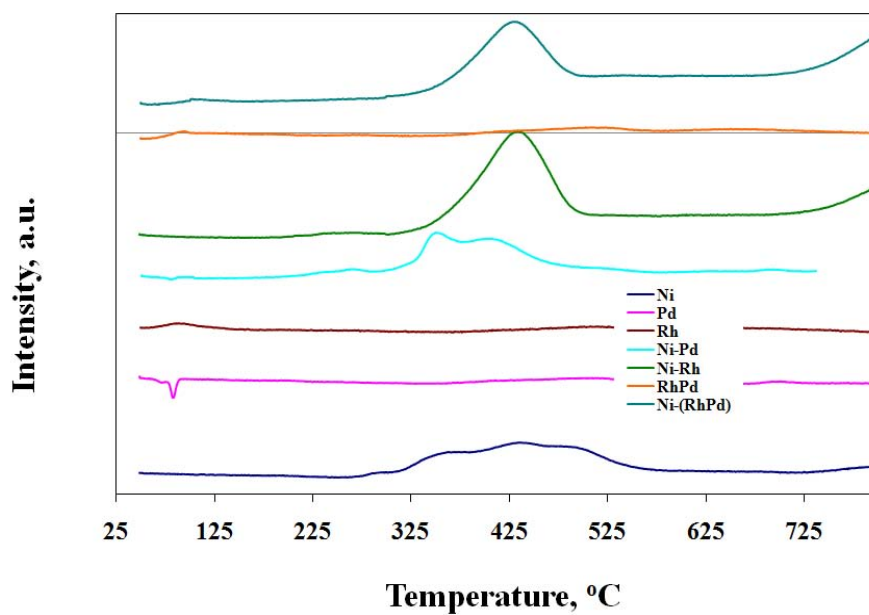
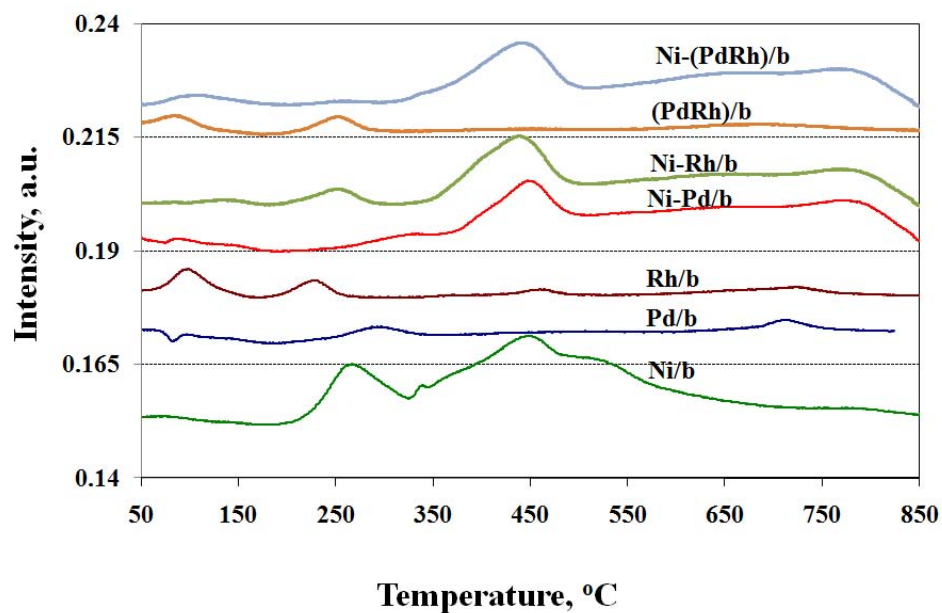
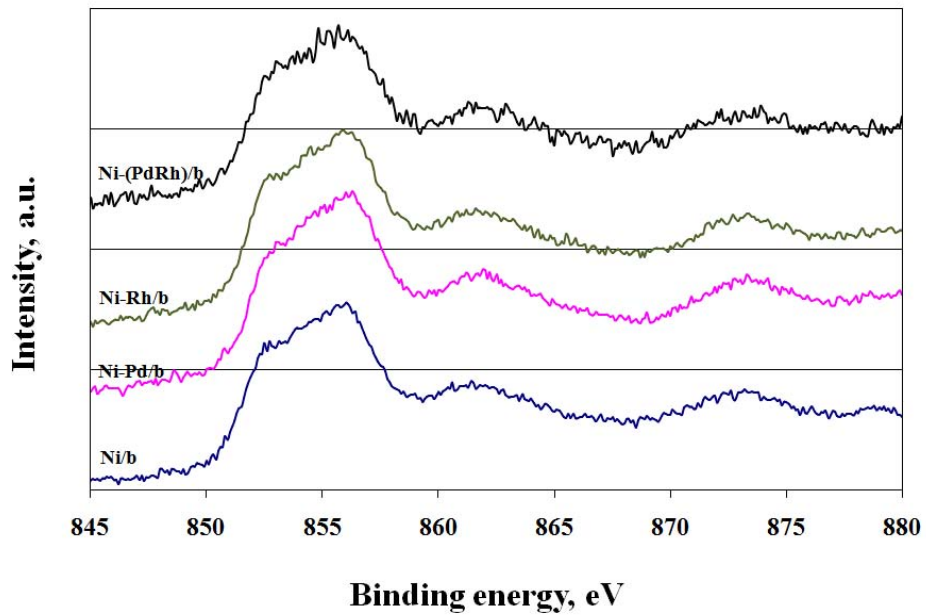


Figure 5-31. TPR profiles of (a) fresh catalysts and (b) used catalysts catalysts after steam reforming of Jet fuel 1000 ppm sulfur at 800°C, S/C=3 and 1 atm

XPS of the used catalysts gave further information about the oxidation states of different metals present. Figure 5.32 presents Ni 2p XPS profiles of all nickel containing catalysts. As mentioned earlier, the peak at around 852.5 eV corresponds to Ni⁰ while that at 856.2 is due to Ni²⁺. XPS is a surface analytical technique and the information obtained can be related to the composition of the material located in the first few nanometers from the surface. The fact that the intensity of peaks is relatively smaller in case of Ni/b and Ni-Pd/b shows that the surface of the catalyst is possibly covered by carbon. In case of Ni-Rh/b and 3J1, the intensity of peaks is fairly high and it can be said that the surface of the catalyst is relatively clean which is characterized by less carbon deposition. The studies concerning carbon deposition are presented in subsequent sections. Ni/b and Ni-Pd/b show higher concentrations of Ni⁰ (852.5 eV) than that in case of Ni-Rh/b and 3J1. Exposure to air causes Ni⁰ to go to Ni²⁺ but only slightly in case of Ni/b and Ni-Pd/b. Since most of the nickel is present in the reduced state, it is suspected that this may be due to the difficulty in the oxidation of nickel when exposed to air. One of the reasons that can cause this is the non-accessibility of nickel partly due to its coverage by carbon. Similar results have been reported in the literature in case of reforming over nickel catalyst systems.

Figure 5.33 shows similar results for used 3J1 catalysts recovered at different times on stream. The XPS profiles look similar until 10h after which the Ni⁰ peak is relatively more intense. As mentioned earlier, there is a gradual deposition of carbon on the surface of the catalyst during reforming. This carbon eventually blocks the access of metal crystallites to the air. Note that after 45 hr on stream, the XPS shows virtually no peaks, suggesting that the metals may be present under a significant coke layer and thus hidden

from view. C 1s XPS results which are presented in the subsequent section showed that there was growth of carbon on the catalyst surface in this time frame. It is for this reason that most of the nickel is present in the reduced state during steam reforming reaction. It is also possible that the bulk of the crystallite might be present in the oxidized form while the surface is mainly concentrated with reduced form of nickel.



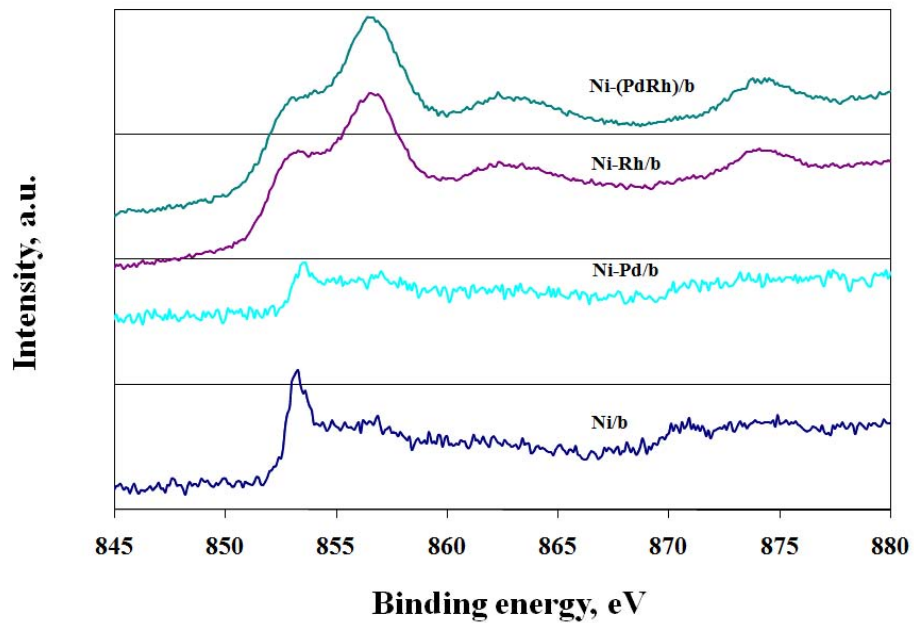


Figure 5-32. Ni 2p XPS of (a) fresh catalysts and (b) used catalysts after steam reforming of Jet fuel 1000 ppm sulfur at 800°C, S/C=3 and 1 atm

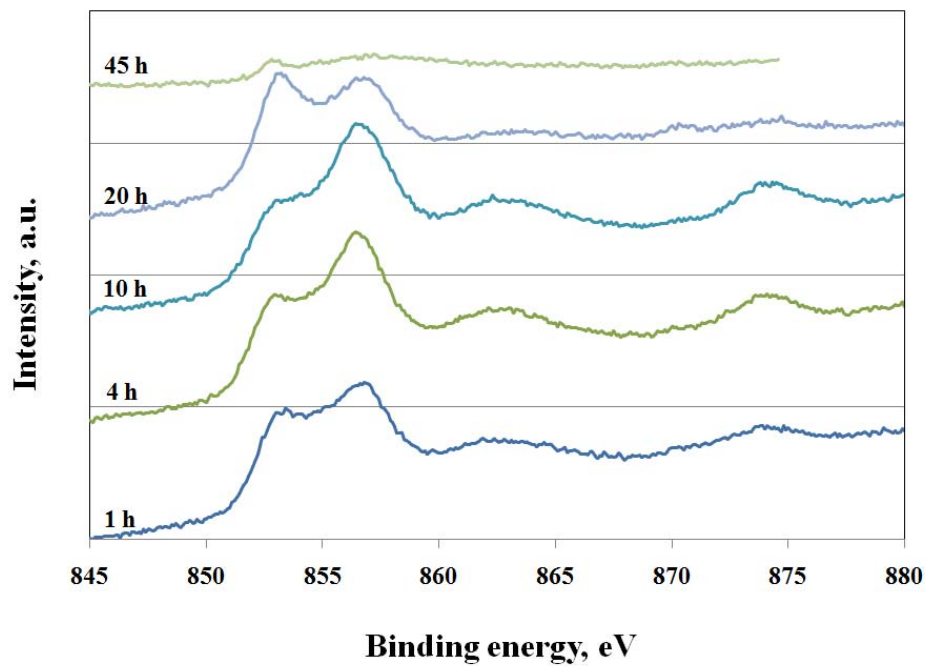
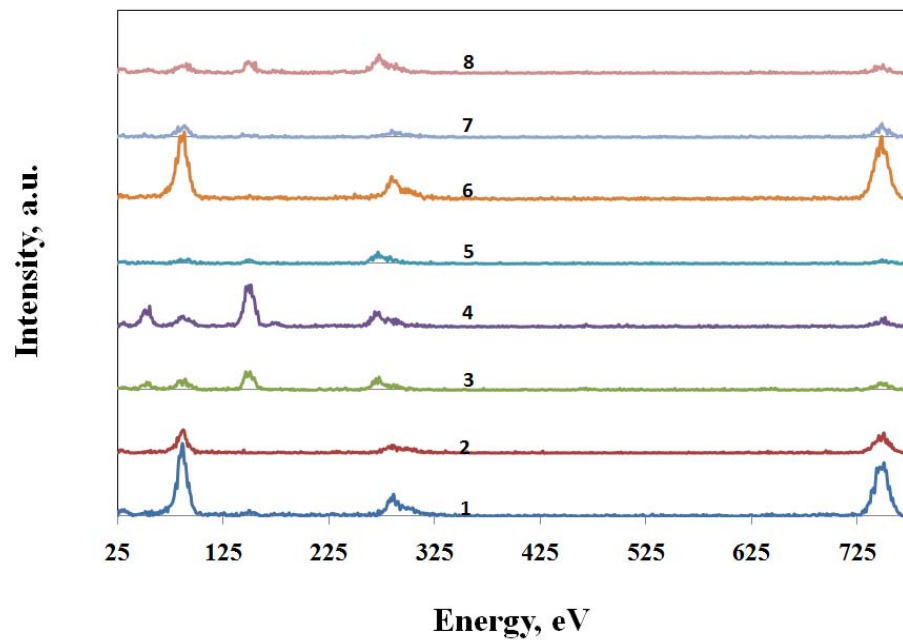
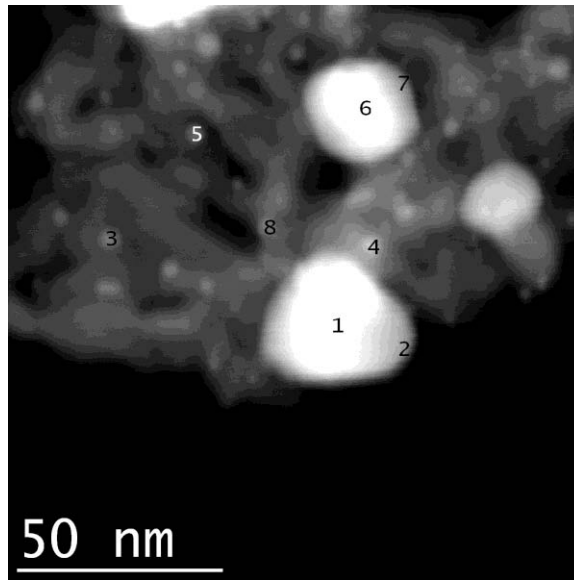


Figure 5-33. Ni 2p XPS of used catalyst 3J1 at different times on stream, catalysts after steam reforming of Jet fuel 1000 ppm sulfur at 800°C, S/C=3 and 1 atm

A STEM image of used 3J1 catalyst was obtained and is shown in figures 5.34. Most of the Ni peaks (large particles) in the used catalyst were characterized by the presence of Pd. This is exactly what was shown earlier in the EDS of fresh catalysts. Positions 1,2,6 and 7 refer to the large particles while 3,4,5 and 8 represent the small particles present on the surface of support. It is important to observe that the identity of the crystallites did not change with reaction. This means that the metal particles did not change their composition during the course of the reaction. There was increase in the size of the nickel particles while crystallites containing Rh were present as small crystallites in the range of few nanometers as seen in the fresh catalyst. Particles containing Rh also showed presence of traces of Ni and/or Pd as observed in the fresh catalysts. The fact that these small crystallites remain small during steam reforming indicates that Rh prevents sintering of the particles giving improved yields and lower deactivation.



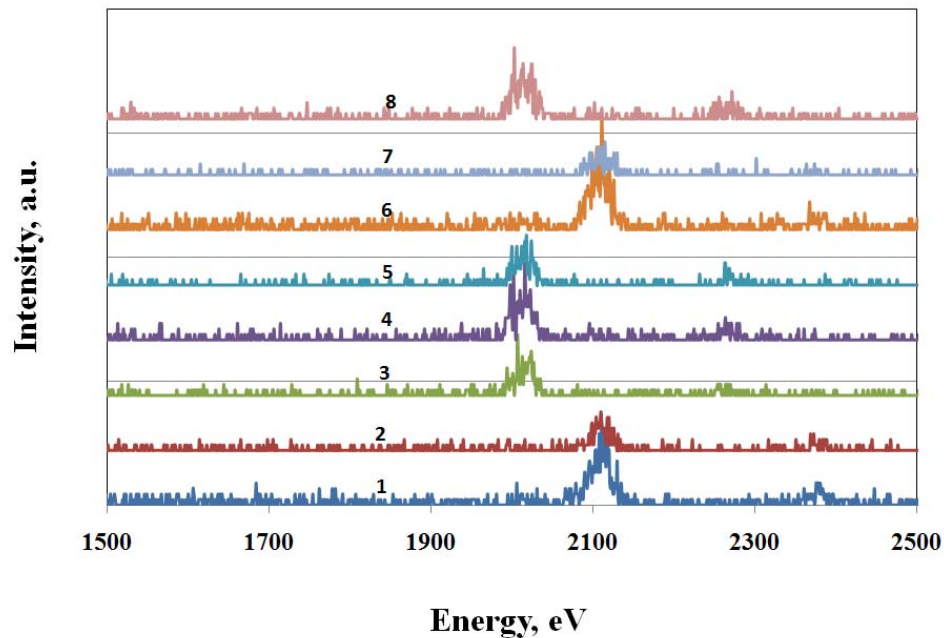


Figure 5-34. EDS analysis of small particles in used 3J1 catalysts after steam reforming of Jet fuel 1000 ppm sulfur at 800°C, S/C=3 and 1 atm

STEM images of used Ni-Rh/b and 3J1 are shown in figure 5.35. Most of the large particles were seen to be in the range of 25-50 nm irrespective of the catalyst composition. Small particles which were predominantly composed of Rh were resistant to sintering to a large extent. The size of the small particles ranged from few nanometers to 8 nm. The particle growth of Ni containing particles was confirmed using XRD and TEM.

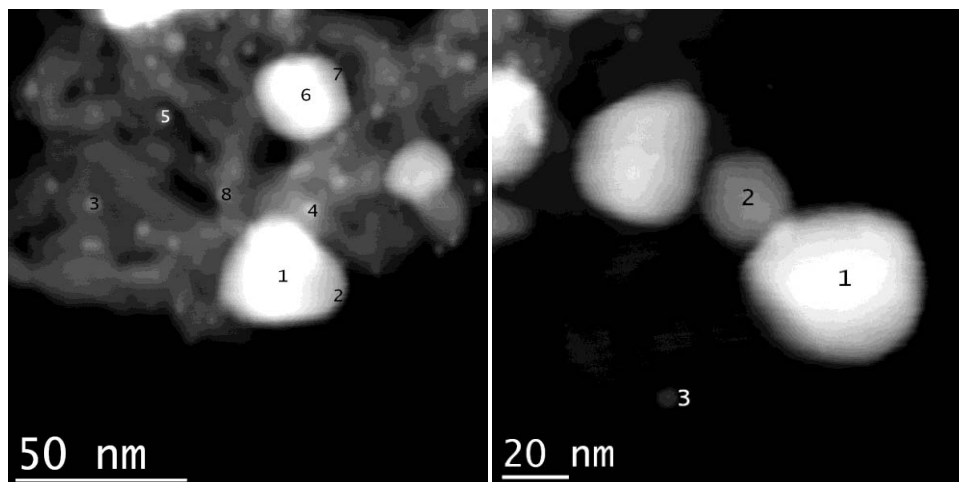


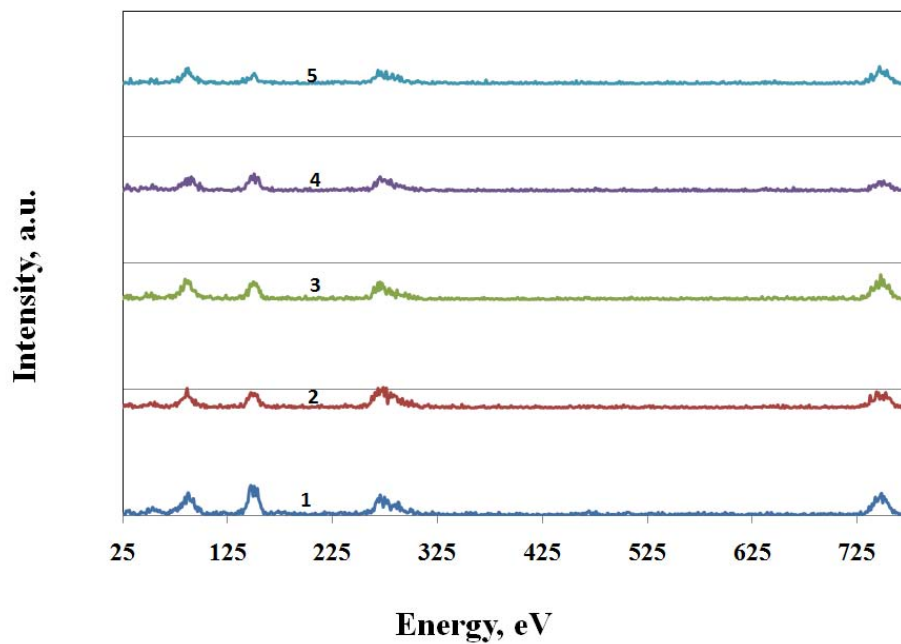
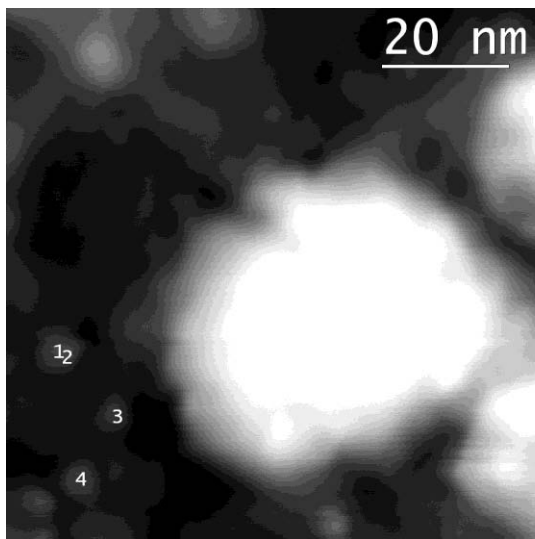
Figure 5-35. STEM images of used (a) 3J1 and (b) Ni-Rh/b catalysts steam reforming of Jet fuel 1000 ppm sulfur at 800°C, S/C=3 and 1 atm

To summarize, the identity of the catalysts was not lost and was found to remain intact during steam reforming. Large particles containing predominantly Ni were found to grow during the course of reaction while tiny crystallites containing mainly Rh exhibited excellent resistance to sintering and thereby retained better steam reforming activity. The catalysts were further investigated for structure-reactivity correlations.

5.6.2. Sulfur adsorption studies

Used catalysts 3J1 and Ni-Rh/b were tested for the presence of sulfur trapped on the surface and/or bulk of the particles using STEM/EDS. Figure 5.36 shows the STEM and EDS for Rh particles found in Ni-Rh/b catalyst. Sulfur presence is detected by a peak at a kinetic energy of 230 eV. In case of EDS of Rh particles shown in the figure below, no such peak was observed and thus sulfur is presumed not to be present on the surface of

Rh particles. This is in accordance to the study conducted in the first part of this project. Sulfur was preferentially seen to accumulate on the surface of nickel crystallites.



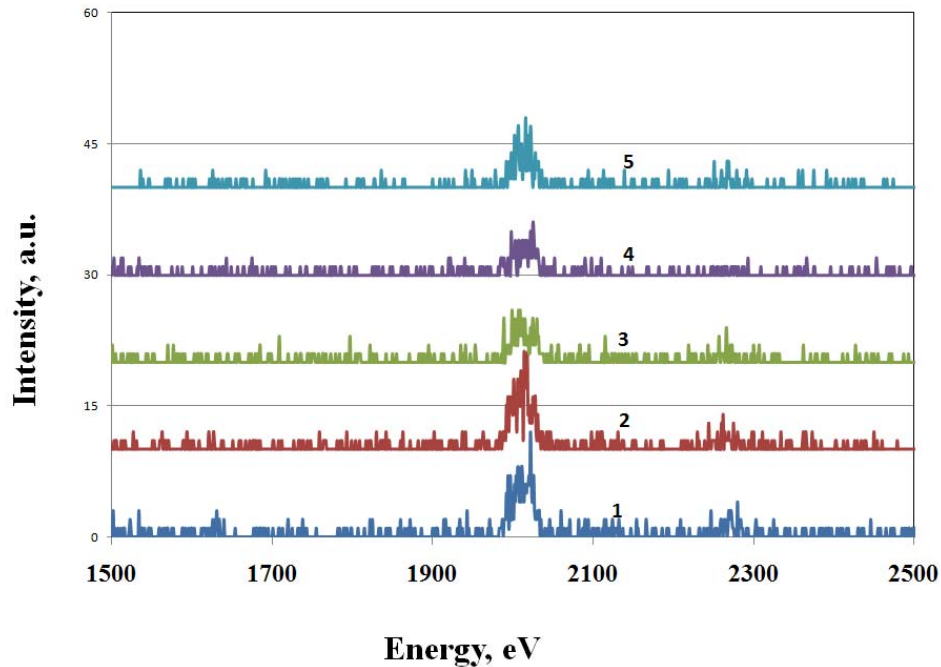
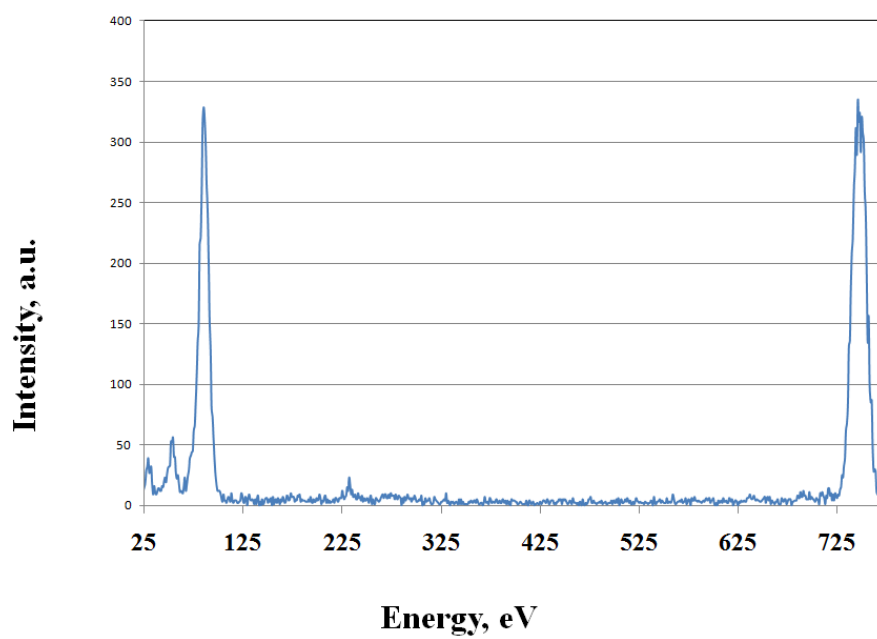
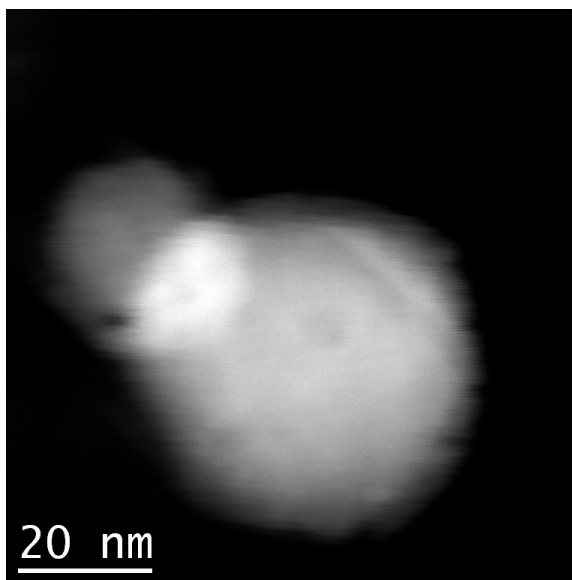


Figure 5-36. EDS analysis of small particles in used Ni-Rh/b catalysts after steam reforming of Jet fuel 1000 ppm sulfur at 800°C, S/C=3 and 1 atm

Figure 5.37 shows some of the STEM and EDS scans of large particles in used Ni-Rh/b catalyst recovered after steam reforming of jet fuel. The small peak at 230 eV suggests that sulfur was present on large crystallites containing nickel and/or palladium. Particles containing Rh did not usually exhibit the presence of sulfur. It should be mentioned that sulfur was seen mostly on the edge of the large particles and not much when the bulk of the particle was the scanning area. This is an important observation and it means that surface adsorption of sulfur was seen and bulk absorption of sulfur was generally not observed.



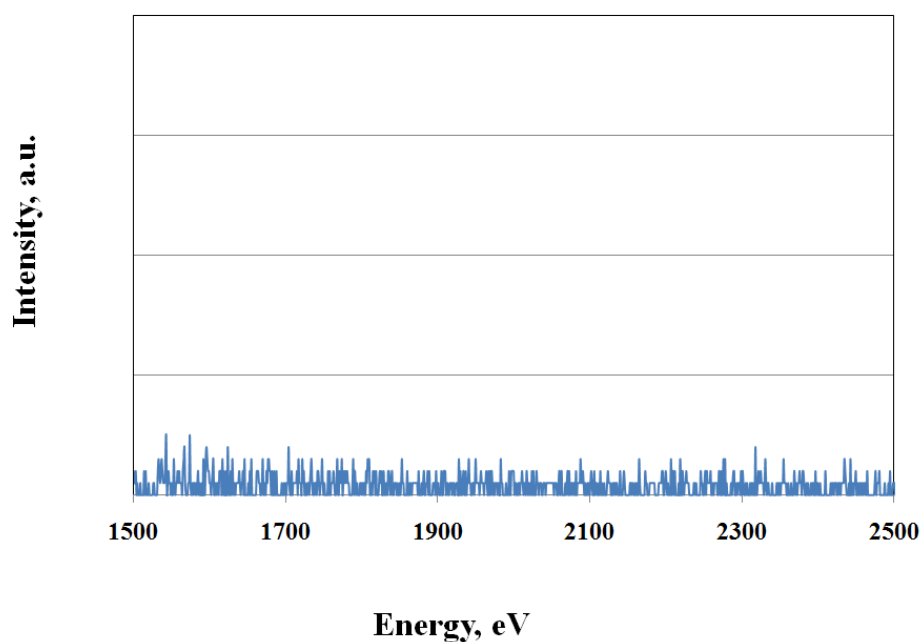
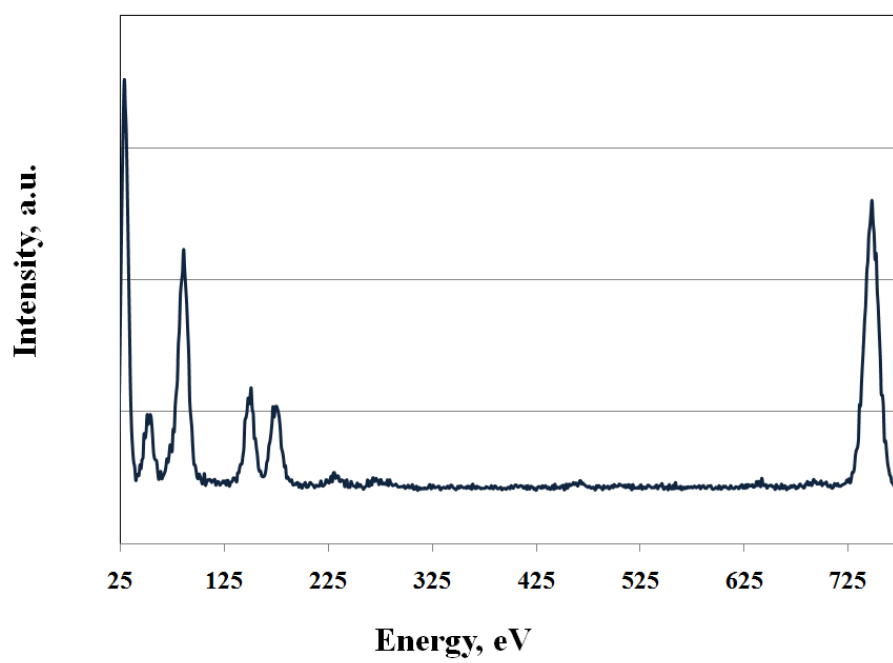
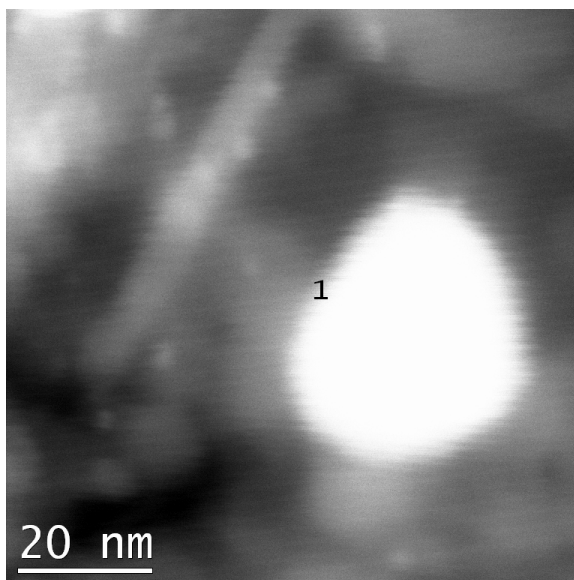


Figure 5-37. EDS analysis of large particles in used Ni-Rh/b catalysts after steam reforming of Jet fuel 1000 ppm sulfur at 800°C, S/C=3 and 1 atm

Figure 5.38 shows similar results in case of used 3J1 catalyst. An edge of the large particle was scanned for sulfur presence. As mentioned earlier, a peak at 230 eV corresponding to sulfur was detected.



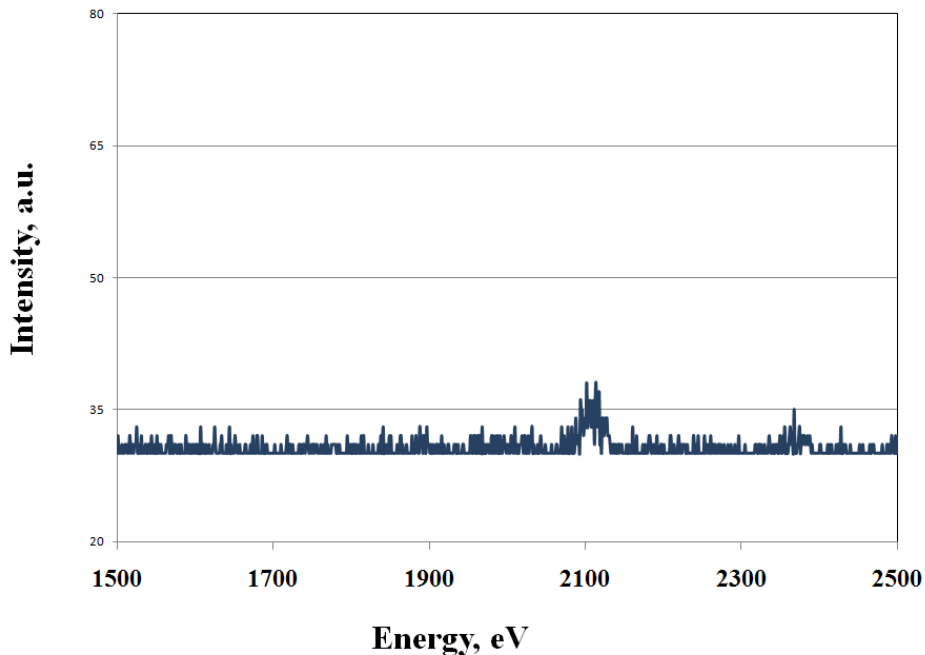
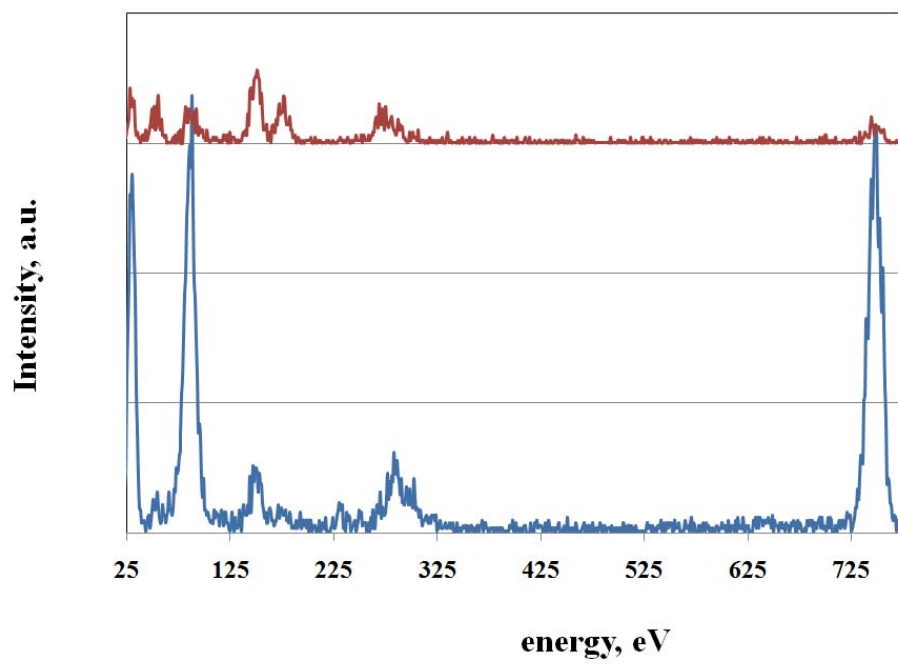
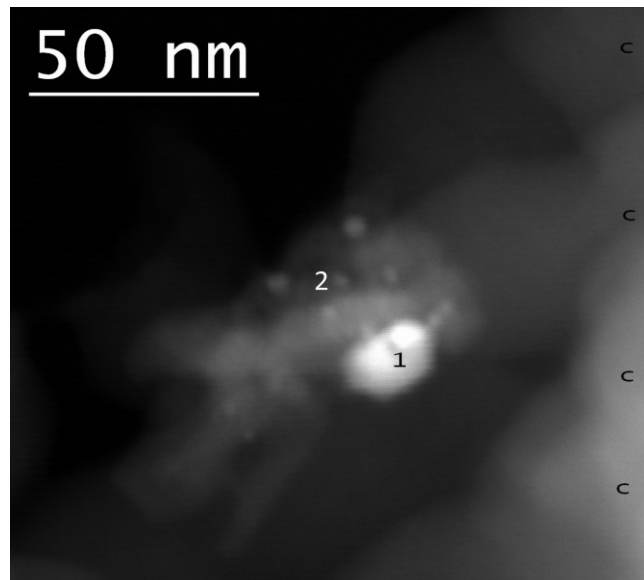


Figure 5-38. EDS analysis of large particles in used 3J1 catalysts after steam reforming of Jet fuel 1000 ppm sulfur at 800°C, S/C=3 and 1 atm

Figure 5.39 shows the STEM image of one of the large particles with few surrounding small particles. As mentioned earlier, the large particles are predominantly Ni and or/Pd while the small particles contain Rh. Position 1 refers the the edge of the large particle while position 2 refers to the Rh particle. EDS profile at these 2 locations suggest that sulfur is not present on the surface of Rh containing particles while is seen to deposit essentially on large particles containing Ni and/or Pd. Figure 4.36 is a confirmation to the observation made that sulfur preferentially sits on the surface of particles with Ni and/or Pd while is generally avoided on the surface of crystallites containing Rh.



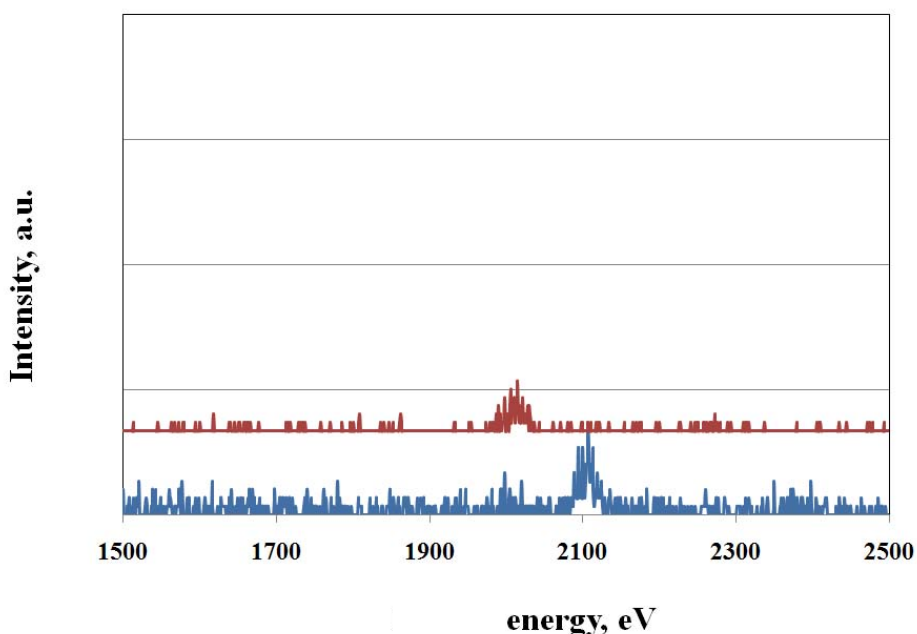


Figure 5-39. EDS analysis of large particles in used 3J1 catalysts after steam reforming of Jet fuel 1000 ppm sulfur at 800°C, S/C=3 and 1 atm

5.6.3. Carbon deposition studies

TPO of the used catalyst was employed to understand both the quantity and quality of coke formed on the catalyst. Figure 5.40 shows the TPO profiles of used catalysts from reforming experiments using jet fuel. Generally, the high temperature peaks are assigned to carbon deposited on or around alumina support while the low temperature peaks are characterized as metals situated around the carbon. In this study, broad peaks corresponding to carbon oxidation were seen starting to appear at temperatures higher than 520 °C. The high temperature peaks were only seen for catalysts Ni/b, Pd/b and Ni-Pd/b and were not observed in any Rh containing catalysts. The low temperature peaks were either very small or absent in most of the catalysts studied. This may indicate that

the carbon was extensively deposited on the surface of the support and not much was observed on the metal sites. It should be emphasized that the Rh containing catalysts with less carbon deposition corresponded with Rh-containing catalysts that gave higher hydrogen yields and lower deactivation, suggesting that one of the causes of deactivation is carbon deposition on the surface of support.

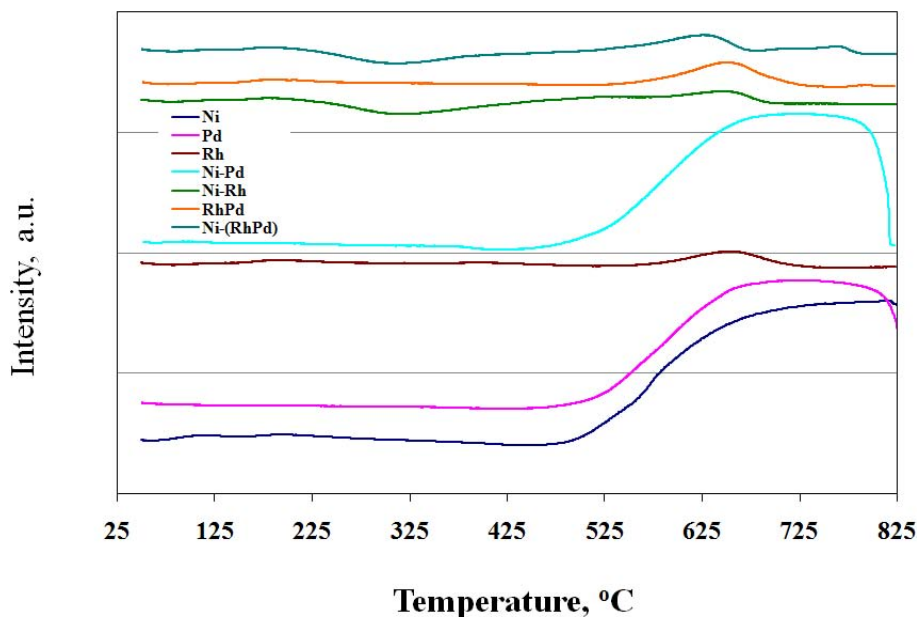


Figure 5-40. TPO of used catalysts catalysts after steam reforming of Jet fuel 1000 ppm sulfur at 800°C, S/C=3 and 1 atm

To further support the conclusion made above, a line scan of one of the Ni/Pd particles found in used 3J1 catalyst is shown in figure 5.41. Composition of different metals can be seen as a function of axial length shown using a line drawn across the image. Ni and Pd are seen uniformly along the length while Al and O showed up at the end of the particle, which represents the support of the catalyst carrying the metal crystallite. What is

important to notice is the spike of carbon seen at the end of the particle which correlates to the spike of the alumina. It is reasonable to postulate that carbon was extensively deposited on the surface of the catalyst support. It should also be mentioned that sulfur and rhodium were below detectable limits.

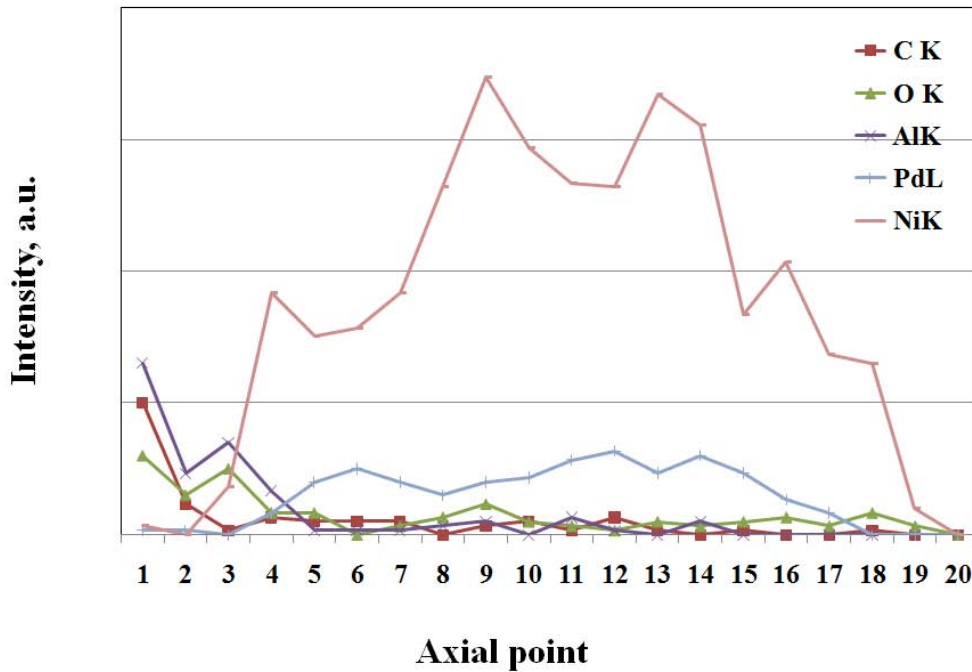
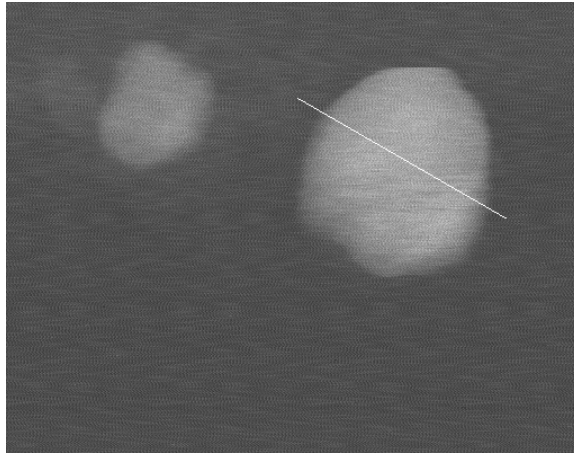


Figure 5-41. EDS analysis of Ni/Pd particle in used 3J1 catalysts after steam reforming of Jet fuel 1000 ppm sulfur at 800°C, S/C=3 and 1 atm

One of the important set of experiments was to study the growth of carbon deposition with time. The used catalysts were recovered at 1, 4, 10, 20 and 45 h on stream and were then characterized using TPO and XPS. Figure 5.42 presents some of the TPO profiles of catalysts recovered after steam reforming at different times on streams. The catalysts did not show appreciable carbon deposition until 20 h time on stream. The large peak observed for 45 h run was due to carbon that is deposited on the catalysts support. This peak starts oxidizing at temperatures above 450 °C and can be assigned to support associated carbon. In short, carbon is accumulated over time on stream and its build up is best observed at longer times on stream. The peak was observed much earlier in case of catalysts not containing Rh and corresponded to an earlier onset of deactivation during reaction experiments. For example, in case of Ni/b, Pd/b and Ni-Pd/b, the peak was observed within the first 10 h on stream. The same is shown using the XPS results below.

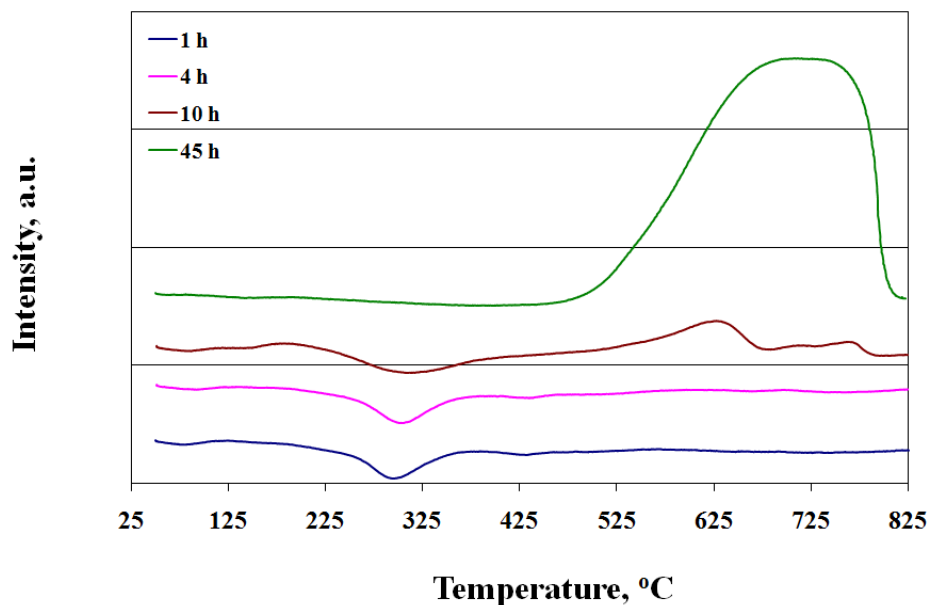


Figure 5-42. TPO of used 3J1 at different times on stream after steam reforming of Jet fuel 1000 ppm sulfur at 800°C, S/C=3 and 1 atm

The carbon deposition was compared with the amount of C₂₊ products (% dry basis) in the effluent stream. A close relation between the cracked products in the reformat and the amount of carbon deposition on the support during the course of steam reforming is observed. Catalysts Ni/b, Pd/b and Ni-Pd/b resulted in high amounts of cracked products, more so with sulfur laden feed. Cracking was observed even in the absence of sulfur, although to a lower level than observed for the sulfur-free fuels. Catalyst formulations containing Rh did not result in excessive cracking products. The cracking results were shown in the initial section of this chapter.

C 1s XPS was conducted on the used catalysts to determine the carbon form present during reforming on different catalyst formulations, as shown in Figure 5.43. Catalysts containing Rh displayed a peak at 284.7 eV, which is generally assigned to the hydrocarbonaceous and/or graphitic type of carbon.¹⁰² Catalysts Ni/b, Pd/b and Ni-Pd/b (non-Rh) displayed a peak at 286.3 eV, attributed to a polymeric and/or aromatic type of carbon species.¹⁰³ This peak also displayed a broad tailing at the high binding energy end. Catalysts containing higher Rh content only contained a single peak at 284.7 eV, indicating that higher amounts of Rh inhibited the formation of aromatic/polymeric type of carbon when sulfur was present. Recall that Ni/b, Pd/b and Ni-Pd/b catalysts deactivated rapidly relative to the catalysts containing higher percentages of Rh, suggesting that formation of aromatic/polymeric carbon was a primary deactivation mechanism.

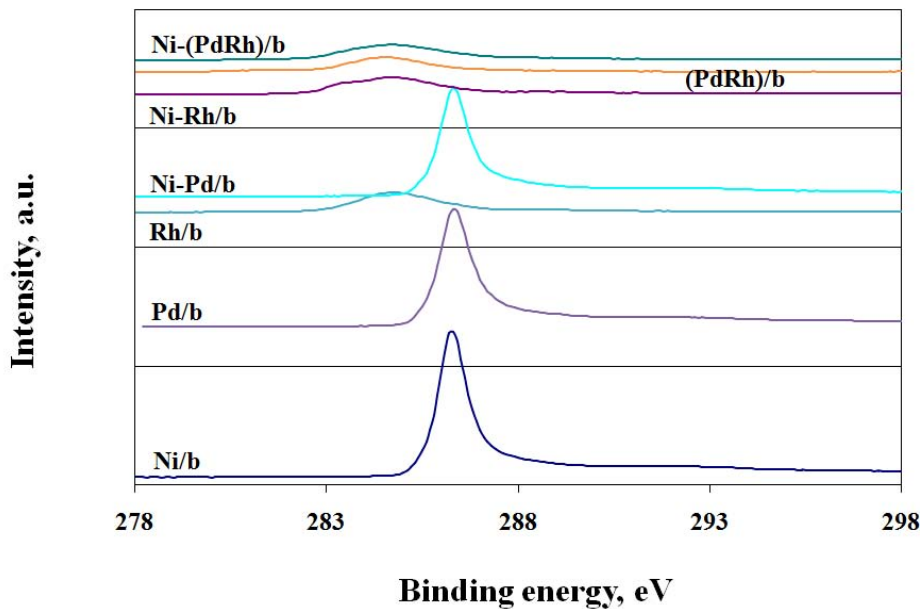


Figure 5-43. C 1s XPS of used catalysts after steam reforming of Jet fuel 1000 ppm sulfur at 800°C, S/C=3 and 1 atm

Characterization of time on stream studies was done to get more information on the build-up of carbon on 3J1 catalysts. The results are shown below in figure 5.48 which presents C 1s XPS of used 3J1 catalysts run at different time on streams, with the maximum of 45 h. The results are in agreement with that of TPO where only 45 h run used catalysts displayed a huge peak at high oxidation temperature.

As mentioned in the previous chapter, aromatization of alkene intermediates occurs by Diels-Alder reaction, as verified by Parera *et al.*¹⁰⁴ and Liu *et al.*¹⁰⁵. This may be one of the crucial routes to the aromatic carbon deposition during steam reforming. To demonstrate this phenomenon, analysis of the C1s peaks was done at different stages of the reaction starting from 1 h to 45 h time on stream. Figure 5.44 shows the evolution of

these peaks as a function of time on stream for reforming of sulfur laden fuel by 3J1 catalyst. Aromatic carbon peak at binding energy 286.3 eV was observed after 45 h on stream, indicating the formation of these species only after longer time on stream. Unlike in case of NM4, the process of deactivation is delayed and the aromatic carbon deposition is observed only after 20 h time on stream. In short, it can be said that the process of deactivation occurs by both sulfur poisoning and carbon deposition and the process is generally delayed by the presence of noble metals, mainly Rh. A detailed mechanism of deactivation during heavy fuel steam reforming is postulated based on these observations and is presented in the next chapter.

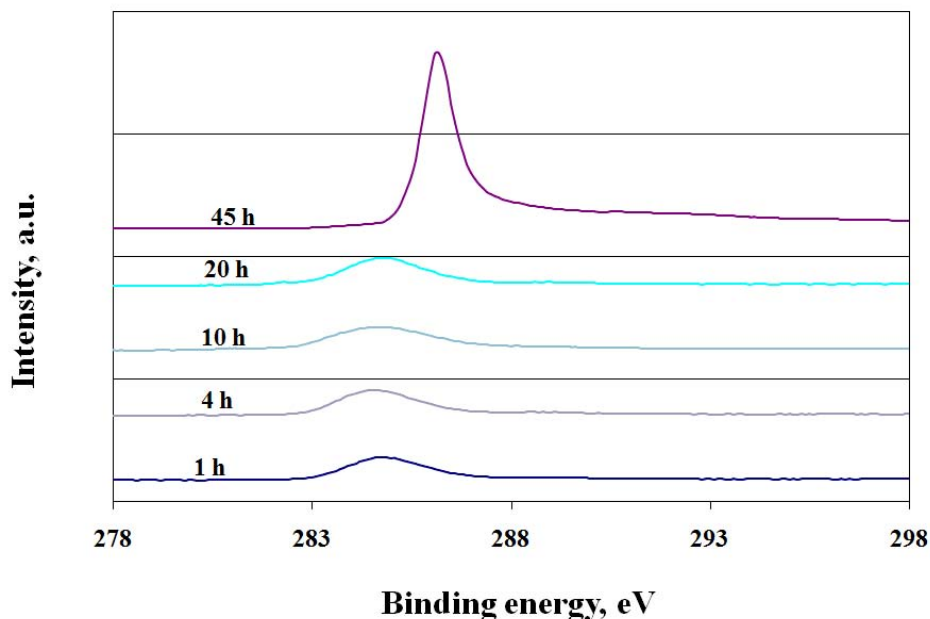


Figure 5-44. C 1s XPS of used 3J1 at different times on stream catalysts steam reforming of Jet fuel 1000 ppm sulfur at 800°C, S/C=3 and 1 atm

Chapter 6

Summary of results and proposed mechanism of deactivation

Two catalyst systems, NM4 and 3J1, were synthesized and characterized to study deactivation mechanism during steam reforming of sulfur containing liquid fuels. A mechanism for the deactivation based on the current results and prior literature is described below and shown schematically in figure 6.1.

Steam reforming of sulfur containing fuel is a collection of many distinct reactions, each of which can occur on Rh, Ni, Pd, alumina support or some combination of them. The hydrocarbon species adsorbed on the surface of active site is converted to hydrogen and carbon oxides by reaction with a water molecule either from the gas phase or adsorbed on the support surface in the vicinity. Results obtained from the monometallic catalysts suggests that the reforming reaction occurs on Ni, Pd, and Rh sites although the rate of reaction differs depending on the nature of the active metal site and the presence of sulfur. In general, catalysts exhibited stable performance in sulfur-free environment. In the presence of sulfur, significant deactivation was observed; the extent of deactivation was limited by the presence of higher amounts of Rh. The surface morphology of the fresh catalyst showed the presence of two groups of crystallites, primarily distinguished based on their relative sizes. A group of particles from a few nanometers to around 6 nm

were shown to consist mainly of Rh, with or without the presence of other metals (Ni and Pd). The other group of particles was larger in size (10 nm-20 nm) and was essentially made of Ni and/or Pd. These particles did not contain Rh. On reaction, the large particles grew in size. Over a period of 10 h on stream, the particles were seen in the range of 30-100 nm, depending on the presence of other metals and whether the fuel contained significant concentration of sulfur. Addition of Rh inhibited the growth of Ni crystallites. This had a beneficial effect on the overall steam reforming reaction in terms of higher hydrogen yields and lower deactivation rates. On the other hand, addition of Pd did not have any identifiable impact on the rate of deactivation, but resulted in excessive cracking products. It should also be mentioned that the growth of support alumina phase was not seen. Recall that the peak width of support alumina did not undergo significant change during pretreatment and activity tests. Therefore, deactivation due to support phase collapse can be ruled out completely.

It is known that the process of sintering occurs by mainly two mechanisms; (a) crystallite migration where entire crystallites migrates over the surface of the carrier followed by coalescence and (b) Ostwald ripening, where metal species emitted by one crystallite travels on the support or in the gas phase and are captured by other crystallite. In the present studies where the temperatures were very high, it is postulated that Ostwald ripening is the dominant cause of sintering. This mechanism seems reasonable considering that it is expected that the energy involved in creating and moving nickel transport species at the surface of nickel particles is lower than the energy involved in nickel transport at a carrier. Sintering of the metal catalysts is accelerated with the presence of steam in the atmosphere around the catalyst. DFT calculations on nickel

steam reforming catalysts show that the combined energy of formation and diffusion for $\text{Ni}_2\text{-OH}$ complexes at $\text{Ni}(111)$ is 40 kJ/mol lower than that for nickel adatoms, strongly indicating that the former species are dominating the surface transport of nickel at nickel surfaces when steam is present in the atmosphere.²² Recall that in case of non-Rh catalysts, the yields were significantly lower which meant higher partial pressure of unreacted steam in the local environment around the catalyst. Higher the concentration of steam, higher is the concentration of $\text{Ni}_2\text{-OH}$ complexes, thereby leading to the accelerated growth of nickel crystallites. It should be understood that the steam to carbon ratio was kept constant for all the catalysts testing. The extent of steam present during the reaction depends on the extent of reaction that consumes steam. Low conversion means more unreacted steam. In case of Rh-containing catalysts, the concentration of steam was relatively lower (and more conversion), which meant that the probability of the formation of $\text{Ni}_2\text{-OH}$ complexes was lower. Sintering has a direct effect on the activity of the catalyst toward steam reforming reaction. The decrease in the activity is directly related to the loss in the surface area due to sintering. Moreover, in case of coking, the effect is more pronounced.

Studies concerning deactivation of reforming catalysts, particularly in case of fuel processing of sulfur containing transportation fuels, has attracted numerous interest in the recent past. Model compound sulfur poisoning studies on single crystals has shown that the adsorption of sulfur on the surface of the metal can lead to profound surface restructuring, leading to changes on activity and selectivity. It is a general assumption that organic sulfur compounds are converted to hydrogen sulfide dictated by strong driving force for the same. It is also well known that the dissociation of thiophene or any

other organic sulfur compounds proceeds via hydrodesulfurization (HDS) where the sulfur compound is first adsorbed and hydrogenated which is then cleaned by hydrogen in the vicinity leading to the formation of hydrogen sulfide.¹⁰⁶ In the present study, it was seen that highly active and stable catalyst formulations gave high sulfur yields. It is proposed that there exists a strong correlation between the tolerance to sulfur and hydrogen concentration during reforming. Catalysts not containing Rh gave substantially low hydrogen concentrations and relatively low sulfur yields. A diminished hydrogen content is inversely proportional to the concentration of hydrogenated sulfur compound, a pre-requisite for the dissociation of sulfur compound. Based on these observations it is reasonable to propose that HDS proceeds normally on the surface of the most active catalyst formulation, leading to equilibrium sulfur coverage. Since this equilibrium sulfur concentration was extremely low, it was never seen in the TEM/EDS studies performed on the used catalysts. Conversely, when this low sulfur coverage equilibrium was not reached, perhaps due to a lower availability of surface-bound hydrogen, site-blocking sulfides accumulated on the less active nickel sites and thereby caused a continuous drop in activity over time.

Sulfur was preferentially adsorbed on the surface of nickel crystallites, thus blocking the reaction sites. No detectable sulfur was found on the surface of rhodium crystallites. Presence of palladium in nickel crystallites did not prevent sulfur adsorption. Bulk sulfur absorption was not observed and only surface adsorption was seen. Since sulfur was preferentially detected on the surface of Ni crystallites, it is likely that the decomposition reaction of thiophene occurred on the same crystallites via HDS as mentioned before. It is also possible that the sulfur adsorbed on rhodium sites of Rh may migrate to nearby Ni

sites, particularly when Ni and Rh particles are present in close proximity, as expected due to co-impregnation method of preparation in the present study. Based on the difference in electronegativities of the elements forming the bonds ($\chi_S = 2.58$, $\chi_{Rh} = 2.28$, and $\chi_{Ni} = 1.91$), the Rh-S bond is less stable than would be a Ni-S bond and thus it is more likely for sulfur to migrate from Rh to Ni than it is in the reverse path. H₂ may assist in sulfur migration via H₂S species, as described by Strohm *et al.*⁹⁹ The potential migration of sulfur from Rh to Ni may further act to retain the reforming activity of the Rh sites. It can be postulated that under more severe conditions, more sulfide layers are formed, but still no bulk sulfide even after full deactivation of the catalyst. This is a reasonable postulation from the result that the yield of sulfur is generally higher and follows the same trend as that of hydrogen yield. Moreover, when the catalyst deactivates, unreacted thiophene was seen in the liquid effluent, suggesting no further adsorption after saturation. This suggests a solid- diffusion-limited process. The solid diffusion process is worsened by the deposition of carbon on the surface of catalyst.

Graphitic carbon was present at all stages of catalyst life irrespective of the catalyst composition. Graphitic carbon formation was significantly higher for sulfur-containing fuels. The formation of graphitic carbon is a byproduct of incomplete conversion of the hydrocarbon, which is catalyzed by both Ni and Rh. As the Ni becomes saturated with sulfur, it becomes less effective for reforming and the formation of graphitic carbon becomes more significant.

The formation of aromatic/polymeric carbon was seen to be effected by the presence of sulfur in the feed and by the Rh content of the catalyst. As the Ni surface becomes

saturated with sulfur, Ni becomes less effective in catalyzing the conversion of the hydrocarbon into hydrogen and carbon oxides. Rather, hydrocarbons adsorbed onto Ni-S sites migrate to the alumina support, where they undergo acid cracking to produce cracked products. In previous work, acid cracking was observed and was seen to be facilitated by the presence of sulfur. The cracked products may then undergo dehydrogenation to give unsaturated hydrocarbons on the support, or through catalytic interaction with Rh may produce hydrogen and carbon oxides. No significant carbon deposition was observed when Rh was present in abundance, due to its good steam reforming ability. Without high Rh content, there is substantial accumulation of unsaturated hydrocarbons on the surface of the support, which eventually lead to aromatic type of carbon, via Diels-Alder reaction.¹⁰⁴**Error! Bookmark not defined.**⁷⁶. These aromatic compounds, over a period of time, may also undergo polymerization to give polymeric deposition, as seen in the TPO results and XPS studies of the current work. Similar propositions were made by Bickle *et al.* in the case of platinum/alumina reforming catalysts.¹⁰⁷

In short, we postulate that sulfur adsorption on nickel sites causes the initial deactivation of the catalyst which suppresses carbon gasification on the active sites, thereby accumulating carbon deposits over time. On the other hand, presence of rhodium inhibits this phenomenon to a large extent, due to high gasifying ability of rhodium metal.

The observations coupled with our postulations were put together to propose a deactivation mechanism model during steam reforming of sulfur-containing liquid fuel on a noble metal promoted nickel based catalyst. The same is shown in figure 6.1. Four different stages of catalyst micro-structure are shown, with relevance to catalyst

deactivation. At time $t=0$, the catalyst is clean and active, free of any carbon and sulfur. At the start of the reaction, the pure catalyst was covered with hydrocarbon fragments along with few thiophene molecules. With the progress of reaction, nickel particles sintered, primarily due to Ostwald ripening. Moreover, it was also covered with sulfide layers, thereby reducing its reforming activity. Meanwhile, rhodium was resistant to sintering and was active for reforming. The adsorbed hydrocarbon on sulfur poisoned nickel crystallite may spill over to alumina support in the vicinity, which leads to the formation of carbon deposits on the support. It is also speculated that sulfur may migrate from rhodium to nickel in the vicinity with the assistance of gas phase hydrogen. Due to poor carbon gasifying ability of sulfur poisoned nickel crystallite, the adsorbed hydrocarbon migrates to adjacent support alumina where it forms aromatic/polymeric type of species, via Diels-Alder condensation reaction as described earlier. Observed deactivation is a combined effect of both sulfur poisoning and excessive carbon deposition that blocks accessibility of reactant molecules to the active sites.

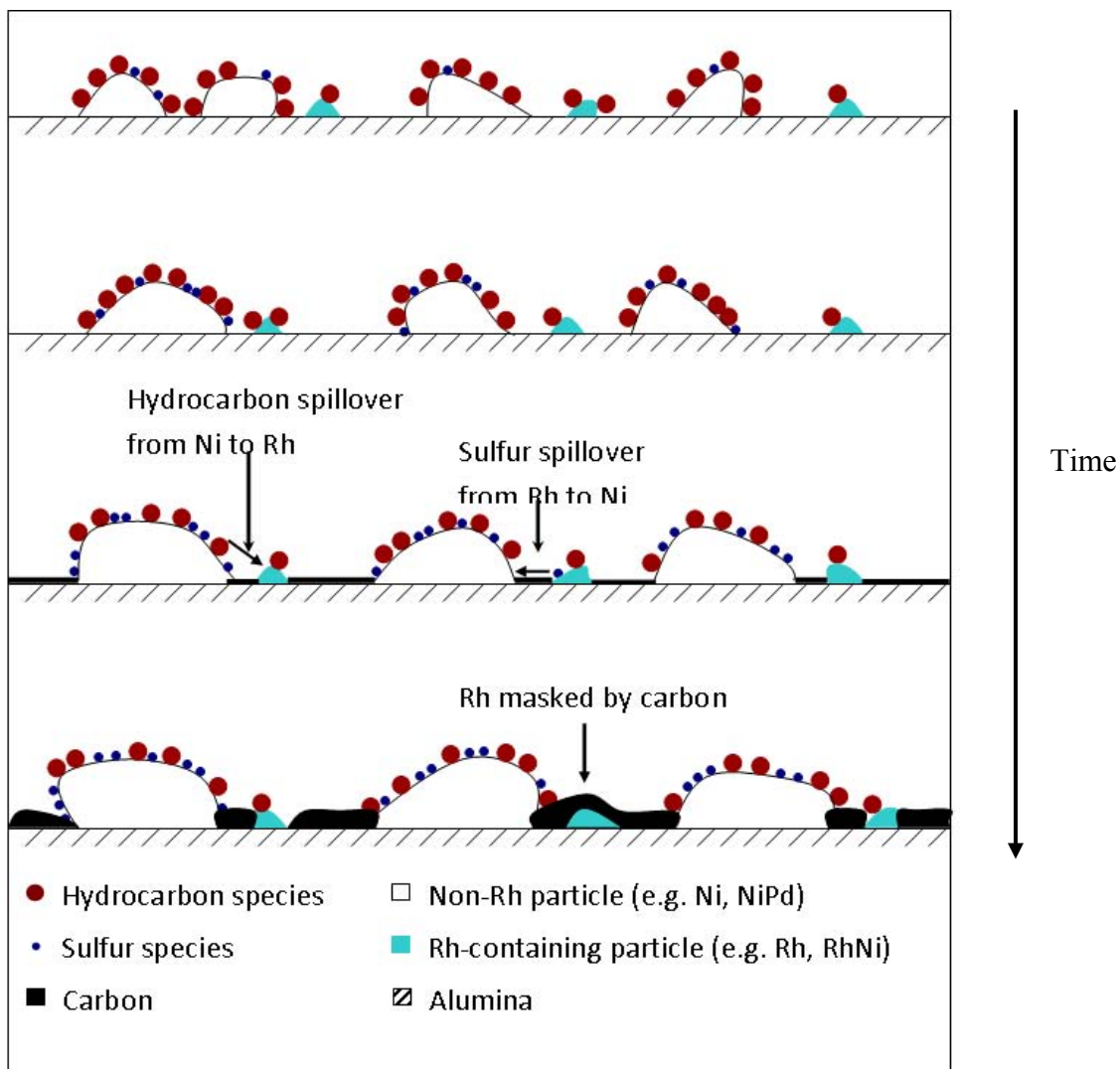


Figure 6-1. Proposed deactivation mechanism on a noble metal promoted nickel based sulfur-tolerant steam reforming catalyst

Chapter 7

Conclusions

In this study, catalyst deactivation during steam reforming of transportation fuels, diesel and jet fuel, was investigated on two previously prepared catalyst formulations, NM4 and 3J1. For comparison purposes, both the catalysts were tested for activity at same conditions of temperature (800°C), pressure (1 atm) and steam to carbon ratio (3).

In general, catalysts showed better activity and stability during sulfur-free steam reforming while they deactivated in the presence of sulfur. Stable and active catalysts, generally those containing Rh, gave complete conversion of thiophene to hydrogen sulfide while those that were less active and stable gave diminished sulfur yields. The latter also coincided with a continuous decline in reforming activity over time.

Addition of Rh to the catalyst formulation had a positive effect on the catalyst activity in terms of hydrogen yield. It was also well established that addition of Rh inhibited the growth of Ni crystallites both during catalyst preparation and steam reforming reaction. This basically meant that there was more metal surface area for reaction which lead to increased hydrogen yields in Rh-containing catalysts. It was convincingly shown that sulfur preferentially adsorbs onto Ni sites while Rh was protected during reforming

reaction. No bulk sulfur was detected and only surface sulfur was formed which was shown to be a thermodynamically favorable process.

Graphitic carbon was present at all stages of catalyst life irrespective of the catalyst composition and it was significantly higher for sulfur-containing fuels. Carbon deposition studies also showed that most of the carbon was present as aromatic/polymeric type. This carbon type was seen to mask metal sites and cause catalyst deactivation.

The research findings from the present work gave new insights into the mechanism of deactivation of noble metal promoted nickel based catalyst during steam reforming of sulfur-containing liquid fuel. One of the important future works should be focused on understanding the nature of different sulfur species (sulfide, sulfate, sulfonate, etc.). It would also be worthwhile to study the effect of steam to carbon ratio on steam reforming activity and deactivation. In-situ studies concerning the interaction of sulfur with well defined metal and oxide surfaces should be conducted to elucidate changes in the structural, morphological, and electronic properties. It has been shown that the chemical activity of a metal can be changed by metal-metal and metal-oxide interactions. Such studies will only help in better scientific design of catalysts, resistant to sulfur poisoning or a high activity for hydrodesulfurization.

References

- ¹ Milliken, J. Transportation fuel cell program, in: Proceedings of the Annual National Laboratory, R&D Meeting of DOE Fuel Cells for Transportation Program, Tri-Cities, WA, June **2000**.
- ² Baujura, R. A.; Fuel cells: simple solutions in a complicated world, in: Proceedings of the Joint DOE/EPRI/GRI Review Conference on Fuel Cell Technology, Chicago, IL, August **1999**.
- ³ Chalk, S. G.; Miller, J. F.; Wagner, F. W. Challenges for fuel cells in transport applications. *J. Power Sources* **2000**, 86 (1), 40.
- ⁴ Song, S. Fuel processing for low-temperature and high-temperature fuel cells: Challenges, and opportunities for sustainable development in the 21st century. *Catal. Today* **1998**, 77, 17.
- ⁵ Thomas, S.; Zalowitz, M. Fuel Cells: Green Power, Publication No. LA-UR-99-3231, Los Alamos National Laboratory, Los Alamos, NM, **2000**.
- ⁶ Carrette, L.; Friedrich, K. A.; Stimming, U. Fuel Cells: Principles, Types, Fuels, and Applications. *Chemphyschem* **2000** 1 (4), 162
- ⁷ Hirschenhofer, J. H.; Stauffer, D. B.; Engleman, R. R.; Klett, M. G. Fuel Cell Handbook, 4th ed., DOE/FETC-99/1076, US Department of Energy, Federal Energy Technology Center, Morgantown, WV, November **1998**.

-
- ⁸ Brown, L. F. A comparative study of fuels for on-board hydrogen production for fuel-cell-powered automobiles. *Intern. J. Hyd. Energy* **2001**, 26, 381.
- ⁹ Momirlan, M.; Veziroglu, T. N. The properties of hydrogen as fuel tomorrow in sustainable energy system for a cleaner planet. *International Journal of Hydrogen Energy* **2005**, 30, 795.
- ¹⁰ Shoesmith, J. P.; Collins, R. D.; Oakley, M. J.; Stevenson, D. K. Status of solid polymer fuel cell system development. *J. Power Sources* **1994**, 49, 129.
- ¹¹ Swami, S. PhD Thesis, University of Toledo, Toledo, Ohio, USA, **2008**.
- ¹² Virent Energy Systems, <http://www.virent.com/Platforms/biofuels.html>, **2010**.
- ¹³ Lindermeir, A.; Kah, S.; Kavurucu, S.; Muhlnert, M. On-board diesel fuel processing for an SOFC–APU—Technical challenges for catalysis and reactor design. *Appl. Catal. B: Environmental* **2007**, 70 (1-4), 488.
- ¹⁴ Qi, A.; Peppley, B.; Karan, K. Integrated fuel processors for fuel cell application: A review. *Fuel Proc. Tech.* **2007**, 88, 3.
- ¹⁵ Babich, I. V.; Moulijn, J. A. Science and technology of novel processes for deep desulfurization of oil refinery streams: a review. *Fuel* **2003**, 82 (6), 607.
- ¹⁶ H. Topsøe, F. E. Massoth and B. S. Clausen. In: J. R. Anderson and M. Boudart, Editors, *Catalysis, Science and Technology*, Springer, Berlin, **1996**, p. 310.
- ¹⁷ Gerritsen, L. A.; Stoop, F.; Low, P.; Townsend, J.; Waterfield, D.; Holder, K. WEFA Conference, Berlin, Germany; June **2000**.
- ¹⁸ Brevoord, E.; Gerritse, L. A.; Plantenga, F. L. The European Refinery Technology Conference, Rome, Italy, November, **2000**.

-
- ¹⁹ Mayo, S.; Plantenga, F.; Leliveld, B.; Miyauchi, Y. A. NPRA 2001 Annual Meeting, New Orleans, March, **2001**.
- ²⁰ Aida, T.; Yamamoto, D.; Iwata, M.; Sakata, K. *Rev Heteroatom Chemistry* **2000**, *22*, 241.
- ²¹ Ahmed, S., Krumpelt, M. Hydrogen from hydrocarbon fuels for fuel cells. *Intern. J. Hyd. Energy* **2001**, *26*, 291.
- ²² Sehested, J.; Gelten, J. A. P.; Remediakis, I. N.; Bengaard, H.; Norskov, J. K. Sintering of nickel steam-reforming catalysts: effects of temperature and steam and hydrogen pressures. *J. Catalysis* **2004**, *223*, 432.
- ²³ Trimm, D. L. Catalysts for the control of coking during steam reforming. *Catal. Today*. **1999**, *49*, 3.
- ²⁴ Borowiecki, T.; Giecko, G.; Panczyk, M. Effects of small MoO₃ additions on the properties of nickel catalysts for the steam reforming of hydrocarbons. *Appl. Catal. A: General* **2002**, *230*, 85.
- ²⁵ Goud, S. PhD Thesis, University of Toledo, Toledo, USA, **2007**.
- ²⁶ Kataria, A, PhD Thesis, University of Toledo, Toledo, USA, **2009**.
- ²⁷ Effendi, A.; Zhang, Z. G.; Hellgardt, K.; Honda, K.; Yoshida, T. Steam reforming of a clean model biogas over Ni/Al₂O₃ in fluidized- and fixed-bed reactors. *Catalysis Today* **2002**, *77*(3), 181.
- ²⁸ Gawade, P. MS Thesis, University of Toledo, Toledo, USA, **2008**.
- ²⁹ J.R. Rostrup-Nielsen, in: J.R. Anderson, M. Boudart (Eds.), *Catalysis: Science and Technology*, vol. 5, Springer, Berlin, **1984**, pp. 1–117.

-
- ³⁰ Bodrov, N.M.; Apel'baum, A.; Temkin, M. I. Kinetics of the reaction of methane with water vapor on a nickel surface. *Kinet. Catal.* **1964**, 5, 614.
- ³¹ Xu, J.; Froment, G. F. Methane steam reforming, methanation and water-gas shift: I. Intrinsic kinetics. *AIChE J.* **1989**, 35 (1), 88.
- ³² Borowiecki, T.; Gołębiowski, A.; Stasińska, B. Effects of small MoO₃ additions on the properties of nickel catalysts for the steam reforming of hydrocarbons. *Appl. Catal. A Gen.* **1997**, 153, 141.
- ³³ Bartholomew, C. H. Carbon Deposition in Steam Reforming and Methanation. *Catal. Rev. Sci. Eng.* **1982**, 24, 67.
- ³⁴ Zhang, Q.; Qin, Y.; Chang, L. Promoting Effect of Cerium Oxide in Supported Nickel Catalyst for Hydrocarbon Steam-reforming. *Appl. Catal.* **1991**, 70, 1.
- ³⁵ Su, B. L.; Guo, S. D. in: Catalyst Deactivation, B. Delmon, G.F. Froment (Eds.), Elsevier, Amsterdam, **1999**, p. 325.
- ³⁶ Teixeira, A.C.S.C. ; Giudici, R. Deactivation of steam reforming catalysts by sintering: experiments and simulation. *Chem. Eng. Sci.* **1999**, 54, 3609.
- ³⁷ Ridler, D. E.; Twigg, M. V.; in: Catalyst Handbook, M.V. Twigg (Eds.), Wolfe, London, **1989**, p. 225.
- ³⁸ Kochloefl, K. in: Handbook of Heterogeneous Catalysis, G. Ertl, H. Knozinger, J. Weitkamp (Eds.), VCH, Germany, Vol. 4, **1997**, p. 1819.
- ³⁹ Rostrup-Nielsen, J. R. Activity of Nickel Catalysts for Steam Reforming of Hydrocarbons. *J. Catal.* **1973**, 31, 173.
- ⁴⁰ Tottrup, P. B. Evaluation of Intrinsic Steam Reforming Kinetic Parameters from Rate Measurements on Full Particle Size. *Appl. Catal.* **1982**, 4, 377.

-
- ⁴¹ Phillips, T. R.; Mulhall, J.; Turner, G. E. Kinetics and mechanism of the reaction between steam and hydrocarbons over nickel catalysts in the temperature range 350 to 500C. *J. Catal.* **1969**, 15, 233.
- ⁴² Muraki, H.; Fujitan, Y. Steam reforming of n-heptane using a Rh/MgAl: I. Support and kinetics. *Appl. Catal.* **1989**, 47, 75.
- ⁴³ Goud, S. K.; Whittenberger, W. A.; Chattopadhyay, S.; Abraham, M. A. Steam reforming of n -hexadecane using a Pd/ZrO₂ catalyst: Kinetics of catalyst deactivation. *Intern. J. Hyd. Energy.* **2007**, 32, 2868.
- ⁴⁴ Borowiecki, T. Nickel catalysts for steam reforming of hydrocarbons: phase composition and resistance to coking. *Appl. Catal.* **1984**, 10, 273.
- ⁴⁵ Tracz, E.; Scholz, R.; Borowiecki, T. High-resolution electron microscopy study of the carbon deposit morphology on nickel catalysts. *Appl. Catal.* **1990**, 66, 133.
- ⁴⁶ B. Stasinska, A. Golebiowski, T. Borowiecki, in: Catalyst Deactivation, B. Delmon, G.F. Froment (Eds.), Elsevier, Amsterdam, 1999, p. 431.
- ⁴⁷ Kepinski, L.; Stasinska, B.; Borowiecki, T. Carbon deposition on Ni/Al₂O₃ catalysts doped with small amounts of molybdenum. *Carbon* **2000**, 38, 1845.
- ⁴⁸ Sidjabat, O.; Trimm, D. L. Nickel–magnesia catalysts for the steam reforming of light hydrocarbons. *Topics in Catal.* **2000**, 11, 279.
- ⁴⁹ Igarashi, A. Catalyst for steam reforming of hydrocarbon. *US Patent 5,130,114*, **1992**.
- ⁵⁰ Ostberg, M.; Hansen, J. H. B.; Nielsen, P. C. I. Aasberg-Petersen, K. Process for pre-reforming of oxygen-containing gas. *US Patent 6,335,474*, **2002**.

-
- ⁵¹ Ferrandon, M.; Krause, T. Role of the oxide support on the performance of Rh catalysts for the autothermal reforming of gasoline and gasoline surrogates to hydrogen. *Appl. Catal., A Gen.* **2006**, 311, 135.
- ⁵² Ayabe, S.; Omoto, H.; Utaka, T.; Kikuchi, R.; Sasaki, K.; Teraoka, Y.; Eguchi, K. Catalytic autothermal reforming of methane and propane over supported metal catalysts. *Appl. Catal. A Gen.* **2003**, 241, 261.
- ⁵³ Mizuno, T.; Nakajima, T. A stable catalyst for hydrogen production by steam reforming of 2-propanol: Rh/Al₂O₃. *J. Chem. Eng. Jpn.* **2002**, 35, 485.
- ⁵⁴ Kikuchi, E.; Ito, K.; Ito, T.; Morita, Y. The reaction of *n*-heptane on rhodium catalysts in the presence of steam. *J. Catal.* **1977**, 46, 382.
- ⁵⁵ Igarashi, A.; Ohtaka, T.; Motoki, S. Low-temperature steam reforming of *n*-butane over Rh and Ru catalysts supported on ZrO₂. *Catal. Letters* **1991**, 13, 189.
- ⁵⁶ Suzuki, T.; Iwanami, H.; Iwamoto, O.; Kitahara, T. Pre-reforming of liquefied petroleum gas on supported ruthenium catalyst. *Intern. J. Hyd. Energy* **2001**, 26, 935.
- ⁵⁷ Kramarz, K. W.; Bloom, I. D.; Kumar, R.; Ahmed, S.; Wilkenhoener R.; Krumpelt, M. Steam reforming catalyst. *US Patent 6,303,098*, **2001**.
- ⁵⁸ Ming, Q.; Healey, T.; Allen, L.; Irving, P. Steam reforming of hydrocarbon fuel. *Catal. Today* **2002**, 77, 51.
- ⁵⁹ Krumpelt, M.; Krause, T. R.; Carter, J. D.; Kopasz, J. P.; Ahmed, S. Fuel processing for fuel cell systems in transportation and portable power applications. *Catal. Today* **2002**, 77, 3.
- ⁶⁰ Okada, O.; Ipponmatsu, M.; Masuda, M.; Takami, A. A study of sulfur poisoning on Ru/Al₂O₃ methanation catalyst. *J. Jpn. Fuel Sci. Tech.* **1989**, 68, 39.

-
- ⁶¹ Suzuki, T.; Iwanami, H.; Yomohiro, T. Steam reforming of kerosene on Ru/Al₂O₃ catalyst to yield hydrogen. *Intern. J. Hydrogen Energy* **2000**, 25, 119.
- ⁶² Oudar, J.; Wise, H. Deactivation and Poisoning of Catalysts, Marcel Dekker, New York, **1985**, p. 1.
- ⁶³ Figuerido, J. L. (Ed.), Progress in Catalyst Deactivation, NATO Advanced Study Institute Series E, Marunus Nijhoff, Boston, **1982**.
- ⁶⁴ Butt, J. B.; Petersen, E. E.; Activation, Deactivation, and Poisoning of Catalysts, Academic Press, San Diego, **1988**.
- ⁶⁵ Bartholomew, C. H. Catalyst deactivation. *Chem. Eng.* **1984**, 91, 96.
- ⁶⁶ Butt, J. B. in: J.R. Anderson, M. Boudart (Eds.), Catalysis, Science and Technology, Springer, New York, **1984**, p. 1.
- ⁶⁷ Farrauto, R. J.; Bartholomew, C. H. Fundamentals of Industrial Catalytic Processes, Chapman & Hall, Kluwer Academic Publishers, London, **1997**.
- ⁶⁸ Delmon, B.; Froment, G. F. Catalyst Deactivation 1980, *Stud. Surf. Sci. Catal.*, Vol. 6, Elsevier, Amsterdam, **1980**.
- ⁶⁹ Bartholomew, C. H.; Butt, J. B. Catalyst Deactivation 1991, *Stud. Surf. Sci. Catal.*, Vol. 68, Elsevier, Amsterdam, **1991**.
- ⁷⁰ Delmon, B.; Froment, G. F. Elsevier 1994, *Stud. Surf. Sci. Catal.*, Vol. 88, Elsevier, Amsterdam, **1994**.
- ⁷¹ Madon, R. J.; Shaw, H. Effect of Sulfur on the Fischer-Tropsch Synthesis. *Catal. Rev. - Sci. Eng.* **1977**, 15, 69.
- ⁷² Bartholomew, C. H.; Agrawal, P. K.; Katzer, J. R.; Sulfur. Poisoning of Metals. *Adv. Catal.* **1982**, 31, 135.

-
- ⁷³ Erekson, E. J.; Bartholomew, C. H. Sulfur poisoning of nickel methanation catalysts: II. Effects of H₂S concentration, CO and H₂O partial pressures and temperature on reactivation rates. *Appl. Catal.* **1983**, 5, 323.
- ⁷⁴ Rostrup-Nielsen, J. R.; Trimm, D. L. Mechanisms of carbon formation on nickel-containing catalyst. *J. Catal.* **1977**, 48, 155.
- ⁷⁵ Trimm, D. L. The Formation and Removal of Coke from Nickel Catalyst. *Catal. Rev.-Sci. Eng.* **1977**, 16, 155.
- ⁷⁶ Trimm, D. L. Catalyst design for reduced coking (review). *Appl. Catal.* **1983**, 5, 263.
- ⁷⁷ Augustine, S. M.; Alameddin, G. N.; Sachtler, W. M. H. The effect of Re, S, and Cl on the deactivation of Pt/ γ -Al₂O₃ reforming catalysts. *J. Catal.* **1989**, 115, 217.
- ⁷⁸ Gates, B. C.; Katzer, J. R.; Schuit, G. C. A. *Chemistry of Catalytic Processes*, McGraw-Hill, New York, **1979**.
- ⁷⁹ Moeller, A. D.; Bartholomew, C. H. Deactivation by Carbon of Nickel and Nickel-Molybdenum Methanation Catalysts. *ACS Fuel Chem. Div. (Preprint)* **1980**, 25, 54.
- ⁸⁰ Barbier, J.; Corro, G.; Zhang, Y.; Bournville, J. P.; Franck, J. P. *Appl. Catal.* **1985**, 16, 169.
- ⁸¹ Coughlin, R. W.; Hasan, A.; Kawakami, K. *J. Catal.* **1984**, 88, 163.
- ⁸² Figoli, N. A.; Beltramini, J. N.; Querini, C. A.; Parera, J. M. *Appl. Catal.*, **1985**, 15, 41.
- ⁸³ Rodriguez, J. A. The chemical properties of bimetallic surfaces: Importance of ensemble and electronic effects in the adsorption of sulfur and SO₂. *Prog. Surf. Sci.* **2006**, 81, 141.
- ⁸⁴ Rostrup-Nielsen, J. *Journal of Catalysis* **1984**, 85, 31.

-
- ⁸⁵ Rostrup-Nielsen, J. R.; Alstrup, I. B. Ensemble control by sulfur poisoning on nickel catalysts for steam reforming. *Stud. Surf. Sci. Catal.* **1987**, 38, 725.
- ⁸⁶ Apestequia, C. R. Barbier, J. *J. Catal.* **1982**, 78, 352.
- ⁸⁷ Duprez, D.; Mendez, M.; Little, J. Evaluation of a method for characterizing coked and sulphided Rh/Al₂O₃ catalysts: study of the space and time dependence of sulphur deposition on Rh/Al₂O₃ in toluene steam reforming. *Appl. Catal.* **1986**, 27, 145.
- ⁸⁸ G. M. Bickle, PhD Thesis, University of Queensland, **1989**.
- ⁸⁹ Khoobiar, S, *Catalysis Supports and Supported Catalysts, Theoretical and Applied Concepts*, ed. A.B. Stiles. **1987**.
- ⁹⁰ Ribeiro, F. H.; Bonivardi, A. L.; Samorjai, G. A. Ensemble size reduction by rhenium-sulfur as a method to lower the rate of deactivation of hydrocarbon reactions over Pt catalysts. *Catal. Lett.* **1994**, 1.
- ⁹¹ Dees, M. J.; den Hartog, A. J.; Ponec, V. Identification of active sites of reforming catalysts by poisoning. *Appl. Catal.* **1991**, 72, 343.
- ⁹² Delahay, G.; Duprez, D. Effect of sulphur on the coking of rhodium in the steam_reforming_of 1-methylnaphthalene. *Appl. Catal.* **1989**, 53, 95.
- ⁹³ Azad, A.; Duran, M.; McCoy, A.; Abraham, M. Development of Ceria Supported Sulfur Tolerant Nanocatalysts: Pd-based Catalyst Formulation. *App. Catal. A: Gen.* **2007**, 332, 225-236.
- ⁹⁴ Heracleous, E.; Lee, A. F.; Wilson, K.; Lemonidou, A. A. Investigation of Ni-based Alumina Supported Catalysts for the Oxidative Dehydrogenation of Ethane to Ethylene: Structural Characterization and Reactivity Studies. *J. Catal.* **2005**, 231, 159.

-
- ⁹⁵ Li, C.; Chen, Y. W. Temperature-programmed-reduction studies of nickel oxide/alumina catalysts: effects of the preparation method. *Thermochimica Acta* **1995**, 256, 457.
- ⁹⁶ Shalvoy, R. B.; Davis, B. H.; Reucroft, P. J. *Surf. Interface Anal.* **1980**, 180, 11.
- ⁹⁷ Heck, R.; Farrauto, R. Catalytic air pollution control: Commercial technology, Wiley publishers, 2nd Ed. **2002**.
- ⁹⁸ Rostrup-Nielsen, J. R. in: J.L. Figuerido (Ed.), Progress in Catalyst Deactivation, NATO Advanced Study Institute Series E, Marunus Nijhoff, Boston, **1982**, 209.
- ⁹⁹ Strohm, J. J.; Zheng, J.; Song, C. Low-temperature steam reforming of jet fuel in the absence and presence of sulfur over Rh and Rh–Ni catalysts for fuel cells, *J. Catal.* **2006**, 238(2), 309.
- ¹⁰⁰ Corro, G.; Fierro, J. G.; Montiel, R.; Banuelos, F. *J. Mol. Catal. A:* **2005**, 228, 275.
- ¹⁰¹ Bickle, G. M. PhD Thesis, University of Queensland, Brisbane, **1989**.
- ¹⁰² Rodriguez, N. M. Anderson, P. E.; Wootsch, A.; Wild, U.; Schlögl, R.; Paál, Z. *J. Catal.* **2001**, 197, 365
- ¹⁰³ Rakass, S.; Oudghiri-Hassani, H.; Abatzoglou, N.; Rowntree, P. *J. Power Sources* **2006**, 162, 579.
- ¹⁰⁴ Parera, J. M.; Figoli, N. S.; Beltramini, J. N.; Churin, E. J. Carbol, R. A. Proc. 8th Int. Congr. Catal. Berlin, **1984**.
- ¹⁰⁵ Liu, B. S.; Jiang, L.; Sun, H.; Au, C. T. *Appl. Surf. Sci.* **2007**, 253, 5092.

¹⁰⁶ Mayne, J. M.; Tadd, A. R.; Dahlberg, K. R.; Schwank, J. W. Influence of thiophene on the isooctane reforming activity of Ni-based catalysts, *J. Catal.* **2010**, 270, 140.

¹⁰⁷ Bickle, G. M.; Biswas, J.; Do, D. D. *Appl. Catal.* **1988**, 36, 259.